Development of an Acoustic Emission Monitoring System for Crack Detection During Arc Welding

Xing Meng

Submitted to meet the degree requirements for

Doctor of Philosophy

School of Metallurgy and Materials

College of Engineering and Physical Sciences

University of Birmingham

2019

Keywords

Acoustic emission

Arc welding

Crack detection

Sensor

Stress waves

Source differentiation

Signal processing

Cross-correlation

Magnitude squared coherence

Abstract

Condition monitoring techniques are employed to monitor the structural integrity of a structure or the performance of a process. They are used to evaluate the structural integrity including damage initiation and propagation in engineering components. Early damage detection, maintenance and repairs can prevent structural failures, reduce maintenance and replacement costs, and guarantee that the structure runs securely during its service life. Acoustic emission (AE) technology is one of the condition monitoring methods widely employed in the industry. AE is an attractive option for condition monitoring purposes, the number of industrial applications where is used is rising. AE signals are elastic stress waves created by the fast release of energy from local sources occurring inside of materials, e.g. crack initiating and propagating. The AE technique includes recording this phenomenon with piezoelectric sensors, which is mounted on the surface of a structure. The signals are subsequently analysed in order to extract useful information about the nature of the AE source. AE has a high sensitivity to crack propagation and able to locate AE activity sources. It is a passive approach. It listens to the elastic stress waves releasing from material and able to operate in real-time monitoring to detect both cracks initiating and propagating. In this study, the use of AE technology to detect and monitor the possible occurrence of cracking during the arc welding process has been investigated. Real-time monitoring of the automated welding operation can help increase productivity and reliability while reducing cost.

Monitoring of welding processes using AE technology remains a challenge, especially in the field of real-time data analysis, since a large amount of data is generated during monitoring. Also, during the welding process, many interferences can occur, causing difficulties in the identifications of the signals related to cracking events. A significant issue in the practical use of the AE technique is the existence of independent sources of a signal other than those related

to cracking. These spurious AE signals make the discovering of the signals from the cracking activity difficult. Therefore, it is essential to discriminate the signal to identify the signal source. The need for practical data analysis is related to the three main objectives of monitoring, which is where this study has focused on. Firstly, the assessment of the noise levels and the characteristics of the signal from different materials and processes, secondly, the identification of signals arising from cracking and thirdly, the study of the feasibility of online monitoring using the AE features acquired in the initial study.

Experimental work was carried out under controlled laboratory conditions for the acquisition of AE signals during arc welding processing. AE signals have been used for the assessment of noise levels as well as to identify the characteristics of the signals arising from different materials and processes. The features of the AE signals arising from cracking and other possible signal sources from the welding process and environment have also collected under laboratory conditions and analysed. In addition to the above mentioned aspects of the study, two novel signal processing methods based on signal correlation have been developed for efficiently evaluating data acquired from AE sensors.

The major contributions of this research can be summarised as follows. The study of noise levels and filtering of different arc welding processes and materials is one of the areas where the original contribution is identified with respect to current knowledge. Another key contribution of the present study is the developing of a model for achieving source discrimination. The crack-related signals and other signals arising from the background are compared with each other. Two methods that have the potential to be used in a real-time monitoring system have been considered based on cross-correlation and pattern recognition. The present thesis has contributed to the improvement of the effectiveness of the AE technique for the detection of the possible occurrence of cracking during arc welding.

Acknowledgements

Foremost, I want to express my heartfelt thanks to my supervisors, Dr Mayorkinos Papaelias and Mr Geoff Melton for the support of my PhD study. Their guidance helped me to research and write this thesis.

I would also like to thank Mr Robert Shaw for his assistance and training with the lab work. For his encouragement, insightful comments, and hard questions.

My sincere thanks also go to my dearest friends, Daniel, Maxime and Meiqi for their support from work to life with countless cups of tea, pints and phone time. I would not have made it without their company in life.

I want to thank my parents, Mrs Ying Zhang and Mr Fanrong Meng. They keep me going.

Table of Contents

List of Figures

List of Tables

List of Abbreviations

AE - Acoustic Emission

NDT - Non-Destructive Testing

TIG welding – Tungsten Inert Gas welding

MAG welding - Metal Active Gas welding

FFT - Fast Fourier Transform

PSD - Power Spectral Density

PR – Pattern Recognition

Chapter 1

Introduction

This chapter begins with an overview of the research background in section 1.1, followed by the goals and scope of the studies in section 1.2 and section 1.3. Section 1.4 describes the original contributions of this work. Finally, section 1.5 is an outline for the rest of the chapters.

1.1 Background

Welding has become an indispensable process in manufacturing various kinds of mechanical equipment as well as in building important engineering structures. Before putting welding products into production, to ensure the welding quality, a considerable amount of welding preparatory work is required. Firstly, to determine the appropriate welding processes and welding parameters. Secondly, to test the standard specimens to verify if the specimens meet the product quality requirements, etc. However, there are various unpredictable elements in the actual welding process. It is difficult to receive good welding quality even with preparatory work. Thus, welding quality monitoring has attracted much industrial interest in recent years. Welding quality monitoring is required to guarantee the usability, reliability and integrity of weldments. Apart from welding technology, welding quality monitoring of weldments is an essential part of welding quality management.

In welding quality monitoring, sensing is an essential part. The task of acquiring real-time phenomena during the process relies on successfully obtaining useful information from the sensors employed. Every sensor that used in welding monitoring has its own deficiencies in obtaining reliable information during welding processes. In fact, techniques and equipment for welding sensors have been widely and successfully used in other fields. However, due to the adverse working condition during welding involving spatter, electromagnetic interference, high temperature, vibration, and dust etc., a more stringent requirement for the welding sensors and more robust systems are needed [1]. Another area where researchers have focused on includes advanced methods for processing signals containing interference. To this end, better

filtering methods for removing noise-related effects and acquiring the useful information of the signals have been undergoing development [2]. Many studies have been carried out, aiming to link the signals which have been gathered from sensors to specific welding defects [3-6]. This can be achieved by employing novel ways to process the acquired signals. However, the study for AE monitoring for arc welding process is still in the initial stages of development. Real-time AE monitoring in particular and feedback control have yet to be proven and implemented in the industry. The present study investigated the development of an AE monitoring system for the detection of the occurrence of cracks using AE signals recorded during the welding process. The study is part of the development work looking to implement a multi-sensor welding monitoring system being developed at TWI Ltd.

1.2 Scope of this research

Signal discrimination is the key to crack detection for the present research. The study of the noise level arising from the working environment during the arc welding processes is one of the priorities since the arc welding process is considered to be noisy and the signal quality could vary broadly from process to process. Welding of different materials can also give rise to a different noise level. It is vital to understand the variations occurring in each case in order to optimise the filtering results according to the noise level arising. The noise during the welding process that could be picked up by the AE sensor could be attributed to many different sources with many of them having different characteristics. Understanding the features associated with noise signals is vital for developing an effective crack detection system. To better study the features of the noise signals, in the present study, the noise-related signals have been categorised into two types [7]. Firstly, the continuous type of noise, which is likely to arise from the welding machine or the background environment. Secondly, the burst type

signals, which are discontinuous, are much more complex to study since they can arise from many different sources and are harder to distinguish them. Under these two categories of signals, many different signals were collected separately for the analysis of their critical characteristics.

Collection and analysis of crack-related signals were carried out. Comparison of the features arising from different sources and observed in the frequency spectra of the acquired AE signals was also performed. The results show the possibility of applying the AE technique for monitoring and detecting signals generated from the occurrence of crack initiation and propagation during the welding process using time-frequency domain-based analysis.

1.3 Objectives of this research

This study forms part of developing a multi-sensing monitoring system and process system to be able to detect imperfections, possibly forming in the weld in real-time. For developing the system, the fundamental features of the obtained AE signals acquired during the welding process need to be understood.

The first important aspect was to investigate the noise level arising from different arc welding processes for various alloys. Subsequently to understand and analyse the spectral (frequency) features of the background signal and investigate the feasibility of filtering background noise sources.

The second important part of the study was to have a comprehensive understanding of the signals arising from the cracking of the weld. AE signals arising from cracking events were collected and analysed.

The third part was to carry out real-time monitoring. The features of the crack-related signal and other types of signals generating from the welding process are used for the development

of the detection system. Two signal processing methods based on signal correlation have been developed for the detection evaluation of cracking-related events.

The ultimate aim of the present study focusing on the development of a useful online welding monitoring tool and a control system which is capable of adjusting the welding process according to the processed signals in a dynamic fashion. The user can set the threshold figure to detect discontinues. Subsequently, the control system can automatically adjust the process by correcting the critical parameters as required. The results of this study have the potential to be integrated into a real-time monitoring system in the future.

1.4 Significance and originality of the research

Previous studies have investigated frequency-related features of signals arising from crack initiation and propagation. However, there has not been a comprehensive comparison of crack-related signals with other sources of signals from the process yet, e.g., signals arise from the welding machine or the background environment This study investigates an AE monitoring system which intelligently combines different signal processing methods.

The major contributions of this research can be summarised as follows. The study of noise levels and filtering of different arc welding processes and materials is one of the areas where the original contribution is identified with respect to current knowledge. The signals arising from the welding process widely vary depending on the exact processes and materials. Each process has its own signature frequencies. The filtering results also vary depending on the process and material.

Another key contribution of the present study is the developing of a model for achieving source discrimination. The different kinds of disturbance signals are collected and analysed

individually. The cracking signals from the Tungsten Inert Gas (TIG) welding process with steel material have been collected and analysed. The crack-related signals and other signals arising from the background are compared with each other. The differences in the frequency range of the signals from different sources have been identified and analysed.

Two methods that have the potential to be used in a real-time monitoring system have been considered based on cross-correlation and pattern recognition.

Publication list:

Welding quality monitoring using acoustic emission techniques

Conference: World Congress on Condition Monitoring - WCCM 2017 At London, UK

Acoustic monitoring system for high-quality arc welding

Conference: 2017 NSIRC Annual Conference at Cambridge, UK

Spectral analysis for crack detection during TIG welding using acoustic emission techniques

Manuscript submitted to Insight Journal (In review)

1.5 Outline of the thesis

This thesis consists of nine chapters.

Chapter 1 provides the scope and background of the study, followed by the original contribution.

Chapter 2 presents different welding methods, their advantages and challenges, different welding defects in welding processes with particular focus on cracking in arc welding.

Chapter 3 presents a summary of traditional NDT methods used for quality control of welding technologies. A short analysis of the advantages and disadvantages is presented. Then a summary of the state of art of online welding monitoring is presented.

Chapter 4 presents the fundamentals of AE technique. The main principles, its advantages and drawbacks of AE monitoring are discussed. Extensive analysis has been conducted with respect to the exploration of different aspects of AE monitoring and problems related to this technique, such as the theory of wave modes and signal processing, past uses and gaps in current knowledge and opportunities for innovative research.

Chapter 5 presents the methodology used in this study. It introduces the AE monitoring system designed and used, along with the materials selected for welding and testing purposes. The welding methods considered are also detailed in this chapter.

Chapter 6 presents the experimental results and the associated analysis of the investigation of continuous background AE signals arising from different welding processes.

Chapter 7 presents the results and analysis of the frequency features associated with crack-related signals and other types of burst signals arising during the welding process.

Chapter 8 presents the results and analysis associated with real-time monitoring.

Chapter 9 summarises the overall findings of the study and discusses possible areas of related work in the future.

Chapter 2

Arc welding and defects in arc welding

This chapter begins with an introduction to arc welding in section 2.1, followed by common defects arising during welding, which are discussed in section 2.2. Section 2.3 details the different types of crack-related defects.

2.1 Introduction on arc welding

Arc welding is an accessible fusion process used to assemble metals. By employing intense heat, the metal at the junction between the two welding parts melts and is directly or more often mixed with the molten intermediate. After cooling and solidification, a metallic bond is produced. Since the seal is a metal mixture, the final weld may have the same strength characteristics as the base metal of the component. This contrasts sharply with non-melting fusion processes where the physical and mechanical properties of the substrate cannot stay the same at the joint [8]. A number of totally new welding principles emerged at the end of the 19th century. Oxygen and gases such as acetylene can be safely combined and stored to produce flames that generate sufficient heat during combustion. At the same time, sufficient current can be generated for resistance welding and arc welding. The intensity of the heat source enabled heat up the work-piece that is quicker than it is lost due to the heat conduct into the surrounding metal. Consequently, it was possible to generate a molten pool which later solidified to form unifying bonds between the parts that are being joined. The basic welding methods of resistance welding, gas welding and arc welding were all developed during the time before World War I [8]. Today, it is still an essential process in steel construction and vehicle manufacturing.

Welding processes can use direct or alternating currents as well as non-consumable or consumable electrodes. The weld area is usually shielded by a shielding gas or slag. The arc welding process can be manual, semi-automatic or fully automatic [9]. Table 2-1 shows the

different types of arc welding processes.

Table 2-1 Different types of arc welding processes.

Consumable electrode methods	Shielded metal arc welding (SMAW)	Current is applied to form an arc between the substrate and the consumable electrode rod. The process is very versatile and requires little operator training and relatively inexpensive equipment. However, the welding time is rather slow because the consumable electrodes need to be replaced frequently, and the slag, flux residue must be removed after welding [9].
	Gas metal arc welding (GMAW), commonly called MIG/ MAG	Gas metal arc welding (GMAW) is also called MIG welding (inert shielding gas) or MAG welding (active shielding gas). Electric arc is created between a consumable tungsten electrode and a weldment. It is a particularly flexible and fast welding type with a wide range of applications [10-12].
	Flux-cored arc welding (FCAW)	A variant of the GMAW technology. The FCAW wire is actually a thin metal tube filled with powdered flux. The shielding gas supplied externally is sometimes used, but the flux itself is usually used to generate the necessary protection to the atmosphere [9].
	Submerged arc welding (SAW)	An efficient welding process in which an arc strikes under the granular flux. The quality of the arc is improved because contaminants in the environment are blocked by the flux. This increases arc quality and working condition.

		SAW is only possible in certain positions [13].
Non-consumable electrode methods	Gas tungsten arc welding (GTAW), or tungsten/inert-gas (TIG) welding	TIG welding (also known tungsten gas arc welding or GTAW) involves creating an electric arc between a non-consumable tungsten electrode and a weldment. The welding pool and the electrodes are shielded by an inert gas (usually argon) fed by a gas cup fixed at the torch end, the electrodes being centred [14].
	Plasma arc welding	The plasma welding process uses plasma as heat source with an internal plasma and an external shielding gas. The shielding gas passes through the external gas nozzle to achieve the same function as the TIG welding. The plasma gas circulates the retracted centre electrode, typically tungsten [15].

2.2 Types of arc welding defects

Welding defects are irregularities that harm the integrity of welded structures. There are a variety of welding defects; some of the common ones are listed in Table 2-2. Welding defects are classified according to ISO 6520, while their acceptance limits are listed in ISO 5817 and ISO 10042.

Table 2-2 Types of welding defects and corresponding cause and identification.

Defect types	Causes	Identification
Cracks	Residual stress, the presence of hydrogen may become susceptible to cracking.	Detailed in section 2.3
Irregular weld shape	The irregular motion of non-uniform and welded cutting edges. During the welding process, when the excess weld metal becomes too high, the current is too low, or the speed of welding is too slow. This can lead to stress concentration [16].	Many conditions, including irregular width and height, overly narrow or wide weld joint, too big or small size of excess weld metal etc.
Slag inclusion	The presence of slag or oxygen cutting off the air at the edge of the weld; the corner grooves and welding current are too low; the welding speed is high. When using an acid electrode, a small current can cause improper weld slag. Slag is also caused when a long arc or a base of an incorrect polarity is used [17].	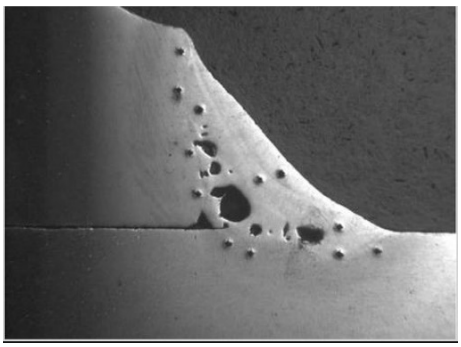 Figure 2-1 Slag inclusion in the weld [17].
Incomplete penetration	The installation space or groove angle is too small, very thick rust on the edge of the weld, excessive diameter electrode, very low current, low	When the weld bead does not penetrate the entire thickness of the base plate, two opposing weld beads do not interpenetrate, or the

	welding speed, too long arc, poor polarity, etc. [18].	weld does not pass through the toe of the fillet weld but only bridges across it. 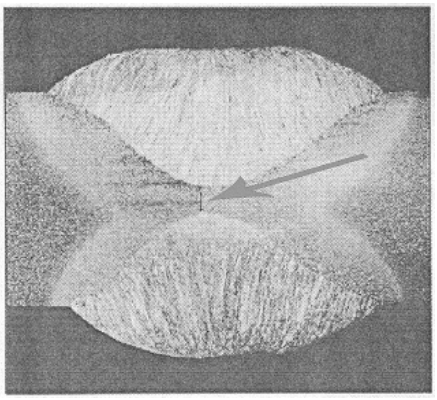 Figure 2-2 Incomplete penetration [18]
Lack of fusion	Too narrow a joint preparation, incorrect welding parameter settings, poor welder technique and magnetic arc blow [16].	Between the weld beads or between weld bead and base metal, the weldment does not melt completely. 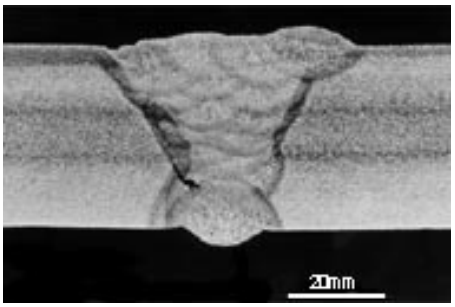 Figure 2-3 Lack of fusion [16]
Undercut	The groove formed by the arc at the molten base metal along the weld edge due to incorrect welding parameters [16].	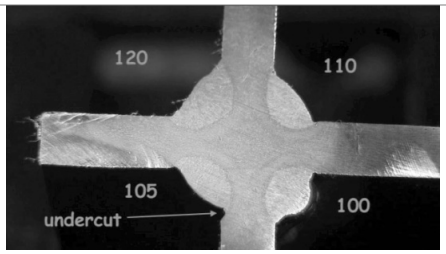 Figure 2-4 Undercut [16]

Porosity	Porosities is caused by the absorption of oxygen, hydrogen and nitrogen in the welding pool and then released upon solidification, trapping the welding metal [19].	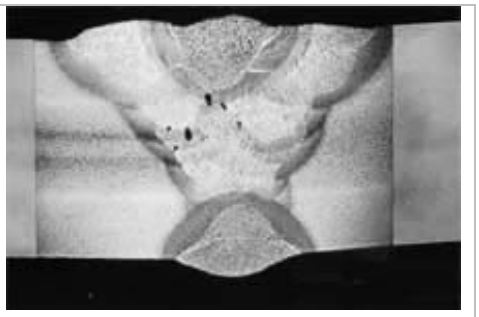 Figure 2-5 Uniformly distributed porosity [19]

2.3 Cracking on welding

Cracking in welds is one of the most common types of welding flaws. Cracks in welding also have different categories. By location, cracks in welding can be categorised, as shown in Figure 2-6. A short introduction of welding cracking by cause followed next.

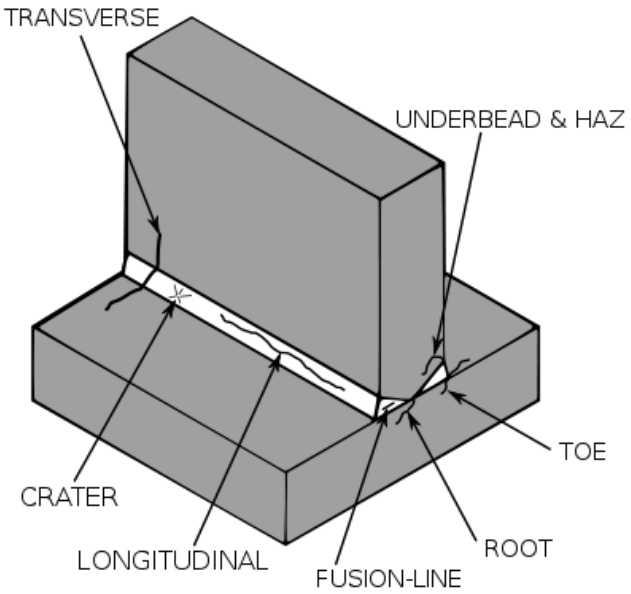

Figure 2-6 Different cracking categories by location [20]

2.3.1 Hot crack

Hot "cracking" welding means the cracking phenomenon which occurs during process as a result of the existence of liquid in the microstructure. Hot cracks are generally related to liquid films exist along the grain boundaries in the melting zone and the partially melted zone in the heat-affected zone. Because these liquid films can continue to reach temperatures well below the equilibrium solidus temperature of the parent alloy, the solidification range of the alloy expands to "effective" solidus temperature. Usually, the effective solid line may be much lower than the solid line at equilibrium due to the influence of segregation of solutes and impurities [20].

The "hot crack" is defined by the American Welding Society as a crack forming before the completion of solidification.

1. Solidification cracks occur in the melting zone at the end of the solidification.
2. Liquation cracking at heat affected zone. It is also inter-crystalline and is produced by a continuous liquid film formed at elevated temperatures.
3. Liquation cracking in the weld metal are usually observed after several welds or weld repairs. These cracks can form at migrated grain boundaries and occur due to the resetting of these limits during reheating at rising temperatures.

2.3.2 Solid cracking

There are many cracking mechanisms related to the area of HAZ or heated weld metal. These include ductility-dip cracking, Post weld heat treatment cracking, stress assisted cracking and copper contamination cracking. These cracking mechanisms cover the entire material range, including steel, stainless steel, nickel-based alloys, copper-based alloys and aluminium alloys [21].

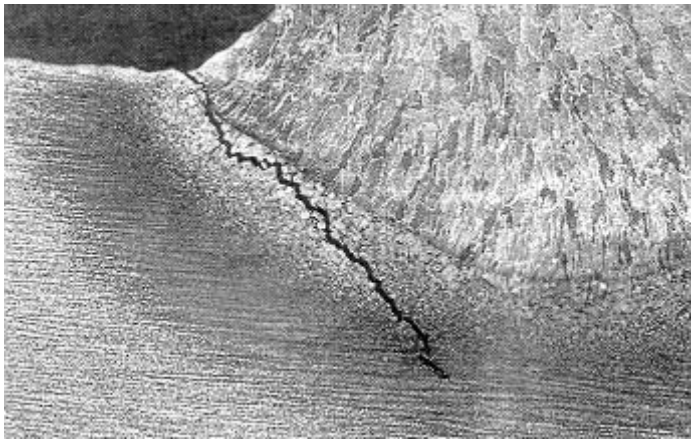

Figure 2-7 Crack along with the coarse grain structure in the HAZ [22].

2.3.3 Cracking induced by hydrogen

The presence of hydrogen in the molten metal or the heated zone can result in a crack defect known as hydrogen-induced cracking (HIC). This kind of cracking is also normally known as cold cracking or hydrogen assisted cracking because it happens at or close to room temperature during the cooling of the welding. The reduce of ductility and reduction of fracture toughness related with the existence of hydrogen is commonly called hydrogen embrittlement. This kind of crack is generally associate to steel. However, the presence of hydrogen in sufficient quantity can cause embrittlement or cracking of other materials. Although hydrogen exists in minimal traces in almost all materials, the introduction of hydrogen will cause the presence of hydrogen over a certain threshold to promote cracking during the welding process. Even at room temperature, atomic hydrogen is very easy to move in the microstructure, allowing it to diffuse into stress-sensitive areas and sensitive microstructures. Although HIC usually appears almost immediately after cooling to room temperature, it can also occur after some delay. This form of HIC is known as the delayed crack. This indicates that it is essential for hydrogen to diffuse and accumulate to the point where cracking occurs after reaching a threshold level of hydrogen [23].

2.4 Summary

Arc welding is the most used joining processing in all industrial applications since it is fast, cheap and able to achieve high quality. However, during the arc welding process, various defects can arise if it is not properly controlled. The most common welding defects are cracking, shape irregularity, porosity, slag inclusion, and undercut. For certain applications, different standards could be applied in order to determine if a defect is within the tolerance limits or not.

Chapter 3

Inspection and monitoring methods for arc welding

This chapter begins with an introduction of the traditional inspection methods for welds in section 3.1, followed by the state of art of monitoring methods for welding process in section 3.2.

3.1 Inspection methods for welds

The principle that often lies in the manufacture of weldments and structures is to ensure welding quality. The term 'welding quality' is relative. The application will decide what constitutes good or defective weld [24]. Generally, any weld will have good quality if it meets the requirements for the appearance and continues to carry out the intended work indefinitely. As a cause of high weld quality, good appearance of the welded surface has been considered very important. However, a good surface appearance does not guarantee a good internal quality. The first step to ensure the quality of welding is to determine the level of welding quality required. Criteria should be established based on service requirements. The criteria designed to give weld quality may vary from work to work, but using appropriate welding techniques can guarantee that applicable criteria are met. Regardless of quality standards, all welds must be inspected after welding is done.

Non-destructive testing (NDT) inspection methods will continue to confirm compliance with the standard by inspecting the weld's surface and the surrounding base material. Five basic methods including vision, liquid penetration, magnetic particle, ultrasonic and radiography (X-ray or gamma-ray based) inspections are commonly used to examine completed welds. As the use of computerisation increases, the image is further enhanced, enabling real-time or close to the real-time display, comparison and storage of the data. By reviewing each method, it can help make the most effective examination by using each process or combination of processes for a particular job.

Visual Inspection:

Visual inspection is generally the most cost-effective method. However, it should be done before, during and after the process. In the requirement of many standards.

Visual inspection only identifies the location of the defects on the surface of the welds. For specifications or applicable specifications, it is also necessary to inspect welds and internals of adjacent metal areas. Although it can be used for non-destructive inspections to determine the presence of defects, unless it affects the correlation between defects and some characteristics of the service [25].

Radiography testing:

The radiographic examination can detect inner defects of ferrous and nonferrous metals. The electrons emitted by the radioactive probe, the gamma-ray pass through the radiation absorbed by the material as they pass through. The thicker the material, the more the absorption of the gamma-ray. These high-intensity light helps to form a latent image that can be developed and fixed in a manner similar to conventional photographic film.

In X-ray inspection, information is displayed visually. It provides a permanent record that can be viewed at a time or location away from the test. This type of test is suitable for parts of various thicknesses and is applicable to all types of materials.

Radiographic film processing and visual equipment are required. Exposure compounds are also required. In radiographic inspection, it is necessary to orient the beam accurately to be able to observe a two-dimensional defect. Furthermore, the radiographic examination does not indicate the depth of the subsurface defects unless measurements from multiple angles have been carried out.

All instructions should be observed carefully in order to get satisfactory results. Radiation testing is permitted only for personnel who are subjected to radiation safety training and qualified as industrial radiological technicians [26].

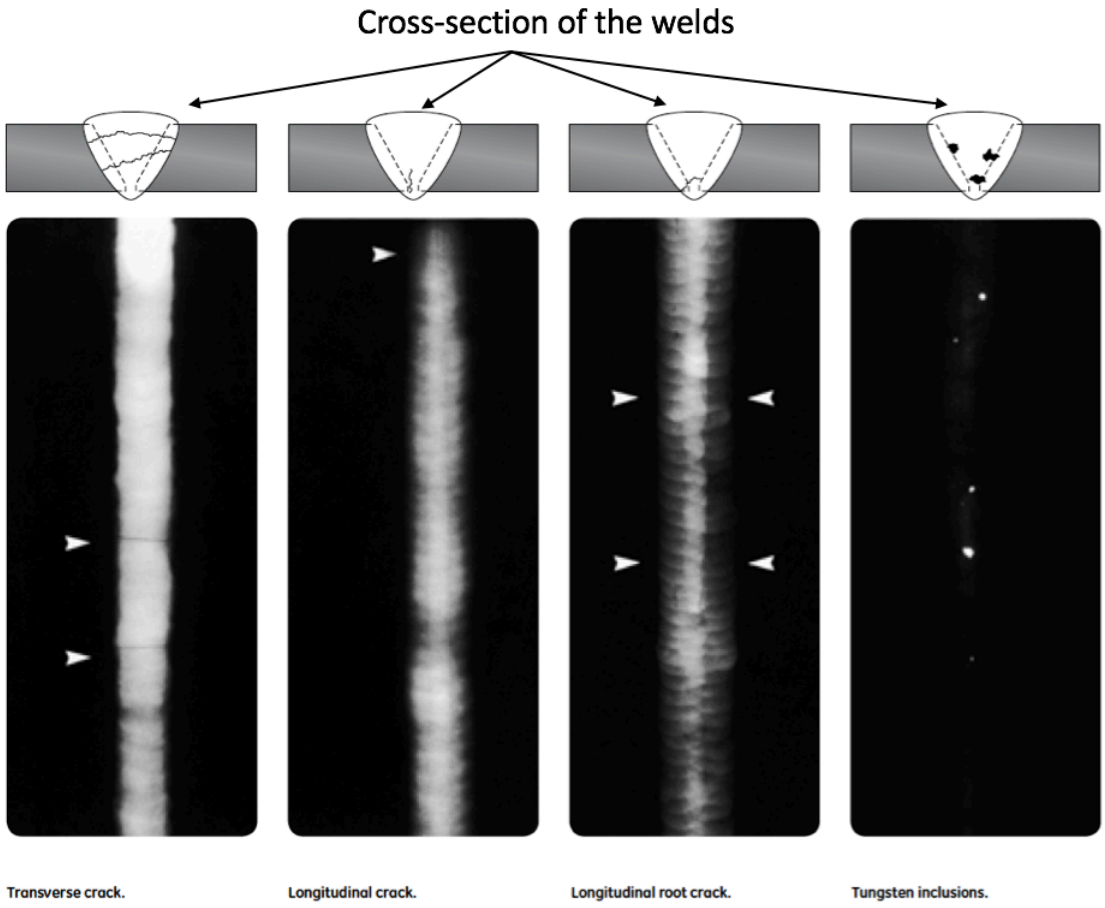

Figure 3-1 Example radiographs [27]

Magnetic Particle Inspection:

Magnetic particle inspection is a mean of specifying and defining defects in magnetic materials. It is ideal for detecting discontinuities on the surface of the welds, including the gaps that are too small to be observed with the naked eye and some discontinuities below the surface. Magnetic particle testing is easy to operate and generally applicable to many applications. The test is quantitative. This type of non-destructive inspection is not only limited to ferromagnetic materials but is also limited to surface or near-surface defects [28, 29].

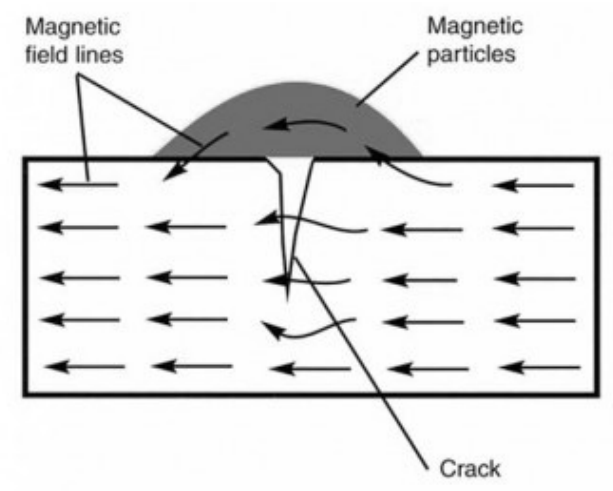

Figure 3-2 Illustration for Magnetic Particle Inspection [30]

Liquid Penetrant Inspection:

Cracks and porosities on the surface that cannot be seen with the naked eye can be confirmed by liquid penetration inspection. It is widely used to identify surface defects in welding and can be applied to austenitic and non-ferrous materials. Magnetic particle detection is otherwise limited to magnetic materials.

Liquid penetration testing is generally considered to have the following advantages:

a. Sensitive to small surface defects.
b. Few limitations with materials —works on magnetic, non-magnetic, metallic, non-metallic, conductive and non-conductive materials.
c. Few limitations with geometric shapes.
d. Visual, real-time results.
e. The apparatus is portable and affordable.

Disadvantages of LPI: Time-consuming pre-cleaning; sensitive to surface contaminants; only able to detect surface defects; can detect defects only on relatively non-porous materials [31].

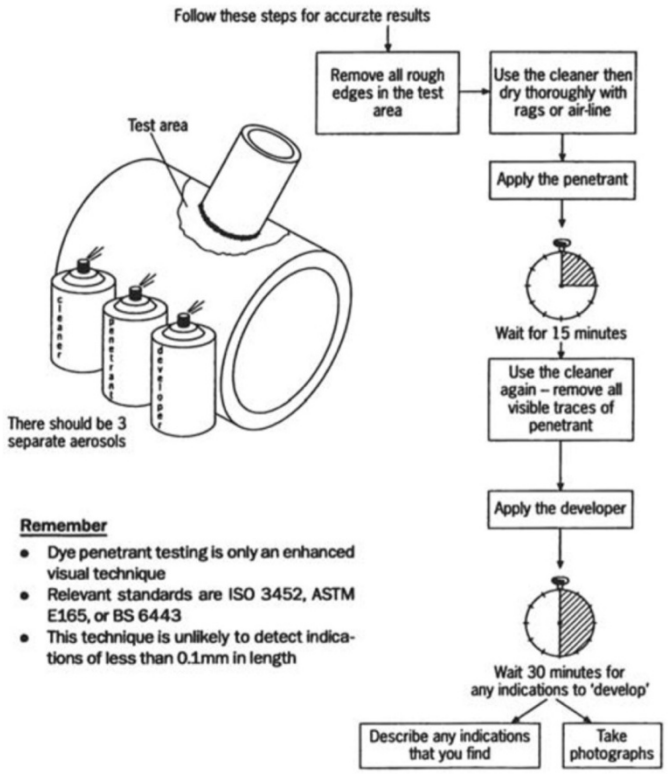

Figure 3-3 Illustration for Liquid Penetrant Inspection [31].

Ultrasonic Inspection:

Ultrasonic inspection is a way of detecting defects by passing a high-frequency sound through a substrate, when the sound beam encounters an interruption in the continuity of the material, a portion of the sound beam will be reflected and returned to the sensor. The instrument collects the returned sound, amplified and displayed, as shown in Figure 3-4.

Detection and measurement of surface and subsurface detection in metals can be discovered and measured, including defects that are too small in size to be otherwise discovered. Ultrasonic testing is not as good as other NDE methods for measuring weld porosity but is a preferred test method for detecting other types of discontinuities and laminations. Portable ultrasound equipment can be used for digital operation. These types of equipment have internal memory that is able to store the recorded data. They can be connected to a computer for further analysis, documentation and archiving. Ultrasound examinations require professional

interpretation of trained and highly skilled technicians [32].

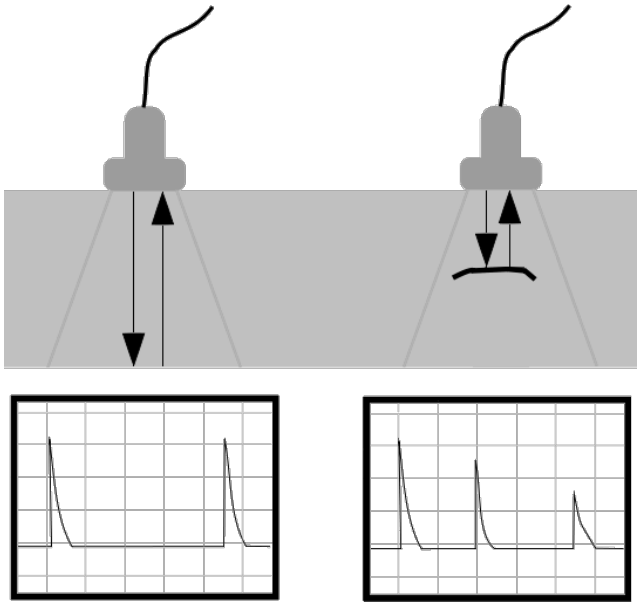

Figure 3-4 Illustration for Ultrasonic Inspection [32].

Eddy Current Testing:

Eddy current technology can detect defects on the surface or under the surface and measure conductivity and coating thickness. This test is sensitive to conductive materials [33]. An eddy current sensor, namely a coil probe that produces an alternating electromagnetic field, is placed next to the measurement target. Coils with a single ferrite core winding are typically used for surface testing of cracks in single or composite parts. The probe is placed on the assembly and "balanced" using the electronic unit controller. A crack is detected when the probe is scanned across the surface of the component. This technology is very flexible due to the high frequency of probes and test frequencies available in various applications.

It is generally accepted that Eddy Current Testing has the following advantages

a. Inspection speed up to approximately 20m per minute.
b. Accuracy and reliability of test results.
c. Able to discover progressive wall thinning or local defects.

d. Offers amplitude and phase information.

For some applications, it is required to select the probe and electronics carefully. In addition, testing is usually limited to surface rupture conditions and small subsurface defects. Many parameters affect the eddy current response. This means that undesired signals such as from hardness changes can cover the desired signals (e.g., cracks) [34, 35].

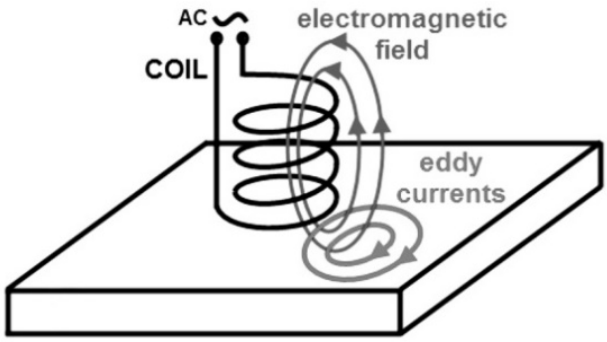

Figure 3-5 Illustration of the principle of Eddy Current Testing [33].

Selection of NDT methods:

A good NDT plan should recognise the inherent limits of each process. For instance, both ultrasound and radiography have different orientation factors that can lead to the process of selecting a particular task. Their advantages and disadvantages often complement each other. Radiographic inspection cannot detect defects similar to lamination reliably, but ultrasound is able to. On the other hand, ultrasonic waves are not suitable for detecting scattering holes, and X-ray photography is outstanding. Then use the correct NDE method as a check to keep the variables online and keep the weld quality within the standard range.

3.2 Online methods for monitoring welds

This section discusses and compares the basic principles and developments of each monitoring method considered in this study. The primary arc welding methods discussed in this study were gas metal gas shielding, arc welding (GMAW) and tungsten arc welding (GTAW). However, other processes such as friction stir welding and spot welding, etc. have been discussed.

3.2.1 Audible sound monitoring

The sound from the welding process includes high-frequency non-audible signals and acoustic signals. The welding process can use AE technology to collect, analyse and monitor the sound signals from the welding process.

The audible tone is mainly generated in an arc in the frequency range of 20 Hz to 20k Hz [36]. It can use non-contact high-fidelity microphones to gather important information about arc conditions and interferences during the processes. Using this method, researchers use the droplets generated by the arc column and splashing during welding to collect sound signals. The most important strength of monitoring the audible sound is that the monitoring sensor does not have to touch the weldment or the system because the welding sound is transmitted to the microphone through the air [37]. This simplifies sensor installation reduces electromagnetic obstruction to the sensor. However, ambient noise from the surrounding environment can affect the quality of the monitoring outcomes.

There are a lot of studies on sound acquisition systems for monitoring arc welding processes. One monitoring method is described in Grad et al. [38] various statistical parameters collected from the recorded acoustic signals are used to monitor the stability of the arc welding process. In 1967, Edman-Jesnitzer et al. found the relationship between arc length and welding current pressure. [39] Sánchez Roca et al. [40] proposed a stability analysis of the GMAW process.

They studied the sound generated by the arc in the short circuit droplet transport process. A variety of welding parameters and conditions were investigated during material deposit. The signals of arc sound were gathered by a system composed of a microphone which has a frequency bandwidth of 20 Hz to 100 kHz. A stability index is also put forward.

In 2010 Bi [41] studied the penetration state of GMAW through sound signal analysis and extracted 11 characteristic parameters from the sound signal. This was done using wavelet transmission. Then, after re-synthesising the 8-dimensional feature vector, an 8-dimensional feature vector is used as input, and four insertion states, namely partial penetration, unstable, complete, and transient penetration are outputs. Then they built a network model to assess penetration.

In 2011, Kamal Pal used GTAW pulses to study the penetration and material transmission modes in acoustic signals [42, 43]. The acquired signal of arc sound is processed with a variety of parameters in the time domain and frequency domain to analyse the transmission mode and penetration state. Figure 3-7 is the protocol of the experiment setup.

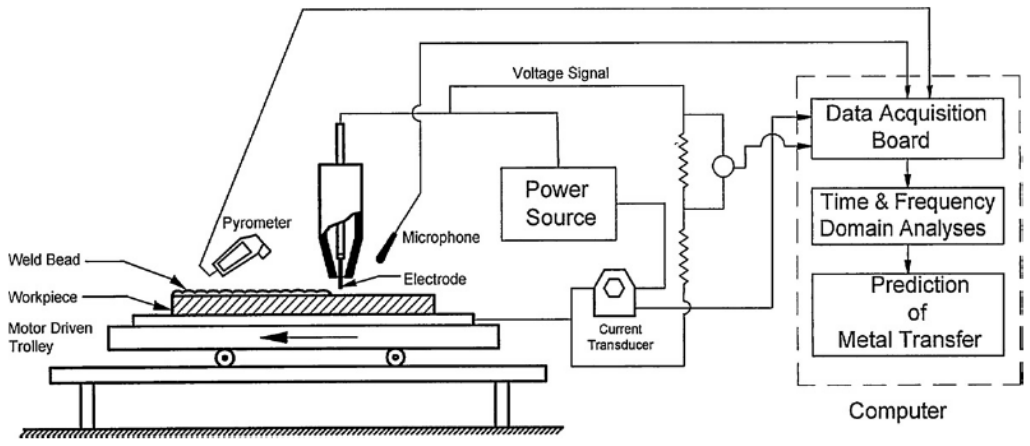

Figure 3-6 Schematic diagram of an arc sound collection system [43].

There is very little literature on GTAW monitoring. Lu Na, et al. used this method to capture sound monitors with GTAW pulses in 2013 and 2014 and studied the relationship between sound signals and arc heights [44] and penetration states [45].

Some commercially available sound monitoring systems are available for arc welding processes. For example, servo robots have developed a sensing system for real-time control of industrial robots integrated with microphones, lasers and cameras. i-CUBE^{TM}. It has many functions such as 3D laser distance measurement, audio signal and video processing [46]. However, the system does not have a sophisticated analysis system.

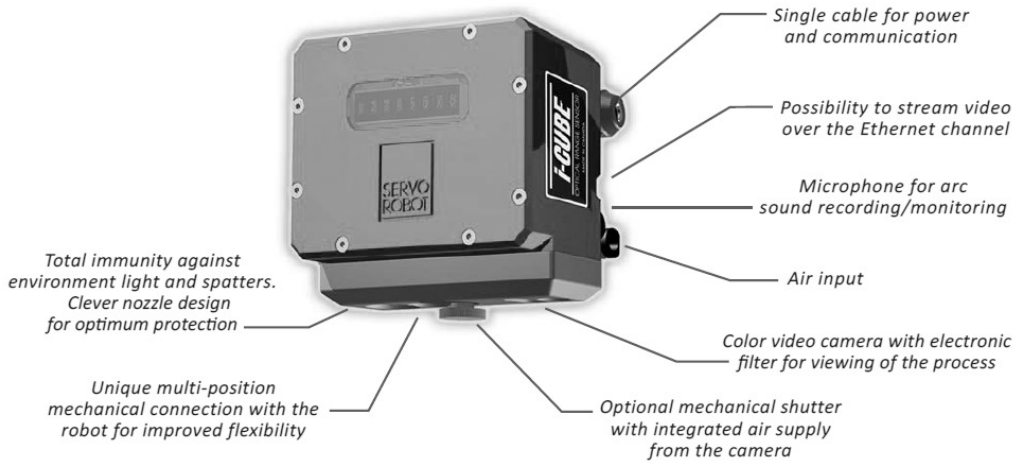

Figure 3-7 Features of i-CUBE ™ laser sensor [46]

3.2.2 Parameters monitoring: welding current and voltage

Parameter monitoring is the most often used monitoring technology in the welding industry. The main monitored parameters involve arc voltage, welding current and travel speed. The current is typically measured with a Hall Effect probe that is fixed around the cable, as shown in Figure 3-8. The voltage measurement schematic is shown in Figure 3-9.

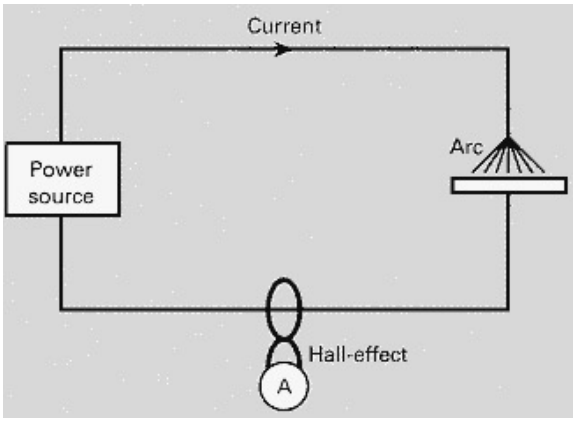

Figure 3-8 Diagram of current measurement technology [47]

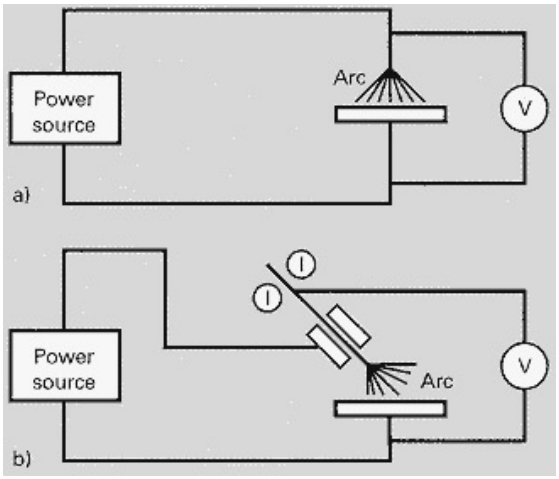

Figure 3-9 Voltage measurement diagram [47]

a) Connection to the back of the TIG torch;

b) Connection to the back of the MIG gun

Welding voltage and arc current signals are related to the physical characteristics of the welding process closely, such as arc stability, arc length, arc height, and droplet transfer [44]. The arc sensor can acquire real-time signals, and the device is simpler and less vulnerable to harsh welding environments. They also have better robustness and stability [48].

There are a lot of commercial welding parameter monitoring systems used in the market or in the development process. For example, the WeldCube^{TM} developed by Fronius can simultaneously monitor 50 welding processes. The AMV 4000 data logger, ADM III and Arc

Guard were developed by Triton Electronics Ltd, they have been on the market for many years. They share a similar operating principle: record arc current, voltage and other signals and compare them to pre-set values. The threshold is set, an alarm will be triggered if the difference between the gathered signals and the pre-set value exceeds the threshold [49].

Figure 3-10 AMV 4000 Data Logger from Triton Electronics Ltd [47]

The WeldPrint^{TM} system was developed by S. W. Simpson [50] of the University of Sydney and consisted of software developed with a front-end interface (see Figure 3-11) and the signature image processing (SIP) technology. Current research explains how to use SIP as a method of monitoring welding: The SIP data is calculated from the welded electrical data as data blocks. In the literature, position error detection of overlapping joint welds has been mentioned. Changes in the position of the welding process can be reflected in changes in physical phenomena. Once the data is collected, the signature of the statistical analysis provides a quantitative assessment of the weld, shows stability and repeatability, and provides defect weld diagnostics and testing [51-53].

TWI Ltd. has launched a project focused on the developing of parameter monitoring [54]. The purpose of the project was to study computer-based parameter monitoring to detect arc

irregularities due to shielding gases or contamination. The welding process considered is AC GTAW and GMAW welded aluminium sheets. The WeldPrint^{TM} system and other analytical algorithms such as FFT and RMS are used to record and analyse electrical parameters under various conditions.

The result is that a voltage signal can be used to discover irregularities effectively in the GMAW process. However, the method used cannot detect arc irregularities due to shielding gas or contamination interference.

Figure 3-11 WeldPrint^{TM} interface. [50]

Many studies have described GMAW quality monitoring using arc voltage and current measurements. Spectral and statistical measurements of welding images and [49] and process stability was discribed [55-57]. In 1991, J. W. Kim and others completed several tasks: they studied the relationship between welding current and workpiece tip distance applied it to the welding tracking system. In this paper, the current of welding was processed by the Runge-Kutta method [58, 59] in the case of reducing and increasing the linear tip distance in GMAW. S.-L. In the study of Ling [60], an on-line classifying metal transfer mode method has been successfully developed and the type of droplet transfer mode can be displayed and quantified

in real-time. The droplet transfer image was recorded using the camera during the recording and analysis of the welding voltage V (t), current I (t). Images of metal drop formation and separation processes are provided as short circuit transmission and spherical transmission. Then observe the physical changes in the welding arc. Prasad's study [61] proposed a statistical model (linear regression model) to estimate droplet transfer patterns in the form of droplets per pulse. Cayo and Alfaro describe the work of evaluating metal droplet transfer stability in the GMAW-S process, including voltage and acoustic acoustical parameters were collected [62, 63].

Some previously published studies have been reported to detect prosities through parameter monitoring. Barborak et al. [64] delivery the absence of shielding gas, porosity in the GMAW has been found to be involved to the welding voltage and current standard deviation and the current-voltage sample envelope shape shown in the V-I diagram. Ludewig [65] used linear Discriminant Analysis (LDA) to apply to the statistical analysis of the prosity formation with the arc current signal and arc voltage signal. Before finally inputting arc current signals and arc voltage to the DAQ board, two active low-pass filters were used to eliminate aliasing. A 12-bit data acquisition board was used to digitise the signals obtained at a rate of 256 Hz. Both filters were of 3-pole Butterworth design and had threshold frequencies of 100 Hz.

For gas-shielded tungsten arc welding (GTAW), the arc characteristics of the non-consumable process are much more stable than the consumption process. There are two difficulties in monitoring the parameters of the GMAW process. One is the severe high-frequency interference of the arc voltage, and the high voltage used to initiate the arc can damage the instrument. These arc sensors must be designed more precisely. The other is to apply the correct signal processing method.

Cook et al. in 1983 [66] a linear relationship between arc length and arc voltage was found under certain conditions of GTAW. 1998 Brent et al. Under certain experimental conditions,

the relationship between arc voltage and arc length in GTAW is also linear [67]. In 2000, Nixon discovered that the arc length arc voltage of the GMAW process were still linearly related to other conditions and shielding gases [68]. Chen announced an aluminium alloy pulsed GTAW welding quality monitoring technology and developed a feature extraction algorithm for time-domain and frequency-domain of real-time voltage signal data [48, 69].

In 2011, Yanling Xu [70] studied the weld height tracking of GMAW welds through parameter monitoring. The eigenvalues of the arc voltage signal are recorded and a linear relationship between the arc length and arc voltage is established using an appropriate voltage drop algorithm. The results show that the actual arc between the linear calculation and the arc calculation error is minimal. Figure 3-12 shows the 6-2 mm, including the total height of the pre-treatment, noise cancellation, linearisation, and fitting analysis of the voltage signal error processing pattern of the welding process.

Experiments have shown that it is possible to have an arc voltage characteristic of at most 0.218 mm consistent with the actual arc length error relationship model for arc length calculation. This means that the accuracy of the relationship model between the arc voltage and the arc length robot fully meets the requirements of the GTAW process — high-speed real-time arc length control.

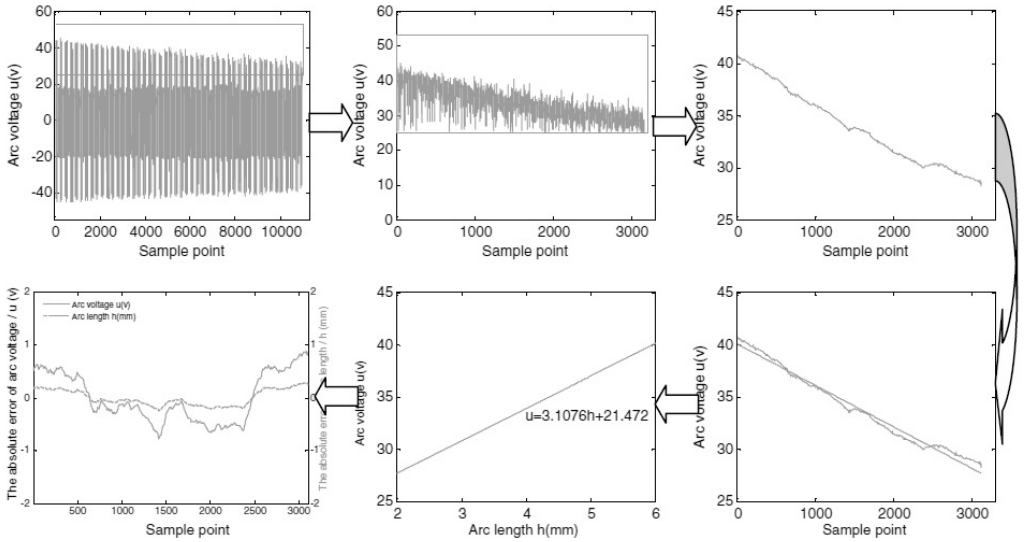

Figure 3-12 The voltage signal processing procedure. (arc height of 6 to 2 mm) [70]

Conclusions can be drawn from the published literature on the developing of parametric monitoring in current commercially available systems and arc welding, with particular physical phenomena such as monitored parameters and arc heights. Establish relationships. However, since many elements can influence the signal acquisition, it is hard to correlate the characteristics of the signal with certain types of defects. For example, Ludwig [65] performed a research to detect porosity in welds using parameter monitoring that can only be useful in certain situations. Similar results have been found in many other studies. This means that the use of only electrical parameters to detect other defects can be very limited. Many researchers have begun to integrate different monitoring methods with electrical parameters [62, 63, 71, 72].

3.2.3 Vision sensors

Visual inspection has always been a hot topic for researchers because it takes direct information from images. It has also been extensively studied in the field of welding process monitoring. The main challenge to be solved in vision-based monitoring systems is strong arc interference. One way to solve this problem is to apply additional illumination to the target and then collect

the information by obtaining a reflected image from the target surface. In this paper [73] Jae Seon et al., a robotic weld seam tracking system consisting of a visual sensing method based on built-in illumination designed to ensure immunity to interference during welding arc, splash and smoke was proposed. A three-dimensional image extraction function and a robot path correction arc of the welded joint are realised. The results show that the system is robust enough to accommodate a variety of welding noises and to monitor weld and workpiece shapes.

Luo and Chen [74] studied the creation of precise welded joint profiles using signal processing of distorted original images. An automatic tracking system for tracking beads has also been developed. The system features training, template saving, automatic start of welding start, automatic calibration, groove dimensioning and seam detection, and tracking control.

There is also a commercially available laser tracking system to monitor the arc welding process. Lincoln Electric Adaptive Fill of Lincoln Ltd is a laser scanning system designed for narrow gap welding [75]. The laser scanning system also has an articulation volume measurement function. With this information and a combination of welding parameters and travel speed control. It can be automatically adjusted to maintenance and filling in addition to i-Cube^{TM}. Servo robots also have a variety of laser scanning systems for a variety of applications. The Power-SCAN^{TM} features a 3-D laser camera with scan speeds of up to 6m / min, which is a fully integrated standard system that includes laser cameras, control units, actuators, teach pendants and software. It tracks all weldable materials, including aluminium. It also has the ability to teach and play [76].

Figure 3-13 3-D laser camera head of Power-scan^{TM} [76]

Recently, passive visual monitoring has become a topic of significant research interest since its low cost and does not require to be in contact with the weld itself. Passive vision technology uses a camera to access the target and capture the image directly without additional means. Some research regarding this technology can be found in the literature. Kuo et al. [77] proposed a passive image tracking system using fuzzy logic. Shen [78] studied the welding process of GTAW and developed a joint tracking system for flange and sheet products [79].

However, processes such as GMAW or pulsed GMAW, which generate many splashes and smoke during the welding process, are more challenging to monitor than other relatively stable welding processes. This paper [80], proposed a GMA pulse weld seam tracking system based on passive vision. The illustration of this system is shown in Figure 3-14. 6-axis Fanuc robots, vision sensors, welding power, wire feeders and control computers are included in this system. In this study, they first performed a spectral analysis to determine which optical filter should be used for image capturing. Next, a robust image processing method for extracting an image from a source image affected by noise is proposed.

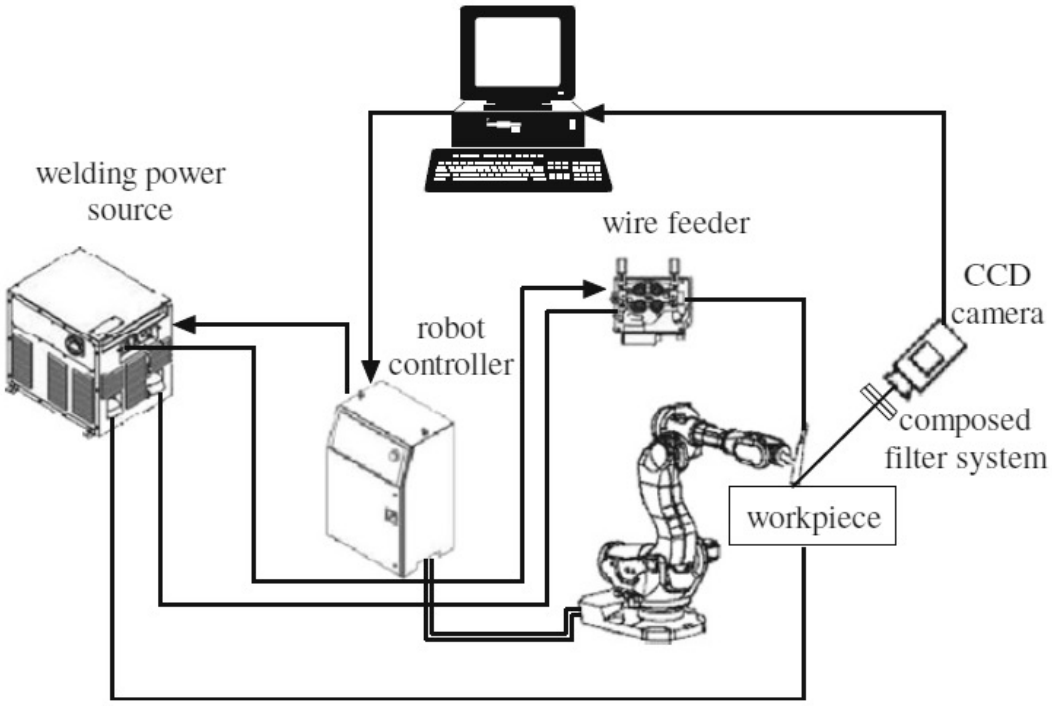

Figure 3-14 Schematic diagram of the system [80]

3.2.4 Other methods and data fusion technology

In addition to those mentioned above, there are many other types of sensors for welding monitoring. For instance, infra-image sensor [81] have been investigated to predict the size of the nugget, penetration depth, weld width and cooling rate during arc welding in resistance welding processes was studied. It also explains the sources of infrared detection interference [82-86]. Plasma electron temperature is a very useful parameter when plasma spectroscopy is applied to weld diagnostics, in this study [87, 88], A relation between the plasma electron temperature and the weld quality was built. Each sensor has its own as only certain aspects of the process can be monitored using a single sensor of a certain type. Therefore, welding conditions cannot be accurately predicted.

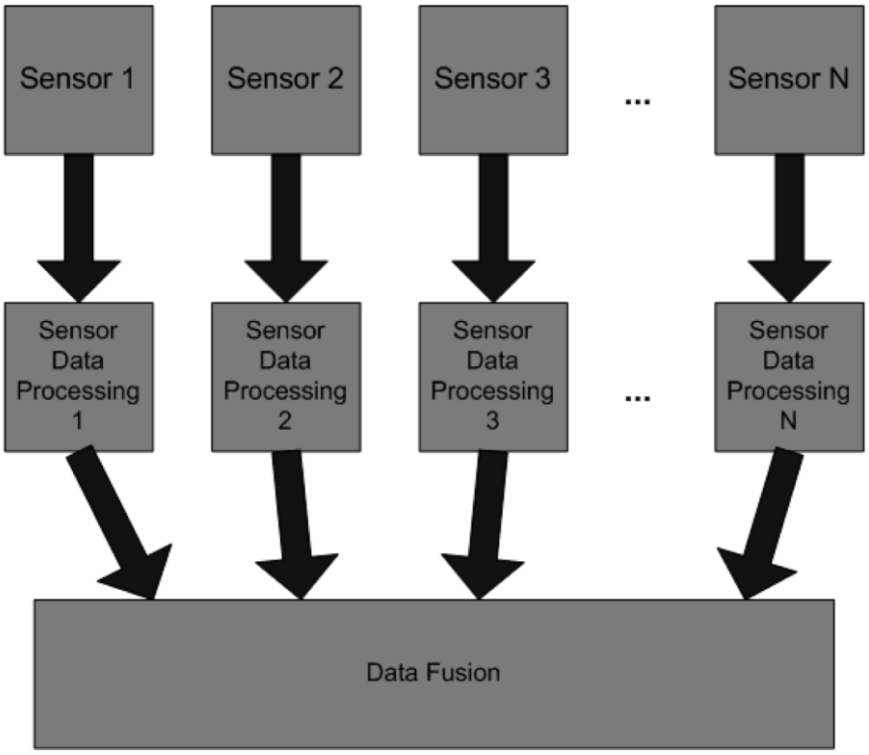

Figure 3-15 A multi-sensing data fusion system [89]

Multi-sensing data fusion is a technology that begun to be developed in the 1970s. Different sensors are employed to get information from different angles of the process. Take advantage of information technology integration and multi-sensing data integration to get more precise results than using just one sensor [90]. Kalman filtering [91], D-S evidence theory [92], neural networks [93] and fuzzy logic [94, 95] are four commonly used multi-sensing information fusion technologies. Multi-sensing data fusion can apply multi-source information to reduce uncertainty and improve weld defect identification accuracy.

The scientific community recognised the benefits of using multi-sensing technology for welding monitoring. For instance, Chen et al. [72] use vision sensors, acoustic sensors and arc sensors to simultaneously collect images, welding currents, welding voltages and arcing sounds during GTAW. This algorithm is then used to collect other parameters. The fuzzy measurement and fuzzy integration method are used to extract the fusion characteristics of the signal to

forecast the state of penetration of the weld. The experiment results show that the fuzzy measurement and fuzzy integration methods can effectively combine the information of different sensors to achieve more countable results than a single sensor.

Cullen et al. [96] use current sensors, electrode sensors, voltage sensors and ultrasonic sensors to collect current, voltage, electrode wearing electrode pressure signals during spot welding and uses neural networks to predict the size of the weld nugget. Pal, Sukhomay et al. [71], six parameters were collected and analysed: pulse width, pulse and post voltage, pulse frequency, welding speed, wire feed rate and RMS values of the current and voltage are used input variables for the prediction of tensile stress of the weldments. In addition, the output produced by multiple regression analysis is used to compare with the output of the neural network model. Artificial neural network models have been used to predict weld strength analysis over models based on multiple regression analysis.

3.3 Summary

The quality of welding becomes increasingly essential as expectations with respect to quality, reliability and cost-efficiency rise. Products and components must be of high quality and unexpected failures must be prevent. For this, engineers and scientists are increasingly interested in discovering efficient, fast and cost-effective means for assessing the quality of welds and detecting defects early.

The welding NDT is a well-developed area that has been applied to the inspection of welding quality for many years; some of them are the requirement for meeting specific standards. However, each NDT method has its own operational principles and hence advantages and disadvantages. For instance, ultrasonic inspection can detect defects only in specific orientations with respect to the interrogating beam. Eddy current technology is less sensitive

to the orientation of the defect but can only be used to detect conductive materials. NDT guarantees the quality of materials and joining processes during the manufacturing and installation stages and to ensure that the product maintains the integrity necessary to ensure its usefulness and public safety.

Due to the need to optimise the quality of the weld, the cost of conventional inspection increases and is more time-consuming. The effective solution to this current technical limitation is the application of real-time inspection enabling the evaluation of weld quality immediately after production or during welding. However, the development of real-time monitoring for welding is still in the early stages and not well implemented in the industry.

Chapter 4

A review on Acoustic emission technology and its application on welding monitoring

This chapter provides a detailed review of AE technology. It discusses the principles of AE and offers a comparison of AE technology with other NDT technologies. The nature of AE signals is discussed together with types of wave modes. Data analysing methods, together with a review of applications of AE for monitoring welding processes, are detailed. The AE instrumentation employed, analysing tools and challenges in applying AE in arc welding processes are discussed.

4.1 Overview of Acoustic Emission Technology

The AE wave is an elastic stress wave that moves within the structure once released from the source. The basic principle of the AE test is built on the use of piezoelectric sensors to detect elastic waves with a frequency of 20 kHz or higher, which occur during deformation in a solid material [97]. The principle of AE technology is shown in Figure 4-1. Piezoelectric sensors are used to detect deformation of a solid due to the propagation of an acoustic wave and convert it to an electrical signal. AE technology has been employed to a variety of components and structures in a variety of industries. Compared to other non-destructive techniques, AE technology has the advantage of observing the damage process of the material under test throughout the entire process.

Weld arc burning, metal deformation and phase deformation, potential movement, crack generating and propagating can release energy along with AE activity. Therefore, the quality of the weld can be checked by analysing the collected acoustic signals.

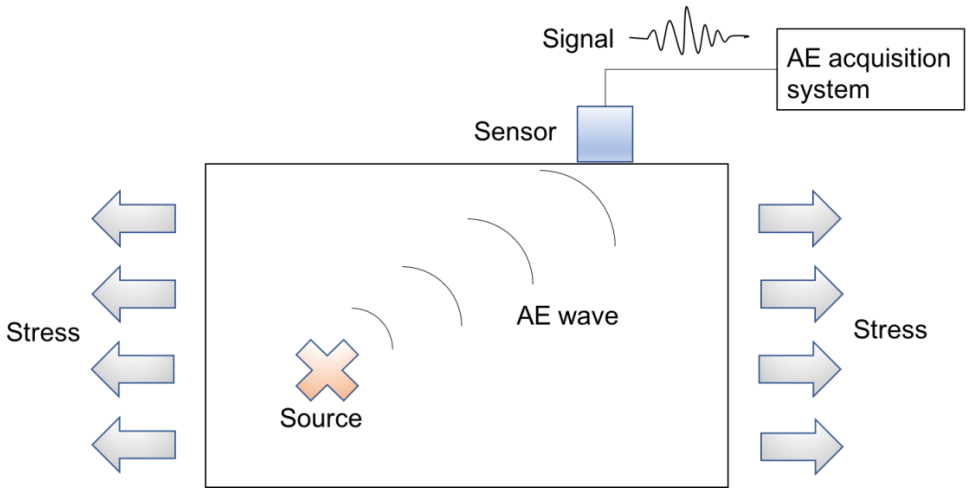

Figure 4-1 Schematic of acoustic emission detection.

AE monitoring is not available for operation under static load conditions. Since the AE phenomenon only occurs during dynamic processes. AE is also very sensitive to various types of noise. The elastic wave propagating process is very complicated because it affects the acquisition of the signal due to attenuation and reflective interference [98].

Unwanted external noise and the way to eliminate it is one of the essential concerns in any AE application. To locate defects during welding or cooling successfully, technology needs to be developed that can suppress signal interference from noise in the environmental. It typically does this by setting threshold levels at the noise level, or by band-pass filtering and post-analysis of the data. In any case, the average amplitude of the noise must be less than 10V to avoid signal saturation. If the noise has a frequency content similar to an AE source, it is necessary to estimate the nature of the noise before making the measurement. Post-processing can be used to separate the signal and noise. Also, for example, because of the nature of the signal source, the entire process cannot be fully reproduced. Sudden cracking occurs randomly from time to time. However, the same shape and the same type of material must lead to similar AE activity [98].

4.2 Comparison with other NDT techniques

Others traditional NDT technologies such as ultrasonic testing have to be applied combined with scanning techniques to detect a defect. They also usually require to stop the process. For AE, the sensor can be fixed on the surface of the component for the whole duration [98]. Another benefit of AE technology is the ability to monitor processes or components that are loaded in real-time. AE can improve operation and maintenance procedures, effectively prevent significant disasters, improve economic efficiency and reduce equipment maintenance costs. AE is suitable for operation in complex environments (hazard, heat, dust, radiation, etc.) and in complex geometric conditions. AE phenomena exist in almost all material types. As a result, AE technology has very few limitations on suitability for a variety of materials [98].
The advantages of AE technology over other monitoring technologies are:

The most crucial advantage of AE is the high sensitivity to crack propagation. Small defects can be detected even in hard-to-reach areas. The location of the technical data source can be determined. AE technology, real-time monitoring of the structure can be realised. Analyse the source of information in the world in real-time. AE can be used to monitor without disturbing the process, thus increasing its practical value. AE technology is a passive technology that does not require the input of external energy but uses energy generated by internal defects of the structure. Although primarily used for local structures, it can also be used with the number of sensors as a semi-global or global technique for monitoring larger regions or complete structures. AE is different from most other methods: First, the signal comes from the material itself and not from an external source. This compares AE with other non-destructive methods such as ultrasound, where the external signal source is introduced into the sample [99]. Second, AE detects motion, while most other methods detect existing geometric discontinuities [100]. The main differences between acoustic emission technology and other detection methods can

be summarised in Table 4-1

Table 4-1 Characteristics of acoustic emission technology compare to other detection methods [100]

Acoustic Emission	Other methods
Detects motions of defects	Detect the geometric form of defects
Detect active defects	Detect existing defects.
Each loading is unique	Inspection is directly repeatable
More sensitive to materials	Less sensitive to materials
Less sensitive to geometry	More sensitive to geometry
Less intrusive on structure/process	More intrusive on structure/process
Requires access only at sensors	Requires access to whole area of inspection
Main problems: noise issues	

4.3 AE signal and wave modes

AE signals that are collected from the piezoelectric sensors which arise from different sources. To discriminate different sources and filter out the useful signal from the unwanted noise has always been a challenge in AE applications. The list below summarises some of the possible AE sources arising from the welding process.

Table 4-2 Possible AE sources arising from the welding process.

Possible AE sources from the transformation in the material during the welding process.	Possible AE sources from the welding process and the environment.
Macro/micro cracks	Background noise in the lab
Phase transformations	Mechanical noise such as displacement of fixtures.
Fracture of inclusion particles	Sound from welding process such as arc burning and torch moving.
Metal deformation	

AE wave is an elastic stress wave that propagates to solids in a variety of modes. The four main types of AE waves can be identified by transverse waves, longitudinal waves and surface waves etc. Reflected and diffracted waves are also frequent. This wave is controlled by the same set of partial differential equations but must comply with other physical boundary conditions [101]. The understanding of the wave modes can help to distinguish the processes of different waves AE because the different wave modes can have different characteristics. An overview of the AE wave mode is given below:

Body waves: longitudinal and shear waves

Both are collectively called body waves. Longitudinal waves are also called compression waves or P waves. With the longitudinal wave, the particles oscillate in the direction of the propagation of the wave. The shear wave is also called S wave, and the oscillation occurs in a direction transverse to the direction of propagation. The mode change can occur between the P and S waves. An illustration of the P and S wave modes can be seen in Figure 4-2.

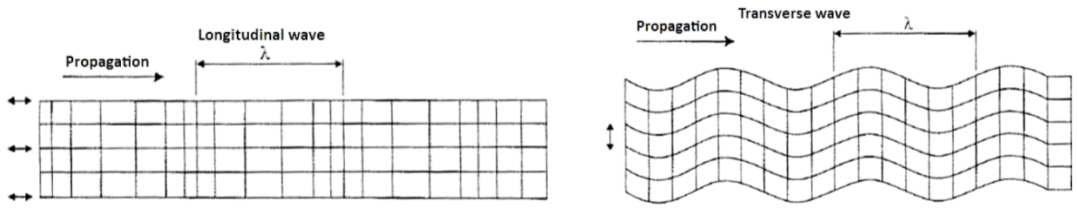

Figure 4-2 Body waves: longitudinal and shear waves [101]

Surface waves

Surface waves (Rayleigh waves) travels over the surface of semi-infinite solids. They are generated by the interaction of shear and longitudinal waves on the surface and travel slightly slower than shear waves. Propagation of surface waves is shown in Figure 4-3.

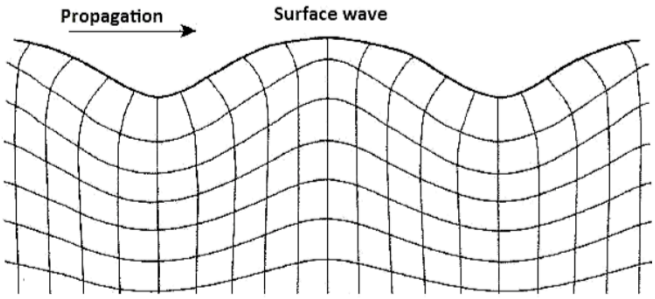

Figure 4-3 Shear waves [101]

Lamb waves

Lamb waves usually appear in the plate structure. They consist of two basic modes: symmetric mode (S0) or extensional mode, which is usually a higher velocity wave but has a lower amplitude (A0) [102] than asymmetrical mode or flexural mode, see Figure 2-7 [102]. The travel speed of the Lamb waves depends on the thickness and frequency of the plate.

The dispersion curve based shows the variation of the mode as a function of plate thickness and frequency [103]. The propagation of the basic model of the lambda wave is shown in Figure 4-4.

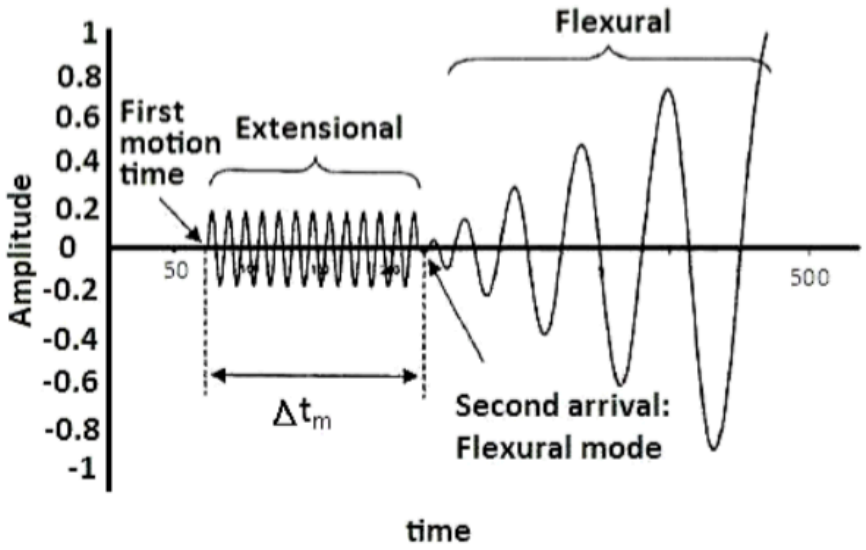

Figure 4-4 Early arriving symmetric (extensional) mode and later asymmetric (flexural) modes [102]

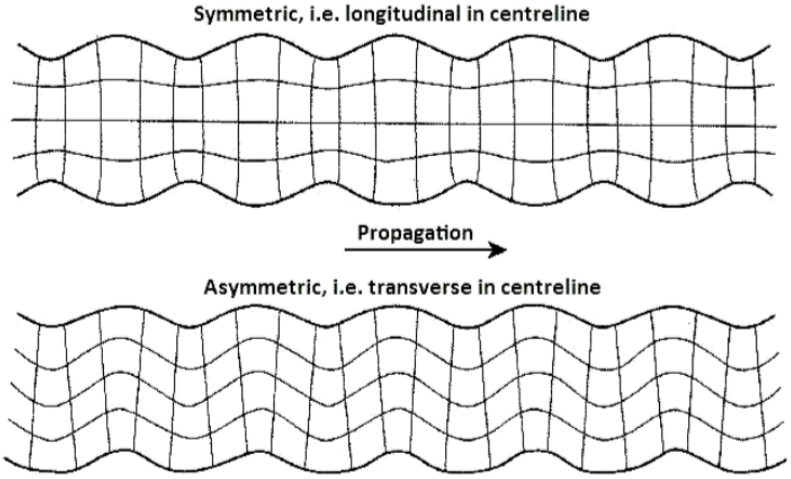

Figure 4-5 Symmetric and Asymmetric Lamb waves [103]

4.4 Data analysis methods

The methods of collecting and processing AE signals can be classified into two types: parameter-based analysis and waveform-based analysis. Parameter-based analysis uses the features extracted from the waveform to represent the AE signal. That includes energy analysis,

single parameter analysis and amplitude analysis. Waveform-based analysis is to analyse the waveform of the collected AE signal. Waveform analysis is a way of processing time and frequency domain of the signal, including evaluating the frequency characteristics of recorded waveforms.

4.4.1 Parameter-based analysis

In a parameter-based approach, signal parameters are used to evaluate the extent of the damage. Typical AE signals and standard parameters are shown in the Figure 4-6. The description of each parameter is listed in Table 4-3.

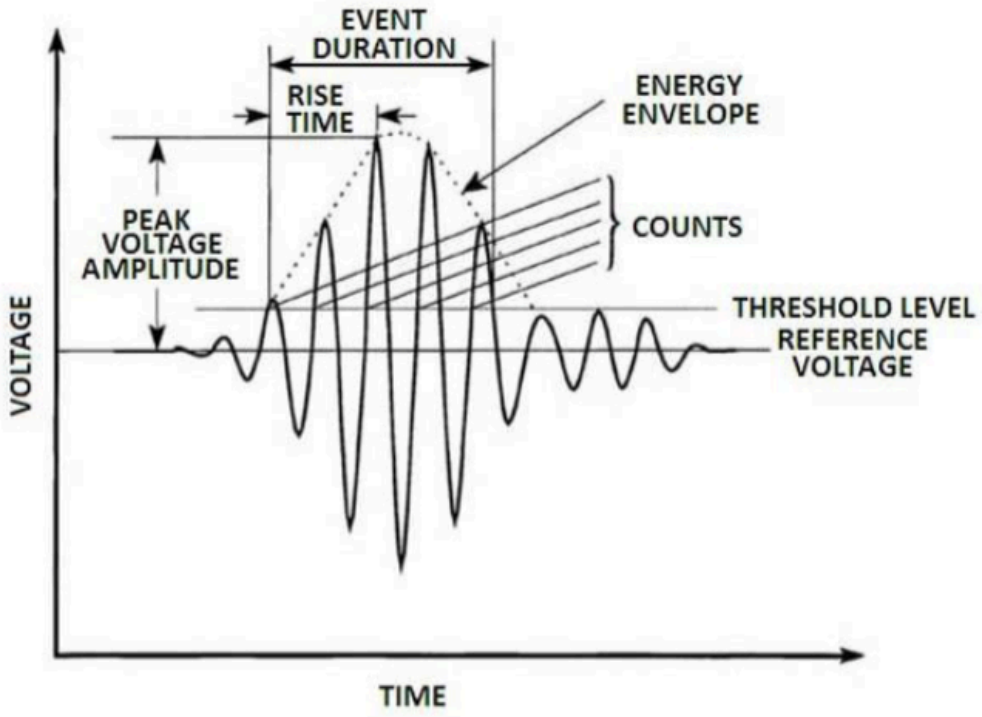

Figure 4-6 Parameters of AE signals [104]

Table 4-3 Parameters in AE signal.

Parameters	Descriptions
Threshold	Once the output signal reaches the set threshold, the recording is triggered. This value is set to eliminate as much noise as possible, but a threshold should be set too high to avoid missing weak signals.
Hit	A signal that exceeds the threshold and causes data accumulation on the system channel is called a hit, thus describing the AE event. The event rate is the number of events/hits per hour.
Amplitude	The peak voltage of the signal waveform is an interesting term because it is closely related to the size of the source event. [105] The amplitude of the signal is expressed in volts or decibels AE, where 1 μV on the sensor is set to 0 dB.
Rise time	The rise time is the interval between the moment the signal is triggered and the moment the signal reaches its maximum amplitude.
Duration	The duration is the interval between the moment the signal is triggered and the moment the signal is below the threshold.
Energy	Signal energy is another parameter that conveys information about the strength of the AE source. There are different ways of expressing energy, such as the area under the amplitude curve, RMS, and the like. The unit energy measured under the ground signal envelope is shown in Figure 4-6. The absolute energy is derived from the integral of the squared voltage signal divided by the reference resistance of the duration of the AE waveform package [106].

Counts	The count is the number of times the signal exceeds the threshold for the duration. In Figure 2-2, you can see success with five counts. The count rate is also used periodically, indicating the count per unit of time.

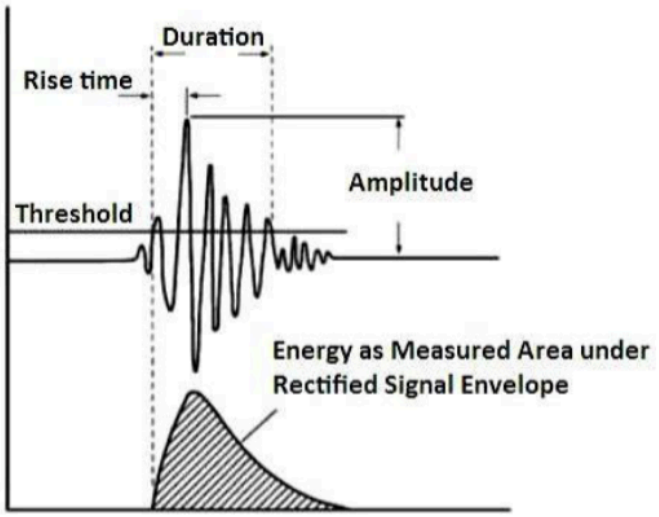

Figure 4-7 Energy as measure area under rectified signal envelope [107]

Hit and count can be employed to quantify AE activity. Since energy is sensitive to duration and amplitude and is less dependent on operating frequency and voltage threshold, it usually use energy to calculate the number of source events that exceed the threshold [2].

Other meaningful parameters include RA (ramp time divided by amplitude) and average frequency (calculated in time), which can be used to classify signals in tensile and shear cracks [2].

4.4.2 Waveform-based analysis

As described in the previous section, only some AE signal parameters were recorded in the parameter-based analysis, but the signal itself was not recorded. This largely reduces the amount of data stored and able to record data quickly. However, as better sensors and more computing resources are available, now it is possible to perform high-speed data acquisition and complete record waveforms [108]. A waveform-based approach [109] uses signal processing techniques and ancillary signal-to-noise ratio identification to provide improved data interpretation than parameter-based methods is described in this research.

The shape of the waveform is affected by the characteristics and geometry of the wave device but still includes information about the source characteristics. Waveform analysis is, therefore, information on the nature of the source is expected to be provided. Moreover, identify the source of the various side effects. Frequency analysing of recorded waveforms is the most commonly used method. Fourier transform or time-frequency analysis methods such as short Fourier transform and wavelet are used. Frequency analysis can be performed while data processing or in real-time with a calculation performance.

Two types of AE signals are usually distinguished, as shown in Figure 4-8: Burst signals and continuous signals. Burst signal occurs only for a short period of time, and continuous signal occurs usually over a longer period of time. Burst signals are usually generated by the growth of cracks, and the continuous signal is mainly noise signal [110].

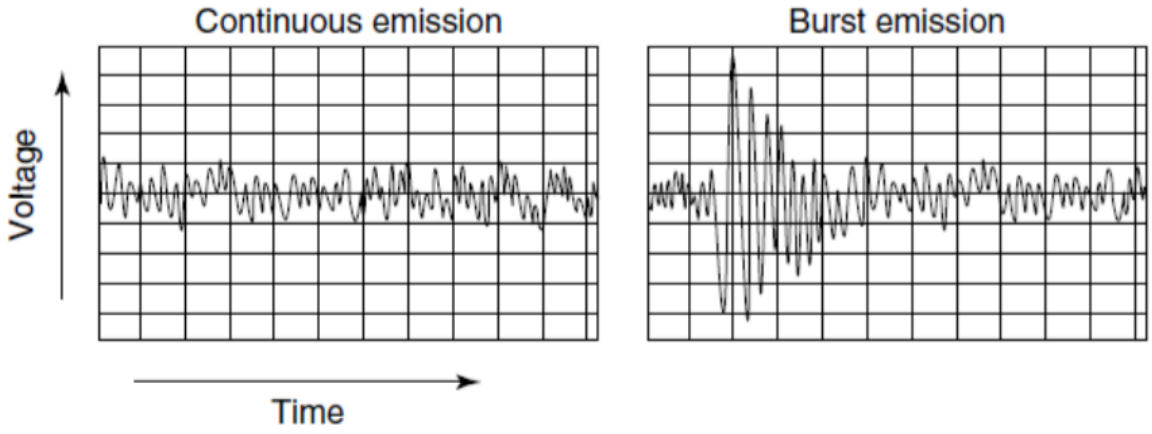

Figure 4-8 Continuous and burst AE signals [7]

The main drawback of the waveform based method is the generation of vast amounts of data. According to the Nyquist criterion, the frequency of the AE wave can range from a few kHz to a few MHz, and for all the frequencies to be recorded. [110] The sampling rate must be at least twice the maximum frequency of the signal. For instance, to effectively record signals at frequencies up to 500 kHz, the sampling frequency must be greater than 1 MHz. Due to the high sampling rate, even a short time signal contains a large amount of data. Despite this problem, waveform-based methods are still widely used. In addition, the AE waves propagate in different modes, it is necessary to employ waveform based analysis for the distinguish of different wave modes.

4.5 Application of acoustic emission in monitoring welding processes

For welding process, much effort has been made to study the capability for the AE technique to monitor welding quality. Given the noisy nature of the process, to achieve the ability to distinguish different AE sources and the controlling of the noise have always been a significant task. Researchers have been working on developing various analysis methods on collected AE signal from the welding and cooling process. The method that was popular in the early stage

of the study is parameter based analysis. In the parameter-based analysis, signal parameters are used to assess the extent of the damage. Parameters of AE signal include amplitude, hits, count number and energy etc. [2]. A study done by D. M. Romrell [111] used the emission rate which equivalent to the amplitude of the raw signal as a measurement, the weld samples that produced high emission rates was found to have several areas in which there were small micro cracks. Weld samples that produced low emission rates had few or no micro cracks. T. Hopwood [112] tried to use emission counts to assess delayed cracking. Some others used similar approaches: using pulse number to identify faulty fusion [5], counts with respect to amplitude to detect weld bead defects [113], they all base on the same principle that to build a relation between count/pulse numbers on a pre-set threshold and imperfection in welds. Some adopted a floating threshold as a refined parameter-based measurement [114], and combine floating threshold with energy (RMS value). The RMS value, which represents the sum of energy the pulse contained has also been used as a tool to measure the severity of the damage. It is often employed in combination with the count number to assess the extent of damage [115]. A finding by S.M.C van Bohemen, etc. [116] suggests that the squared RMS value is proportional to the volume rate of martensite formation during spot welding. The disadvantages of the conventional parameter-based analysis method are: first, by only recording some of the parameters, much information in the AE waveform has lost. Secondly, the relationships built between the parameters and the welding defection is easily influenced by other factors during the welding process, the results are hard to reproduce, given many variables in the test. In the actual application, given the complexity of controlling the noise, the discrimination of different AE sources is hard to approach by parameter-based analysis.

Wave pattern analysis has received more attention due to the wave pattern method providing the ability to interpret data better than the method of using parameters by allowing the use of signal processing techniques and signal separation. Frequency analysis can be used during data

post-processing or in real-time [105]. Kikuta et al. describe the monitoring of thermal cracking in inert tungsten gas (TIG) welding [117, 118]. In their study, cracks were stimulated by restraining stainless steel plates. The crack signal can be classified using the cumulative frequency and the frequency response that represents the crack in the frequency range of 290kHz to 320kHz. Apasov et al. [119] also studied AE for detecting hot cracking during the welding process. The ultrasonic waves emitted from the crack in the frequency range formed by the weld is 400 kHz to 700 kHz. The characteristics of the weld after cladding welds are proposed in the frequency range from 200 kHz to 300 kHz [120]. The frequency of the hot cracking signal was found to be 260 kHz - 270 kHz, and in the study by Sittisak Charunetratsamee et al., the weld solidification and phase transition will have a frequency between 100 kHz and 130 kHz [6].

4.6 Instrumentation

Signal detection, filtering, amplification and analysis are important components of AE technology, and AE monitoring systems normally consist of sensors, preamplifier and AE receiver and analysis system with simple measurement chain layout. AE values are shown in Figure 4-9.

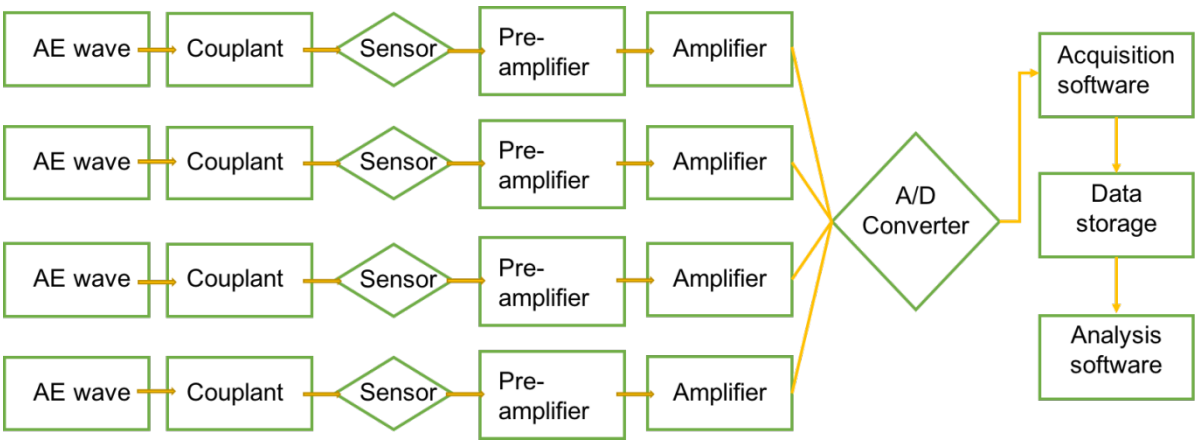

Figure 4-9 AE measurement chain

Sensors usually mounted on the surface of weldments to record acoustic emanation signals. Sensors are accessible in a full extent of sizes and shapes. Excellent coupling of the sensors to the test example is vital for compelling transmission of AE signals. Sensors are connected on the surfaces utilising attractive holders, pastes or indeed elastic groups and tapes. A layer of couplant such as vacuum oil or glue is connected between the two surfaces. Working recurrence run is critical amid sensor determination. The common recurrence extends for AE testing in respectful frameworks is 100-300 kHz [121].

Piezoelectric sensors are the most commonly used sensor type for inspection purposes. AE piezoelectric components change mechanical vibration to electrical signals. Traditional AE sensors consist of lead, zirconium, and titanium. Alternatively, crystal which is commonly utilised piezoelectric ferroelectric ceramic. The dimensional changes arising from the application of stress are in the range of 1 pm (10−12 m) and result into the generation of electrical signals of 1 μV due to changes in polarisation of the crystal [122]. The wear plate is mounted on the surface of the sensor with the piezoelectric component being placed behind it in order to protect it from accidental damage and wear. A simplified schematic of an AE sensor can be seen in Figure 4-10.

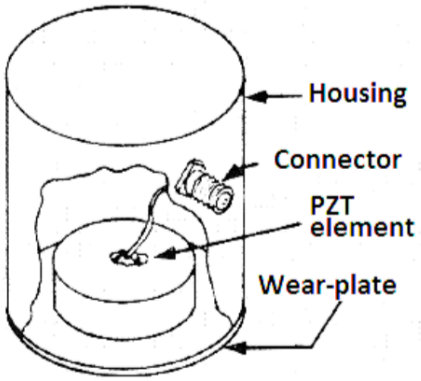

Figure 4-10 AE sensor of the piezoelectric element [122]

Sensor selection and optimal positioning are important to detect damage effectively. As AE waves propagate through the material, their amplitude decreases (this process is called attenuation). The attenuation can be calculated using an exponential relationship:

$$A_f = A_0 e^{-\alpha d} \quad (1)$$

Where A_f is the amplitude of the induced position, A_0 is the initial amplitude of the location of the source, d is the distance travelled by the waveform and α is the attenuation coefficient [102]. The causes include dispersant attenuation, diffusion, and is converted to other kinds of energy, such as heat. Due to attenuation, wave can only effectively be recoded at a certain distance, which limits the separation distance of the sensors. The number of sensors that can be used is limited by the number of channels available in the data acquisition system used, or due to economic reasons since sensors and associated data acquisition equipment can be expensive.

In terms of frequency response, piezoelectric sensors can be classified into two categories: resonant and broadband. Diagram describes the response behaviour of a resonant and broadband sensor in a specific frequency range, shown in Figure 4-10. The two curves in Figure 2-12 represents two different means to measure the sensor response (not shown here, see [105]. However, it can be seen that the effectiveness of resonance sensor is in a small frequency range, while the broadband sensor has a wide frequency range. With a better signal-to-noise ratio, the resonant sensor is preferred in practical applications. On the other hand, a low-sensitivity broadband sensor can record additional background noise [123]. However, since the resonant sensor tends to have a resonant frequency independent of the source, which may distort the original waveform [124], attention is required to select the appropriate frequency range of the resonant sensor.

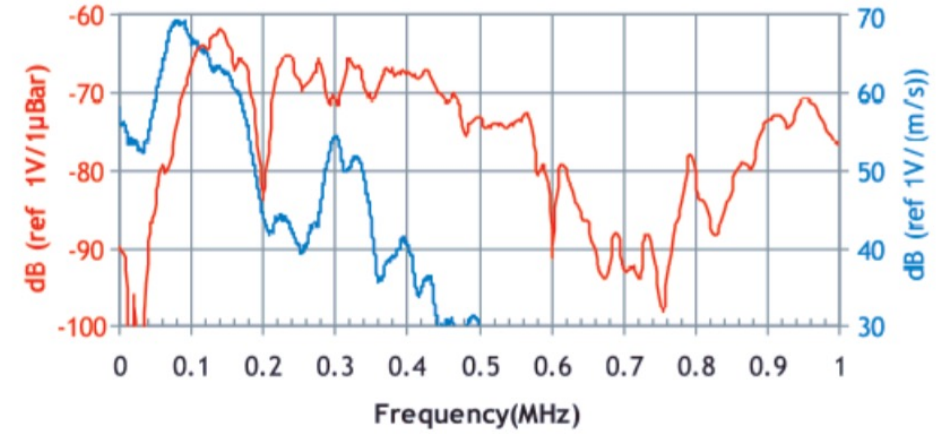

(a)

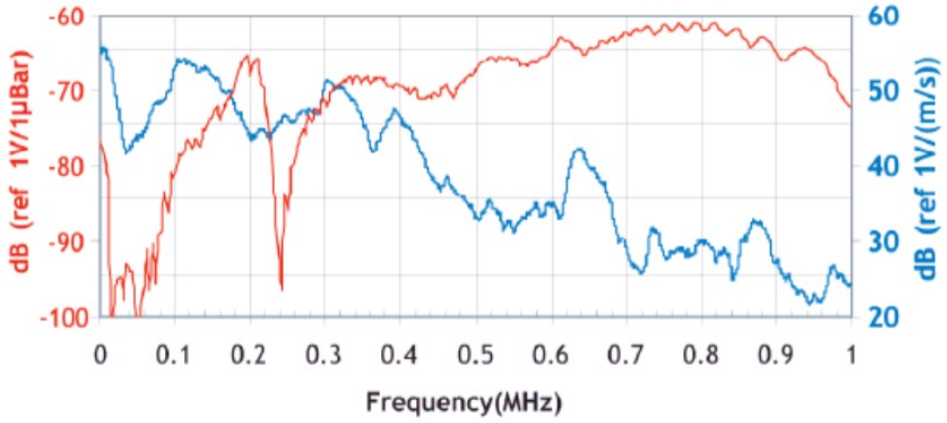

(b)

Figure 4-11 Responses of resonant sensor (a), broadband sensor (b) [125]

The recorded AE signal is typically too small. The preamplifier is used to amplify the signal captured by the sensor prior to any subsequent processing. A typical amplification gain is 40 to 60 dB. The amplification level can be predefined or used alone to define the range of the frequency filter. The amplified AE signal is then going to the acquisition system, which is connected to a PC. With data acquisition and analysis software, collected data can be processed to assess signal parameters, display images and waveform records, perform other signal conditioning tools and track waveform parameters.

4.7 Analysing tools

The recording of the waveform of the AE signal itself is not sufficient and the signal must be processed to evaluate and quantify the damage. The most common signal processing methods for AE signal analysis are time series analysis, such as Fast Fourier Transform (FFT) and Short Term Fourier Transform (STFT) and the Wavelet Transforms (WT). FFT is a standard tool for identifying the frequency content of a signal. However, the main drawback of the FFT technique is the loss of information regarding time at which the frequency component occurs. In order to obtain time and frequency data, STFT and WT come in place. STFT consists of multiplying a signal by a short window function then calculating the Fourier transform of the product, then move the window to the new location and repeat the calculation. This gives the time-frequency information of the whole signal. However, due to the fixed length of the window, the resolution will be corrected in the time domain and frequency. Wavelet analysis uses different window alignment techniques than the fixed window size. Require more accurate low-frequency data and shorter areas, Use long-term interval windows that require more accurate low-frequency information and shorter areas where high-frequency information is needed [126]. Thus, wavelet analysis divides the signal into different levels, each level corresponding to a specific frequency. In the signal, Appendix B provides a brief description of the mathematical details of the STFT and WT.

WT is used for AE signal analysing, fracture modes identification of composite AE signals and signal detection with a low signal-to-noise ratio [127]. Qi et al. [128] and Qi [129] uses wavelet AE analysis to recognise signals with different frequency ranges and different wave modes. Found that wavelet filtering can be used to improve the signal-to-noise ratio (SNR) [130, 131] The wavelet has been proven to be useful in some other condition monitoring methods - an outline of the various condition monitoring methods applications can be found in the article by M.M Reda Taha etc. [132].

4.8 Summary

The literature review found that AE is able to be used to monitor the structural state of the arc welding process. However, effectively analysing the huge amount of data produced during monitoring is still a challenge. Instrument and sensing technology is relatively developed, and data collection is largely simplified. However, novel ways to manage large amounts of data to collect useful information is the focus of research.

Chapter 5

Experimental Methodology

This chapter describes the methodology of this project. Section 5.1 discusses AE equipment and system. Section 5.2 details materials selected and characteristics of them. Section 5.3 and section 5.4 provides details of welding trails design and mechanical noise collection design. Finally, section 5.5 describes the analysing methods.

5.1 AE equipment

The AE system uses high frequency passive piezoelectric sensors which were mounted on the surface of the welding area to detect elastic waves, such as cracks, porosities or slags created by different types of defects during the welding process. Figure 5-1 shows the appearance of the piezoelectric sensor. The frequency response of the sensor is illustrated in Figure 5-2. After the AE signal is acquired using a passive piezoelectric sensor, the signal is amplified with a preamplifier and an amplifier.

A customised AE analysis system has been in developing from researchers at the University of Birmingham. The AE analysis system consists of the following parts: 2/4/6 pre-amplifier from PAC, amplifier from PAC, R30α resonant acoustic emission sensors from PAC, U2531A Agilent data acquisition card four-channel hub from Agilent and customised PC with data logging software.

The whole setup for the test is shown in Figure 5-3, the Operating Specifications of the R30α are in Table 5-1.

Figure 5-1 R30α resonant acoustic emission sensors manufactured by PAC.

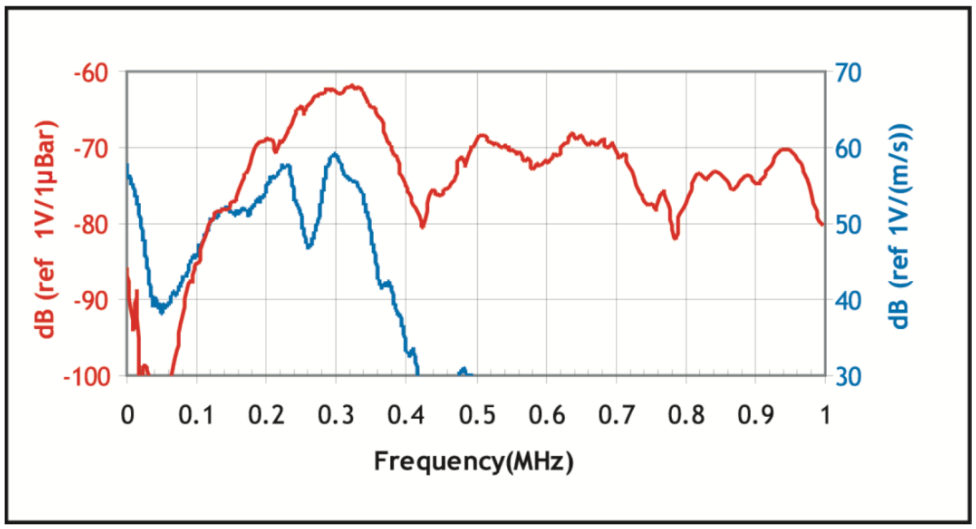

Frequency response of the R30a. Calibration based on ASTM E1106; Calibration based on ASTM E976.

Figure 5-2 Frequency response of the R30a.

Table 5-1 The Operating Specifications of the R30α.

Peak Sensitivity V/(m/s); [V/μbar]	58 [-62] dB
Operating Frequency Range	150 - 400 kHz
Resonant Freq. V/(m/s); [V/μbar]	300 [330] kHz
Temperature Range	-65 to 175°C
Shock Limit	500 g
Dimensions	0.75” dia. x .88” h (19 x 22.4 mm)
Weight	29 g

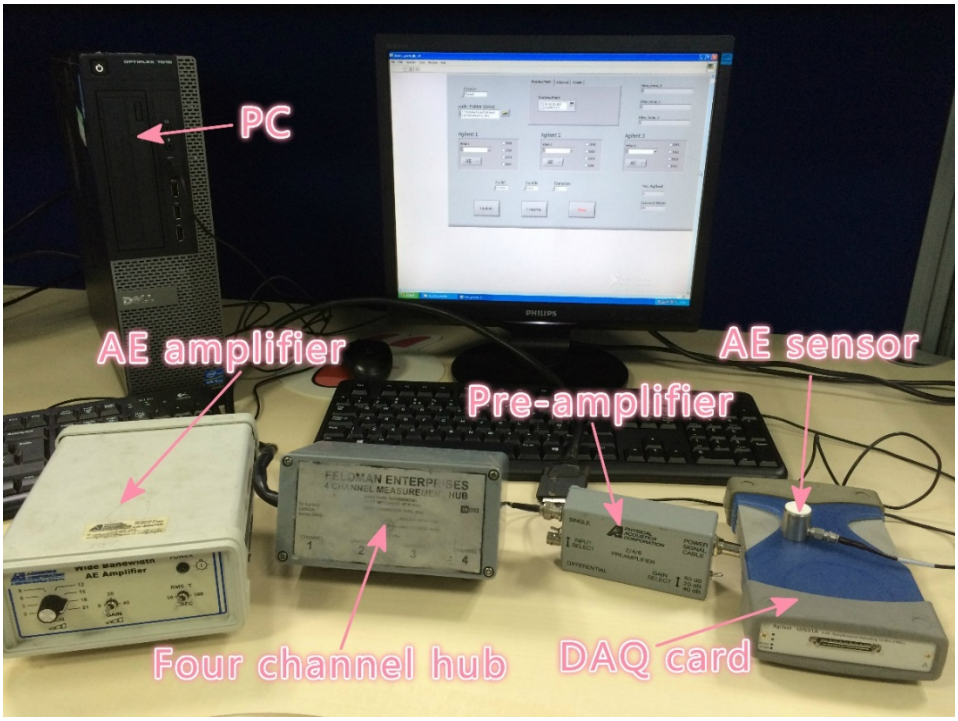

Figure 5-3 AE system setup.

5.2 Materials

The materials used in this project involve stainless steel, carbon steel and aluminium. The materials are CS70 carbon steel, EN8 carbon steel, 304 stainless steel and 6082 aluminium.

CS70 hardened & tempered tool steel is selected for the project for the stimulation of the cracks in the weld. The chemical composition is in Table 5-2. The equivalent carbon content of CS70 carbon steel is CE=0.84, using the equation below. The carbon equivalent is a measure of the tendency of welds to form martensite and undergo brittle fracture during cooling [133]. When the carbon equivalent is above 0.60, if no pre- or post- weld thermal treatment is applied, the welds will have a high tendency to crack. The test plates are in the dimension of $500\text{mm}\times50\text{mm}\times3\text{mm}$.

$$\mathrm{CE_{IIW}} = \mathrm{C} + \frac{\mathrm{Mn}}{6} + \frac{\mathrm{Cr+Mo+V}}{5} + \frac{\mathrm{Ni+Cu}}{15} \quad (2)$$

Table 5-2 The chemical composition of the CS70. (%)

Carbon	0.65-0.75	Phosphorous	0.045 max
Manganese	0.50-0.90	Sulphur	0.045 max
Silicon	0.05-0.35		

EN8 is a very popular grade of through-hardening medium carbon steel. Welding of EN 8 can be done with the advice of a specialist welding material expert, but welding with hardened, flamed or induction hardened materials is not recommended. It normally needs to be preheated by the furnace, heating mats or heating coils. The composition of the EN8 is in Table 5-3. This kind of steel is not suitable for welding, however, the fact that it is easy to crack can provide cracking signal easily and in a constant manner.

Table 5-3 The chemical composition of the EN8. (%)

Carbon	0.36-0.44	Phosphorous	0.050
Manganese	0.60-1.00	Sulphur	0.050
Silicon	0.10-0.40		

304 stainless steel is the most commonly used form of stainless steel in the world, mainly due to its great corrosion resistance and value. It contains 16 to 24% by weight of chromium and up to 35% by weight of nickel, as well as small amounts of manganese and carbon. These alloys can be easily welded using any arc welding methods. Because they do not harden upon cooling, they exhibit good toughness and do not require heat treatment before or after welding.

Table 5-4 The chemical composition of the 304. (% in wt)

Carbon	0.08	Nickel	35 Max
Silicon	1.0	Chromium	16-24
Manganese	2.0	Sulphur	0.03
Phosphorous	0.045		

Aluminium 6082 alloy exhibits medium strength and great corrosion resistance. It has the highest strength of 6000 series. 6082 alloy is a common engineering alloy. In the form of aluminium alloy sheets, 6082 is the most commonly used machining alloy. Table 5-5 summarises the composition of aluminium 6082 alloy. Aluminium 6082 alloy has good welding ability. But the strength of the weld is reduced.

Table 5-5 The chemical composition of the aluminium 6082 alloy. (% in wt)

Silicon	0.7-1.3	Zinc	0.0-0.2
Iron	0.0-0.5	Titanium	0.0-0.1
Copper	0.0-0.1	Chromium	0.0-0.25
Manganese	0.4-1.0		

5.3 Welding experiment design

There are three types of welding processes involved in this project, which are detailed below.

5.3.1 TIG welding trials

The illustration of the TIG welding experiment setup is in Figure 5-4. TIG welding is an arc welding process that employs non-consumable tungsten electrodes to create welds. The sensor is attached on one side of the weld to collect the signal generated from the welding process and cooling process. The real condition of the experiment is in Figure 5-5. Different materials are used for the purposes of the study of the noise levels of background signal from a different material and the signal collection of cracking signal. The parameters of the TIG welding are detailed in each result chapter.

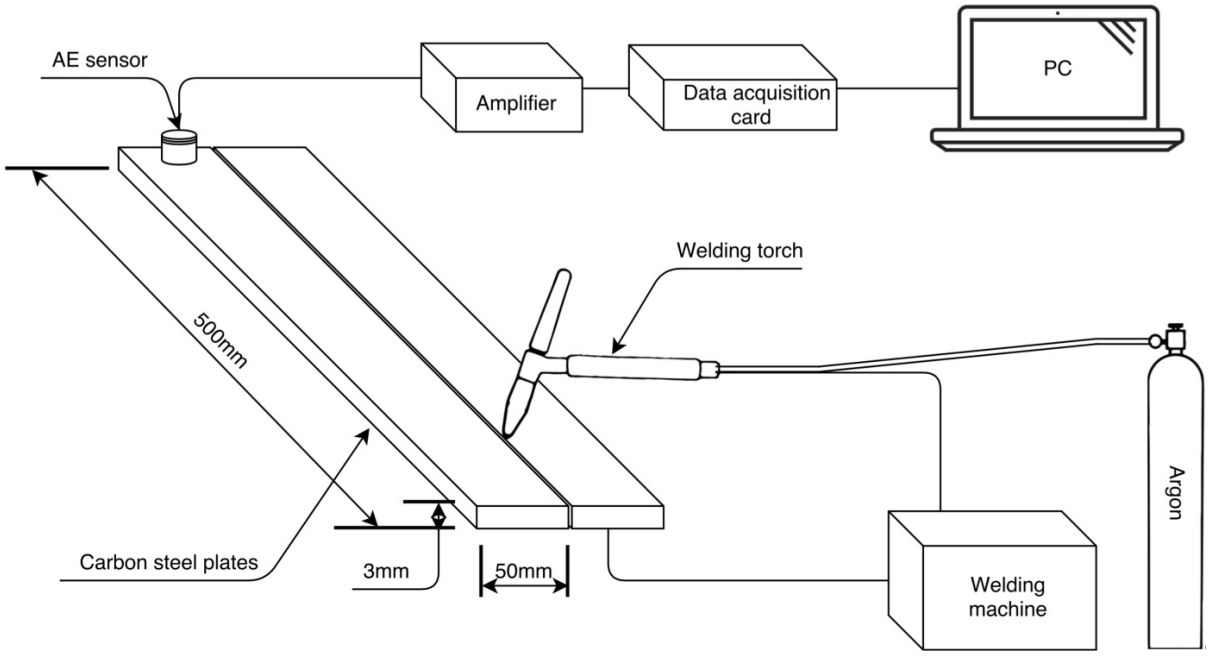

Figure 5-4 The illustration of the TIG welding experimental setup.

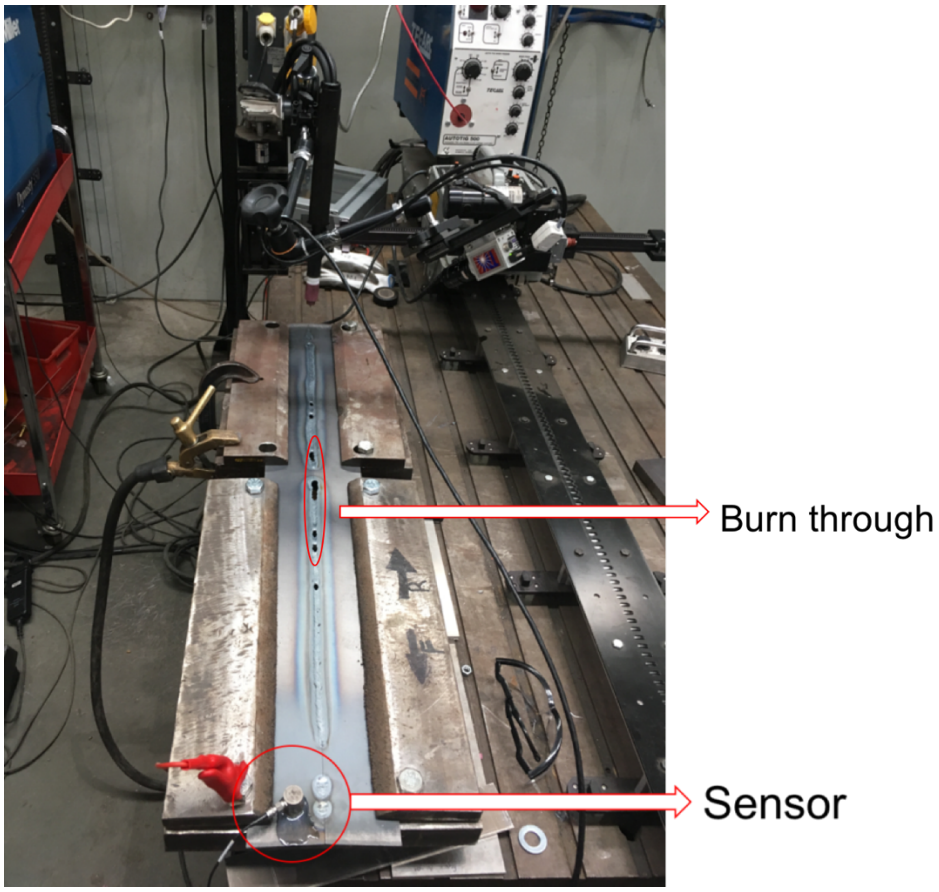

Figure 5-5 TIG experimental setup

5.3.2 CMT welding trials

The CMT welding equipment in TWI Ltd. is shown in Figure 5-4. This process is compared to conventional MIG, namely "cold" and quiet (reduced heat). In general, this welding system employs the same hardware as the traditional MAG/ MIG system. It is integrated with a dynamic wire feeder fixed directly on the torch. When the digital control panel detects a short circuit, it is fed back to the wire feeder, the wire feeder responds by pulling out the wire to separate the wire from the droplet. After separating the wires and droplets, the wires will move forward again and repeat the cycle. The period of heat used in the process is very short, thus reducing heat. The short circuit frequency can be up to 130 times per second.

Figure 5-6 CMT welding setup and AE system.

Figure 5-7 AE sensor attached on one side of the weld.

5.3.3 MAG welding process

Metal active gas (MAG) welding is an arc welding process that takes place between a consumable wire electrode and a workpiece, causing the metal workpiece to heat up and melt together. When combined with the wire, the gas is passed through the torch to protect the process from contaminants in the air. Compared to TIG welding and CMT welding, MAG welding is a much noisier process. During the experiment, the sensor also attached on one side of the welding to collect the signal from the welding and cooling process. The parameters of each test are detailed in the results chapters.

5.4 Collection of various signal from the environment

The environmental noise has been collected including background noise in the laboratory area, noise arising from the gas flow, torch movement, arc ignition and mechanical noise which arises from the direct contact with objects and the welding plate. The collection of the AE signals from the environment is achieved by mounting the AE sensor on the side of the parent material and clamped on the welding Table. This represents the same condition as during the TIG welding process. The background noise in the laboratory was recorded using 60 dB gain with the pre-amplifier. The AE signal from the torch moving was collected as the torch moved with a speed of 98cm/min. The AE signal arising from gas flow was recorded using a release rate of Argon gas of 15L/min rate for 5/10s long intervals. The AE signals from arcing sound were collected during the TIG welding process. The AE signal was cropped from the beginning of the signal from welding as that was the arc ignition period.

The direct-contact mechanical noise was simulated based on a) object dropping and a light hammer knock on the plate which were used to imitate the accidental dropping of an object during the welding process, b) an object sliding on the plate, which imitated the displacement between the plates and fixtures arising from the dilation and contraction of the plates during heating and cooling. The dropping and knocking experiment was carried out using a nut drop at a preselected height and distance from the sensor on the plate and by a small hammer used to knock the surface of the plate. The sliding signal collection was carried out by a metal plate sliding against the other at a certain distance from the sensor. The experimental configuration parameters are summarised in Table 1 below.

Table 5-6 Experiment configuration of the collection of signal from the environment.

Signal type	Data collection condition
Background signal	AE sensor attached to the side of the parent material while it is clamped by a fixture. AE sensor for all of the tests below is under the same condition
Torch moving	Torch moves at 98 cm/min
Arc ignition	The beginning of each welding signal
Gas purging	Gas flow at 15L/min
Nut dropping	DIN 934 HEXM5 stainless steel nut drops from 20 cm height and 20 cm far from the sensor
Hammer knocking	A small hammer lightly taps on the plate 20 cm from the sensor
Plate sliding	A plate sliding on the plate at 20 cm from the sensor

5.5 Processing tools

The introductions of processing tools that were used in this project are listed in this section, the MATLAB algorism for the processing tool is in Appendix B.

5.5.1 Root mean square

The root mean square (RMS) method is used to calculate the square root of the arithmetic mean of the squares of a set of values. It applied here as the simplified indicator for the mean energy for the signal. It has the flexibility to find useful information in large data sets. The equation of RMS is provided below:

$$\mathrm{RMS} = \sqrt{\frac{1}{\mathrm{N}}\sum_{\mathrm{n}=1}^{\mathrm{N}} \mathrm{x}_{\mathrm{n}}^{2}} \qquad (3)$$

5.5.2 Fast Fourier Transform

Fast Fourier Transform (FFT) is used to convert the AE signal from the time domain to the frequency domain and then investigate the power spectral density (PSD) of the signal used for defect detection by specifying the presence of the resonance of the AE sensor. It is mathematical representation is given below:

$$\mathrm{X}(\mathrm{j}\omega) = \int_{-\infty}^{+\infty} \mathrm{x}(\mathrm{t})\mathrm{e}^{-\mathrm{j}\omega\mathrm{t}}\mathrm{dt} \qquad (4)$$

The equation (4) is the mathematical representation of FFT, which shows that is possible to represent a function in time (original signal) as a function in frequency (decomposed signal).

5.5.3 Discrete Wavelet De-noising

The wavelet transform (WT) is a powerful tool of signal processing for its multiresolutional possibilities. Unlike the Fourier transform, the WT is suitable for application to non-stationary signals with transitory phenomena, whose frequency response varies in time [134].

The wavelet coefficients represent a measure of similarity in the frequency content between a signal and a chosen wavelet function. These coefficients are computed as a convolution of the signal and the scaled wavelet function, which can be interpreted as a dilated band-pass filter because of its band-pass like spectrum.

Discrete Wavelet De-noising (DWT) is an implementation of WT using mutually orthogonal set of wavelets defined by carefully chosen scaling and translation parameters. This leads to a very simple and efficient iterative scheme for doing the transformation [135]. The scaling

function should meet several requirements such as orthogonality, the normalised area between the functions et. The translation equation is given as:

$$\mathrm{DWT}\left[\mathrm{n}, a^{j}\right] = \sum_{m=0}^{N-1} x[m]\, \psi_j * [m-n]\,,\ \psi_j[n] = \frac{1}{\sqrt{a^j}}\psi\left(\frac{n}{a^j}\right) \tag{5}$$

where n is delay parameter, N is the length of signal, ψ is the discretised mother wavelet. Since in DWT, computation performed on discrete set of wavelets, it provides a significant yield in terms of computational time. Therefore, DWT is useful when compression of the signal is needed.

5.5.4 Cross-correlation analysis

Cross-correlation calculates the similarity of two sequences as a function of the time-lag shift. In signal processing, it reflects various frequency components that are held simultaneously between the two signals. The coherence (sometimes called magnitude-squared coherence) between two signals x(t) and y(t) is a real-valued function that is defined as:

$$C_{xy}(f) = \frac{|G_{xy}(f)|^2}{G_{xx}(f)G_{yy}(f)} \tag{6}$$

where $G_{xy}(f)$ is the Cross-spectral density between x and y, and $G_{xx}(f)$ and $G_{yy}(f)$ the spectral density of x and y respectively. The magnitude of the spectral density is denoted as |G|. Given the restrictions noted above (ergodicity, linearity) the coherence function estimates the extent to which y(t) may be predicted from x(t) by an optimum linear least squares function.

There are two main elements in the proposed correlation analysis: the features that are needed for the template and related processing. Templates are important for getting accurate and reliable results in the correlation analysis. It usually consists of a set of signals generated from specific defects.

Therefore, the energy spectrum density (PSD) can, therefore, be used as a correlation processing feature. By calculating the similarities between the PSD of the template and the resulting emission data can determine whether the signal is caused by a defective connection. Spectrum coherence analysis is performed to calculate the similarities between the template and each window. Signs that have the same functionality as the template should have higher similar results. The workflow diagram of the algorithm is shown in Figure 5-8.

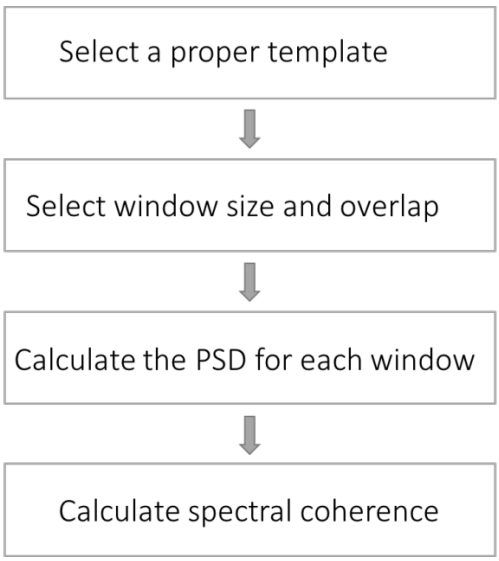

Figure 5-8 Cross-correlation analysis

5.5.5 Pattern Recognition analysis

This is a customised analysing method to accommodate the frequency features of the cracking signal, frequency distribution of cracking signal and mechanical signal. Similar to the cross-correlation, this analysis method also gives similarity to the cracking related signal. The difference is this method could give a result which can distinguish mechanical signal and cracking signal. The design of these methods will be detailed in the result in chapter 8.

Chapter 6

Investigation of continuous background AE signal from different welding processes

This chapter describes the background, experimental setup, results and subsequent analysis performed during the welding process to eliminate material-independent signals. Section 6.1 discusses the research plan and proposed methods. Section 6.2 details the experimental setup, equipment, and settings. Section 6.3 provides analysis and discussion of the results. Finally, Section 6.4 summarises the main findings of this study.

6.1 Approach

Unwanted noise elimination is a vital part of the present research study. The noise during the welding process that could be detected up by the AE sensor arises from many different sources of different characteristics. It is important to understand major noise signal sources before getting into the study of the signal from the actual welding and the material defects. To better study the features of the noise signal, in this project, the noise has been categorised into two types. The first type of noise signal is the noise from the welding machine itself, which is likely to be the continuous type of signal and the burst type of signal. The second type of noise signal is the burst type. In this chapter, the continuous signal from the welding machine will be discussed. The signal that the AE sensor captured from different welding process will be analysed. The discontinuous type of signal will be discussed in chapter 7.

The possible continuous background signal sources could come from electromagnetic noise, welding machine, and other cyclic signals from the machines in the lab environment. Some might not be easy to identify. The nature of the continuous background signal would also quickly change from process to process, including noise level and frequency characteristic. The noise level affects the detection of cracking activity, so the levels of the noise and the frequencies characteristics from different processes need to be studied, the way to assess the noise levels is by observing the raw signal and by comparing the RMS values of them. The

feasibility of the de-noising of the signal will also be discussed. The method that adopted for de-noising of the signal is 1-D wavelet transformation.

Different welding process including Cold Metal Transfer (CMT) welding, Tungsten Inert Gas (TIG) welding and Metal Active Gas (MAG) welding with varying materials including stainless steel, carbon steel and Aluminium are performed for the collection of various types of background signal.

6.2 Experiment

Three types of arc welding processes and different parameters settings were performed. The first part is the collection of signals from the CMT welding process. The second part is the collection of signals from the TIG welding process. The third part is the collection of the signals from the MAG welding process.

6.2.1 CMT welding trials

The CMT trials carried out at NSIRC/ TWI laboratories, the basics of this process are explained in chapter 5 the methodology chapter. The experimental configuration of the trials is shown in Table 6-1. The material used in CMT welding trials is 304 stainless steel. Attach the AE sensor to the weldment surface using Araldite Rapid glue. Each weld length is 125 mm for 15 seconds. The AE system begins recording a few seconds before the start of welding. Figure 5-2 shows the cold metal transfer (CMT) process of the AE sensor mounted on the weld side during additive manufacturing. The sampling frequency is 500k Hz. The CMT welding parameters are listed in Table 6-1.

Table 6-1 CMT parameters

Current	120 A
Voltage	11.5 V
Wire feed speed (WFS)	5 m/min
Shielding gas	80% Ar – 20% CO_2
Gas flow	25 L/min
Short circuit frequency	70 Hz – 130 Hz

6.2.2 TIG welding trials

The TIG welding trials were performed in NSIRC/TWI laboratories. The materials that used in TIG welding trials are CS70, S304, EN8 and Al6082. The experimental setup is shown in Figure 5. The experimental configurations are listed in Table 6-2. The signals were collected in 1Mk Hz.

Table 6-2 Experiment parameters

ID	Material	Thickness (mm)	Current (A)	Voltage (V)	Speed (cm/min)	Heat input (kJ/min)
784	CS70	3	70	12	9.8	0.308
941	CS70	3	110	12	9.8	0.485
1021	CS70	3	130	12	9.8	0.573
1423	304	0.9	70	15	30	0.126
1424	304	0.9	70	15	30	0.126
1425	304	0.9	70	15	30	0.126

1487	Al6082	4	150(7/3)	20	15	0.504
1489	Al6082	4	150(7/3)	20	20	0.378
1492	Al6082	4	175(7/3)	20	30	0.294
1593	EN8	3	50	12	9.8	0.22
1616	EN8	3	90	12	15	0.259
1604	EN8	3	90	10	9.8	0.331

6.2.3 MAG welding trials

The trials were produced in TWI Middleborough. The principle of MAG welding is explained in chapter 5. The materials used in the trials include CS70 carbon steel, EN8 steel. The experiment configurations are listed in Table 6-3. The signal was collected with 1M Hz.

Table 6-3 Experiment configurations of MAG trials

ID	Material	Thickness (mm)	Current (A)	Voltage (V)	WFS (m/min)	TS (cm/min)	Heat Input (kJ/min)
1782	CS70	3	166	19	6.37	41	0.369
1783	CS70	3	168	19	6.37	41	0.374
1785	CS70	3	160	21	6.37	41	0.394
1804	EN8	3	154	15.5	5.91	59	0.194
1806	EN8	3	152	16.5	6.22	59	0.204
1807	EN8	3	153	16.5	5.5	59	0.205

6.3 Analysis and discussion

6.3.1 CMT process

6.3.1.1 Raw signal and noise level discussion of CMT process

In this section, the raw signals from CMT welding and 304 stainless steel are plotted. And the noise level of them were discussed.

The raw signal from the CMT process is plotted in Figure 6-1. From Figure 6-1, the continuous background signal is less than 0.2 V, which is low. Apart from the continuous emission, there is some burst emission in the signal with the voltage less than 1 V. CMT process is quiet, the AE emission from CMT process is as low as 0.1- 0.2 V.

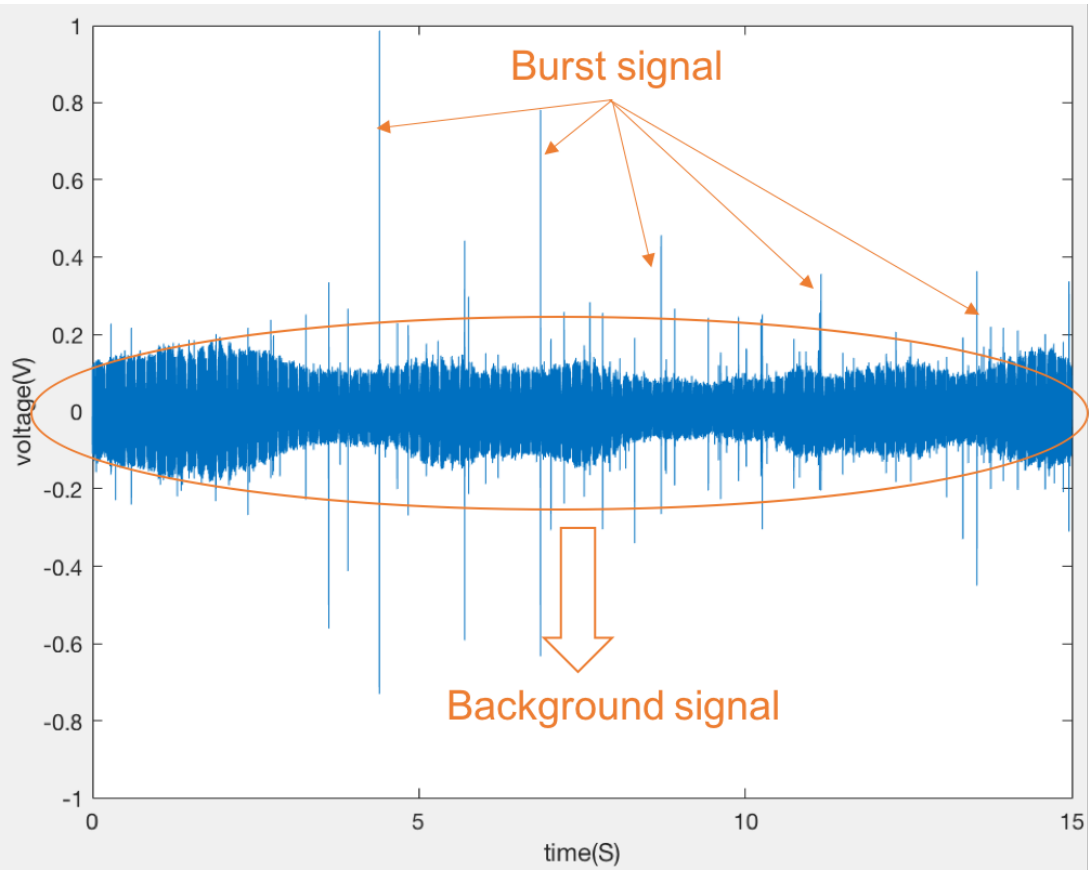

Figure 6-1 Raw signal from CMT process

6.3.1.2 De-noising of the raw signal from CMT process

In this section, the raw signals from the raw signals from CMT welding and 304 stainless steel are processed with wavelet de-noising. The principle of wavelet de-noising is explained in chapter 5.

The De-noised signal for CMT is shown in Figure 6-2B. The background signal is mostly filtered out using undecimated wavelet transform. However, the burst signal in the raw signal is mostly preserved in the filtered signal.

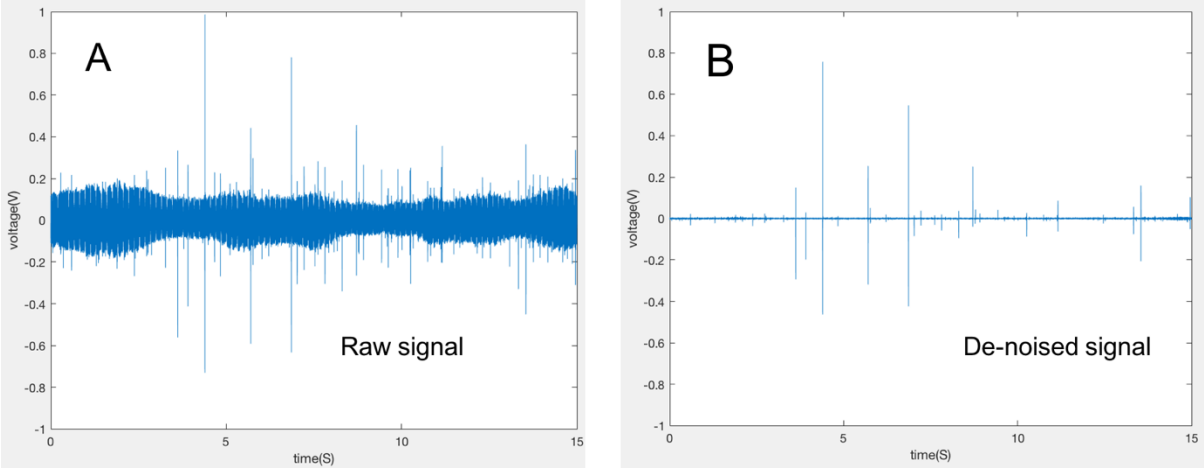

Figure 6-2 Raw signal from CMT process and de-noised signal

6.3.1.3 Frequency analysis of signal from CMT process

In this section, the raw signals from CMT process are processed using Fast Fourier Transform (FFT) and the Power Spectral Density (PSD) values are obtained for detailed frequency analysis.

Figure 6-3A is the raw signal of the trial of 304 stainless steel with the CMT process. Figure 6-3B is the FFT result of the raw signal. A few noticeable frequencies are marked in Figure 6-3B. The exact origins of the marked frequencies are hard to identify. They may be from the CMT machine. The FFT result for the filtered signal is plotted in Figure 6-3D: most of the

marked frequencies in B are filtered out. This means that the noted frequencies in Figure 6-3B are filtered out, proving that the background signal in the raw signal with a CMT trial is mostly cyclic and easy to filter out.

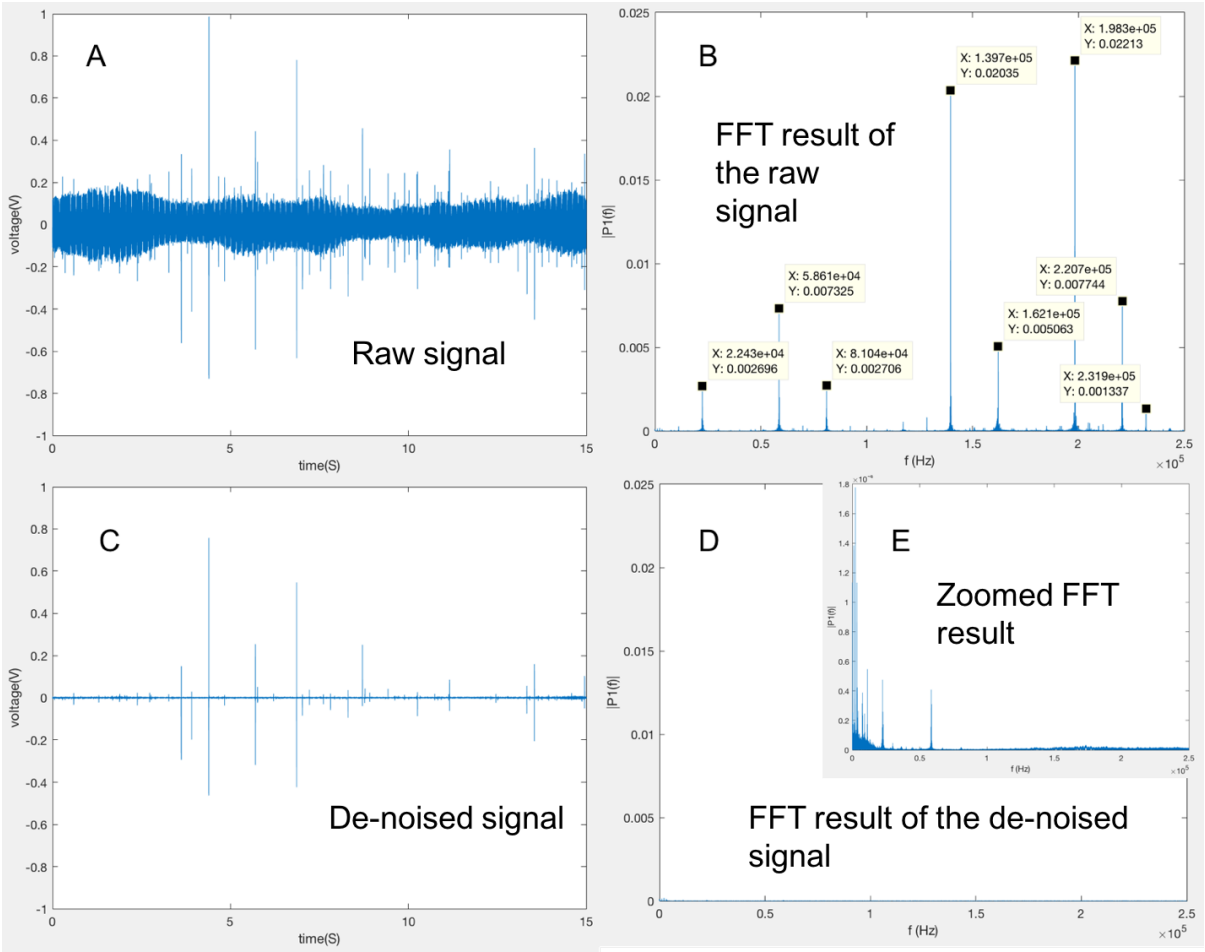

Figure 6-3 Comparison of raw and de-noised signal and FFT results of CMT trial

A. Raw signal from CMT trial. B. FFT result of the raw signal. C. A de-noised signal from CMT trial. D. FFT result of the de-noised signal. E. Zoomed FFT result of the de-noised signal.

6.3.2 TIG process

6.3.2.1 Raw signal and noise level discussion of TIG process

In this section, the raw signals from TIG process are plotted. The noise levels of them were discussed. The RMS values for each trial are calculated for the comparison of the noise levels. The principle of RMS is explained in chapter 5.

The RMS values for the signals collected from the TIG trials are calculated and listed in Table 6-4. RMS values provide the flexibility to find useful information in large data sets. It's a simple index of acoustic energy during welding trials. It could be used to build a relationship with the background signal level.

Table 6-4 The RMS values for the signal collected from the welding trials

ID	Material/ Process	Heat input (kJ/ min)	RMS raw (V)	RMS WD (V)
784	CS70/ TIG	0.308	0.1049	0.0048
941	CS70/ TIG	0.485	0.1471	0.0155
1021	CS70/ TIG	0.573	0.2414	0.1437
1423	304/ TIG	0.126	0.0085	0.0063
1424	304/ TIG	0.126	0.0112	0.0084
1425	304/ TIG	0.126	0.0069	0.0034
1487	Al6082/ TIG	0.504	0.0675	0.0301
1489	Al6082/ TIG	0.378	0.1613	0.1195
1492	Al6082/ TIG	0.294	0.4723	0.3898

The raw signals from the TIG process with different materials and parameters are plotted below. The levels of background signals vary between different materials and settings. Raw signals from TIG process trials with 304 is plotted in Figure 6-4, the weld ID is 1423, 1424 and 1425.

The background signal is overly low from the observation from the raw signal. From the RMS value in Table 6-4, RMS values for these three trials are very low. TIG welding process is a low noise process. The stainless steel has a low spatter level.

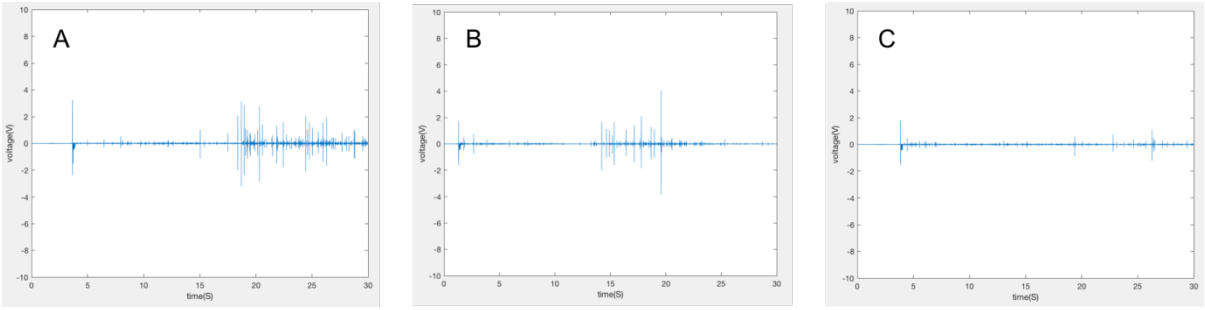

Figure 6-4 Raw data from TIG welding process with 304 stainless steel

A: Weld ID: 1423. B: Weld ID: 1424. C: Weld ID: 1425.

The raw signals from material EN8 are plotted in Figure 6-5; the background signal is also low but higher than 304 steel. From Table 6-4, trial 1593 has the lowest heat input: 0.3673, trial 1616 has the medium heat input: 0.432 and trial 1604 has the highest heat input: 0.551. From the observation of the plotted raw signals in Figure 6-5, the level of background signal has a positive correlation with the heat input. The RMS values for these three signal are 0.0593 V/ 0.1526 V/ 0.2227 V. RMS value is the indication of the mean energy for the raw signal, form the result, the heat input and the RMS of the signal have a positive correlation.

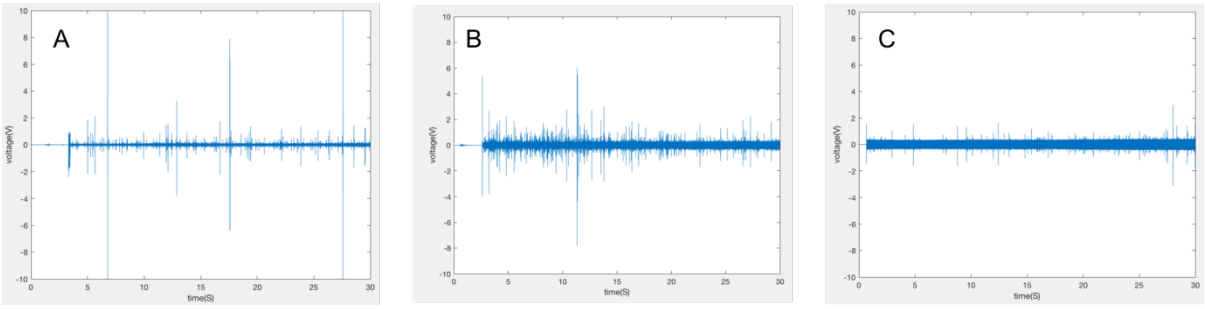

Figure 6-5 Raw data from TIG welding process with EN8 steel

A: Weld ID: 1593. B: Weld ID: 1616. C: Weld ID: 1604.

The raw signals from material CS70 are plotted in Figure 6-6; the background signal is also low. From Table 6-4, trial 784 has the lowest heat input. Trial 1021 has the highest heat input. From the raw signals, the level of background noise has a positive correlation with the heat input. The RMS value also has a positive correlation with the heat input. For CS70 and EN8, since they are both carbon steel material, and the thickness of the material is the same, so the raw signal and background signal level are similar.

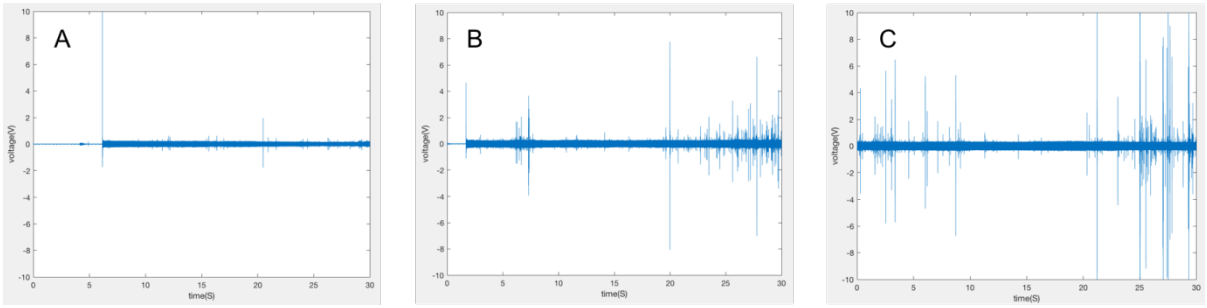

Figure 6-6 Raw data from TIG welding process with CS70 steel

A: Weld ID: 784. B: Weld ID: 941. C: Weld ID: 1021.

The raw signals from aluminium material Al6082 are plotted in Figure 6-7. The levels of background signal vary from different parameters, overall is higher than with steel material. Trial 1487 has the lowest heat input; trial 1489 has the medium heat input; trial 1492 has the highest heat input. From the raw signal, the level of background noise also has a positive correlation with the heat input. The raw signal for Al 6082 is overall 'noisier' than the signal from steels. Since there are more spatters with aluminium material, and in this trial, thicker material was used. With Aluminium, the AE signals that collected are less stable than steel material, with the background level as in trial 1492, some burst emission could be buried under the background signal.

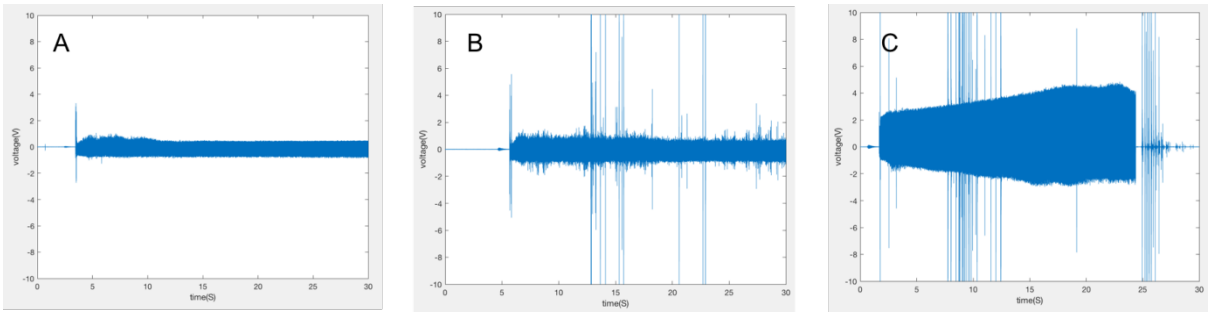

Figure 6-7 Raw data from TIG welding process with Al6082 aluminium

A: Weld ID: 1487. B: Weld ID: 1489. C: Weld ID: 1492.

6.3.2.2 De-noising of raw signal from TIG process

In this section, the raw signals from different processes and materials are processed with wavelet de-noising. The principle of wavelet de-noising is explained in chapter 5.

Figure 6-8 is the comparison between the raw signal and the filtered signals from the TIG process with 304 stainless steel. The background signal from the TIG process with 304 is very low, so the result is not very obvious. From the RMS values, the mean energy is reduced. The discontinuous spikes were preserved.

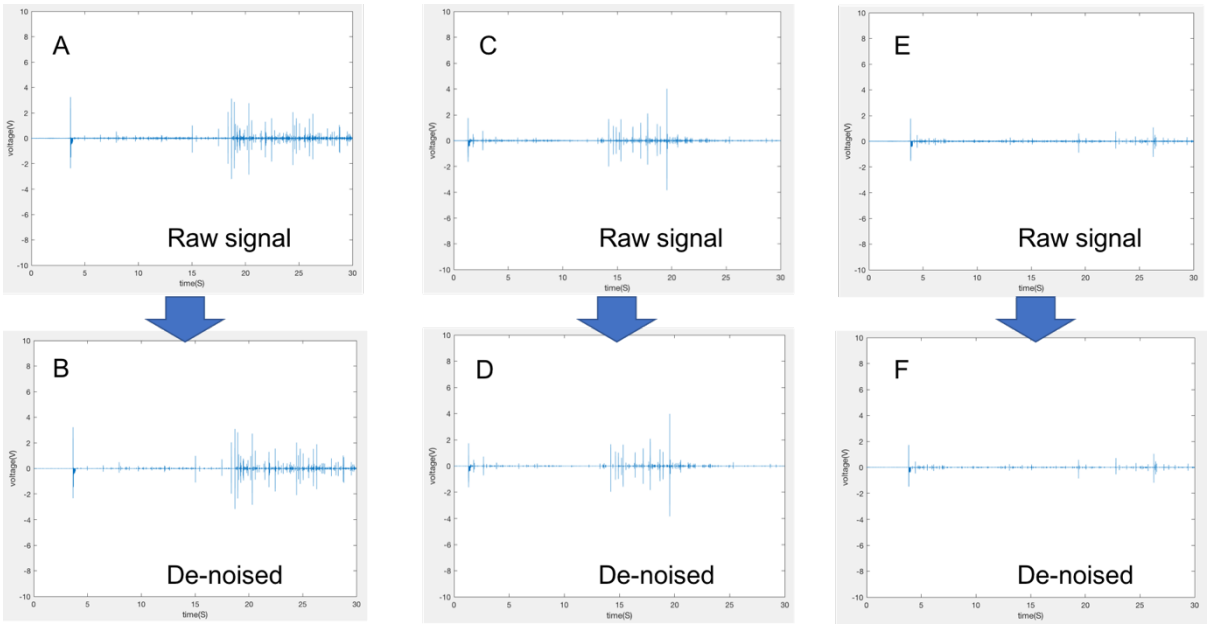

Figure 6-8 Raw signal and the filtered signals from TIG welding process with 304 steel

A: Weld ID: 1423. C: Weld ID: 1424. D: Weld ID: 1425.

B. De-noised signal (1423) D. De-noised signal (1424) F. De-noised signal (1425)

Figure 6-9 shows the comparison between the raw signal and the filtered signals from the TIG process with EN8 steel. From the results in Figure 6-9B, Figure 6-9D and Figure 6-9F, the background signals are mostly filtered out. Also, the discontinuous spikes are preserved. The results from the TIG process with CS70 steel are in Figure 6-10. The results are similar to EN8 steel.

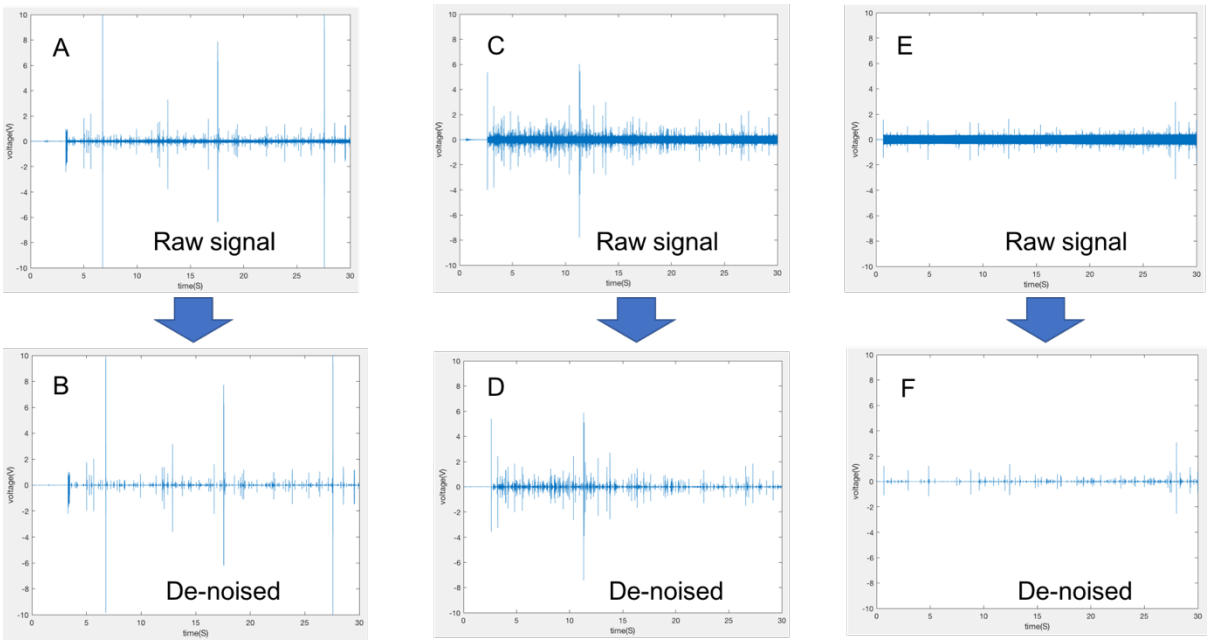

Figure 6-9 Raw signal and the filtered signals from TIG process with EN8 steel

A: Weld ID: 1593. C: Weld ID: 1616. D: Weld ID: 1604.

B. De-noised signal (1593) D. De-noised signal (1616) F. De-noised signal (1604)

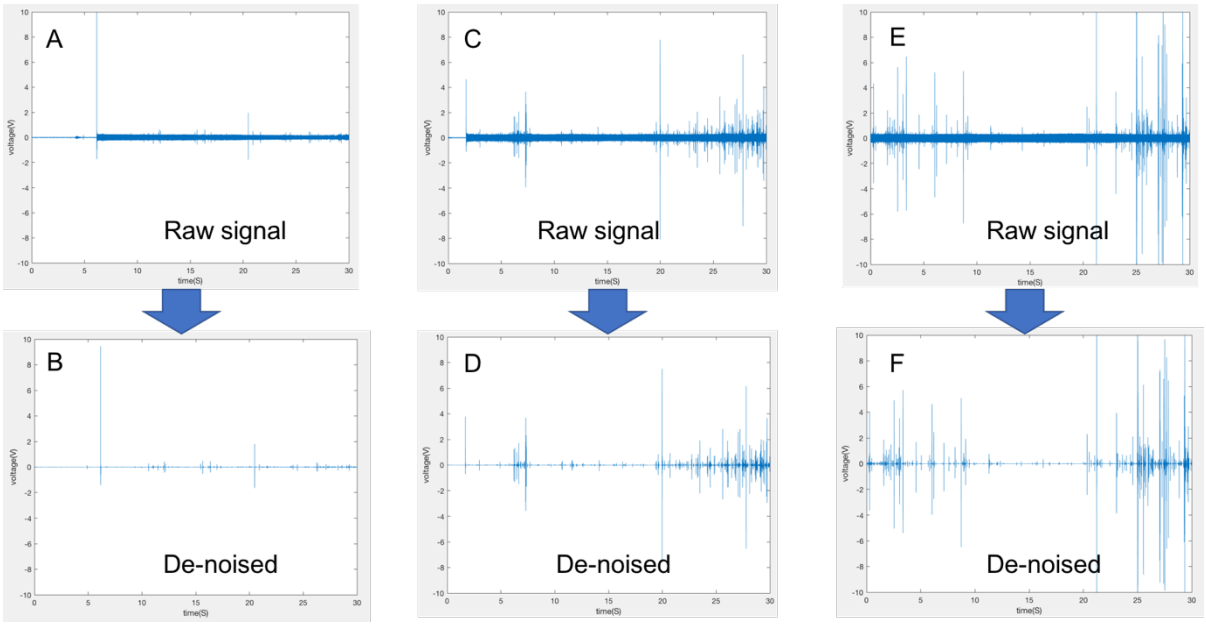

Figure 6-10 Raw signal and the filtered signals from TIG with CS70 steel

A: Weld ID: 784. C: Weld ID: 941. D: Weld ID: 1021.

B. De-noised signal (784) D. De-noised signal (941) F. De-noised signal (1021)

Figure 6-11 is the comparison between raw signals and the filtered signals from the TIG welding process with Al6082 aluminium. The background signals from the TIG welding process with Al6082 are higher than with steels. After de-noising, the background noise is reduced by a small percentage. The reason for this is it is that the nature of the background signal from Aluminium and steel are different. The reduction in the value of RMS is similar in comparison with other materials. Since aluminium is a high spatter material, it is possible that during the trial with aluminium, the background noise is mixed with other types of noise like noise from spattering.

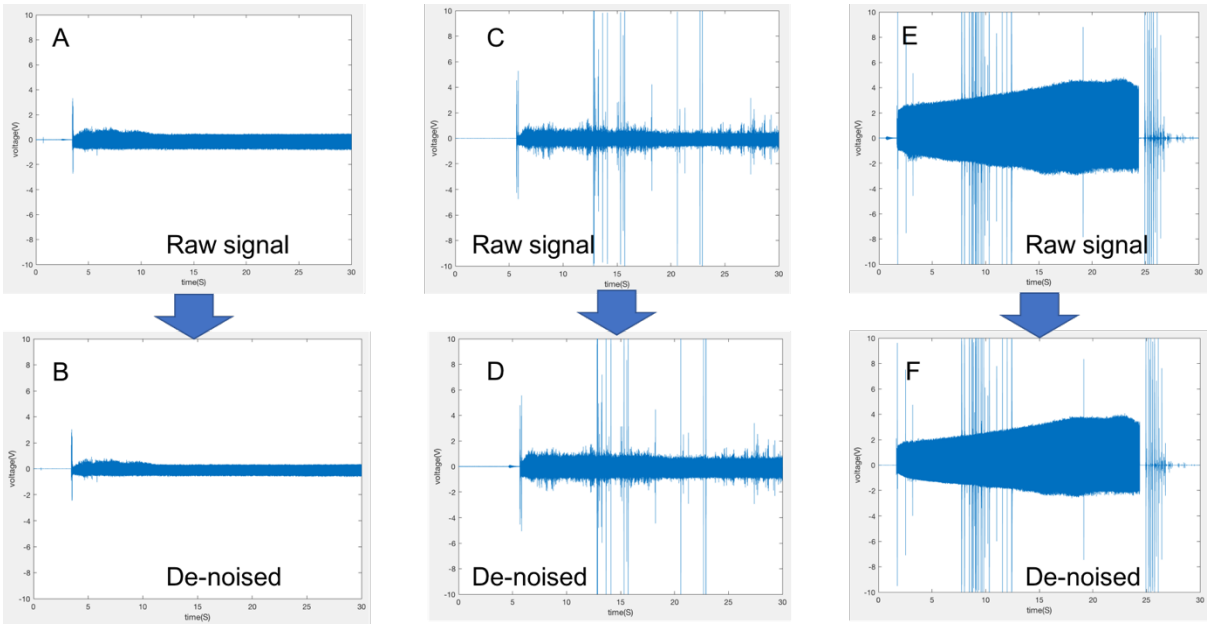

Figure 6-11 Raw signal and the filtered signals from TIG with Al 6082

A: Weld ID: 1487. C: Weld ID: 1489. D: Weld ID: 1492.

B. De-noised signal (1487) D. De-noised signal (1489) F. De-noised signal (1492)

6.3.2.3 Frequency analysis of signal from TIG process

In this section, the raw signals are processed using Fast Fourier Transform (FFT) and the Power Spectral Density (PSD) values are obtained for detailed frequency analysis.

Figure 6-12A is the FFT result of the raw signal. In Figure 6-12B, the signal is from weld ID 784: CS70 with the TIG process. A noticeable frequency of 56 kHz is marked. After zooming in as in Figure 6-12E, the frequency range is a frequency range around 56 kHz. The FFT result for the filtered signal is plotted in 6-12D. The marked frequency is filtered out. In Figure 6-13 and 6-14, which are weld ID: 941 and 1021 (CS70 with TIG welding process) can be seen that they have the same frequency range 56 kHz. This proves that the background signal for the TIG process with steel is also mostly cyclic and they can be easily filtered out by the wavelet transform method. From Figure 6-14. There is also another noticeable frequency range around 100 kHz, which is related to the burst signals in the raw signal, which cannot be filtered out by

the wavelet transformation. This part of the signal is more likely to be related to AE activities in the material itself rather than from the TIG welding process itself.

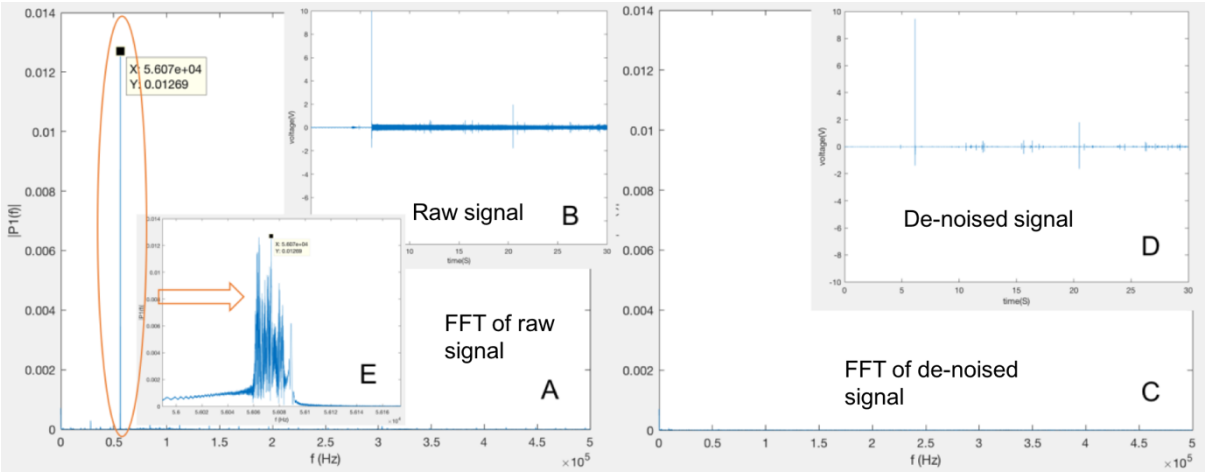

Figure 6-12 Comparison of raw and de-noised signal and FFT results of trial 784

A. FFT result of the raw signal, weld ID: 784. B. Raw signal from TIG trial.

C. FFT result of the de-noised signal. D. A de-noised signal from TIG trial.

E. Zoomed frequency range from FFT result.

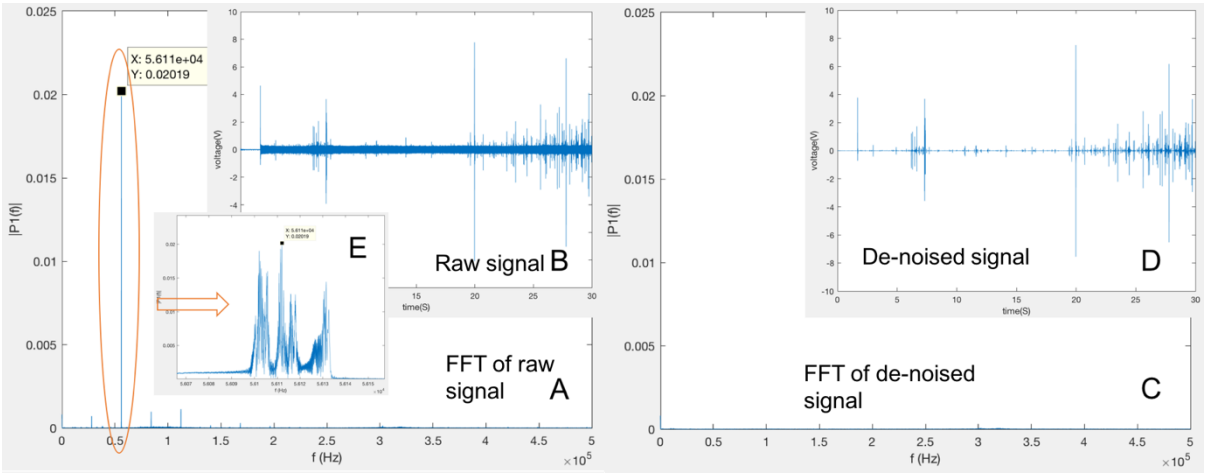

Figure 6-13 Comparison of raw and de-noised signal and FFT results of trial 941

A. FFT result of the raw signal, weld ID: 941. B. Raw signal from TIG trial.

C. FFT result of the de-noised signal. D. A de-noised signal from TIG trial.

E. Zoomed frequency range from FFT result.

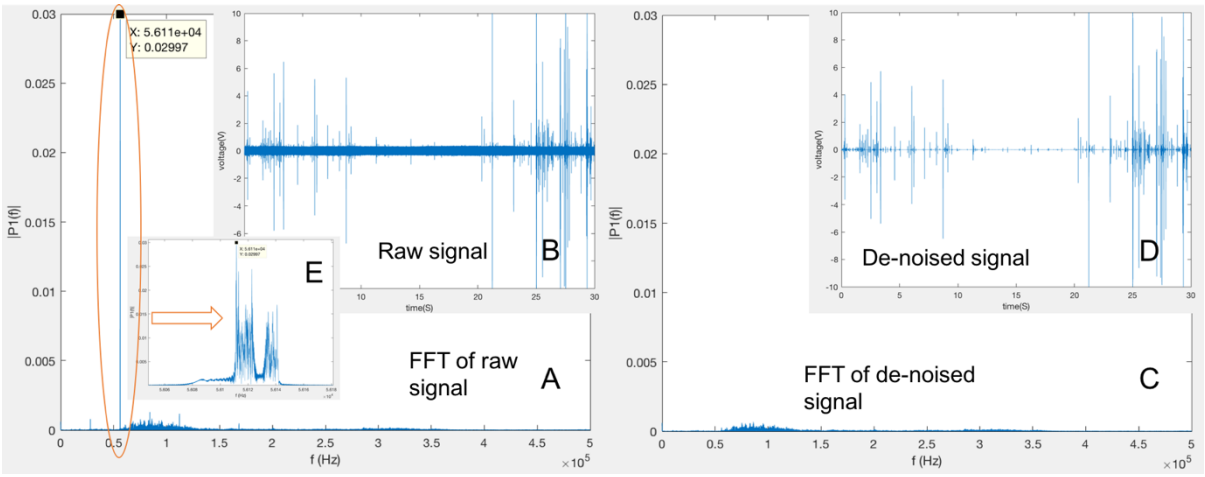

Figure 6-14 Comparison of raw and de-noised signal and FFT results of trial 1021

A. FFT result of the raw signal, weld ID: 1021. B. Raw signal from TIG trial.

C. FFT result of the de-noised signal. D. A de-noised signal from TIG trial.

E. Zoomed frequency range from FFT result.

Figure 6-15A, Figure 6-15C and Figure 6-15E are the FFT results of the raw signals 1487, 1489 and 1492 (Al6083 with TIG welding process). Figure 6-15B, Figure 6-15D and Figure 6-15F are the FFT results of the de-noised signal. The signature peak frequency is the same as with the TIG process with steel at 56 kHz. The signature frequency is filtered out after the de-noised process. However, apart from the peak frequency at 56 kHz, some other characteristic frequencies can be observed which are likely to relate to signal from material melting and solidification or the formation of defects or other non-cyclic noise from the background which is hard to filter out.

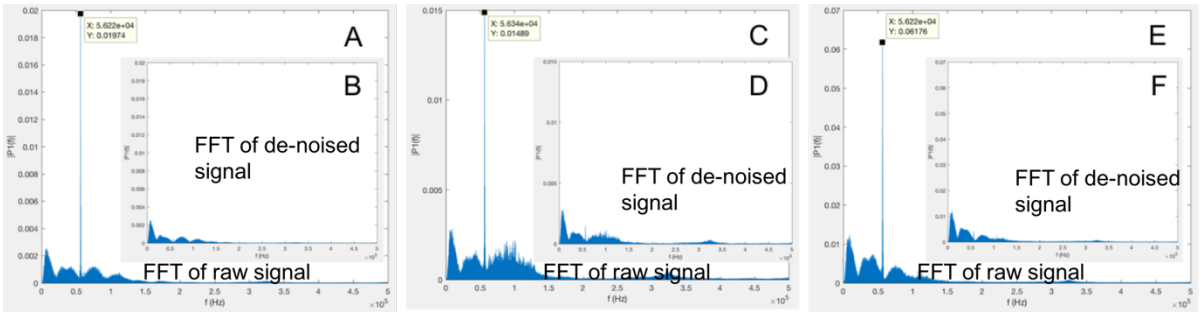

Figure 6-15 Comparisons of the FFT results between raw and de-noised signal

A. FFT of signal 1487 B. FFT of signal of de-noised signal 1487

C. FFT of signal 1489 D. FFT of signal of de-noised signal 1489

E. FFT of signal 1492 B. FFT of signal of de-noised signal 1492

6.3.3 MAG process

6.3.3.1 Raw signal and noise level discussion of MAG process

In this section, the raw signals from MAG process are plotted. The RMS values for each trial are calculated for the comparison of the noise levels. The principle of RMS is explained in chapter 5. The RMS values for each trial are calculated for the comparison of the noise levels. The principle of RMS is explained in chapter 5.

Table 6-5 The RMS values for the signal collected from the welding trials

ID	Material/ Process	Heat input (kJ/ min)	RMS raw (V)	RMS WD (V)
1782	CS70/ MAG	0.369	0.1601	0.1152
1783	CS70/ MAG	0.374	0.0521	0.0381
1785	CS70/ MAG	0.394	0.1594	0.1249
1804	EN8/ MAG	0.194	0.6212	0.5624
1806	EN8/ MAG	0.204	0.3984	0.2955
1807	EN8/ MAG	0.205	0.2284	0.1729

The raw signals from the MAG welding process with material CS70 and EN8 are plotted in Figure 6-16. and Figure 6-17. The raw signal from the MAG process has an overall higher level of background noise than the TIG process from observation of the plotted raw signal. The MAG process is a noisier process with higher spatter level, which can be observed during the trials. Especially with EN8 steel, the signals have a very high level of noise, without proper filtering process, the useful information which can be used for the identification of cracking activities can be easily buried by redundant background signal. The raw signal is not possible to be used for the identification of the defects in welds directly.

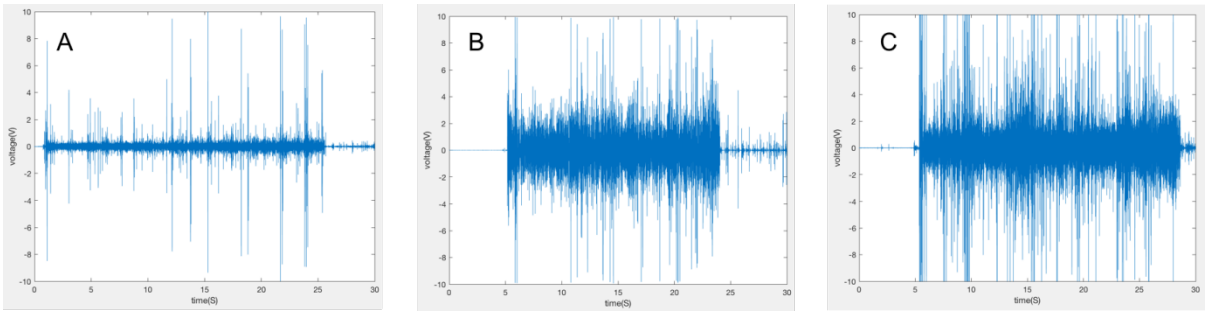

Figure 6-16 Raw data from MAG welding process with CS70 carbon steel

A: Weld ID: 1783. B: Weld ID: 1785. C: Weld ID: 1782.

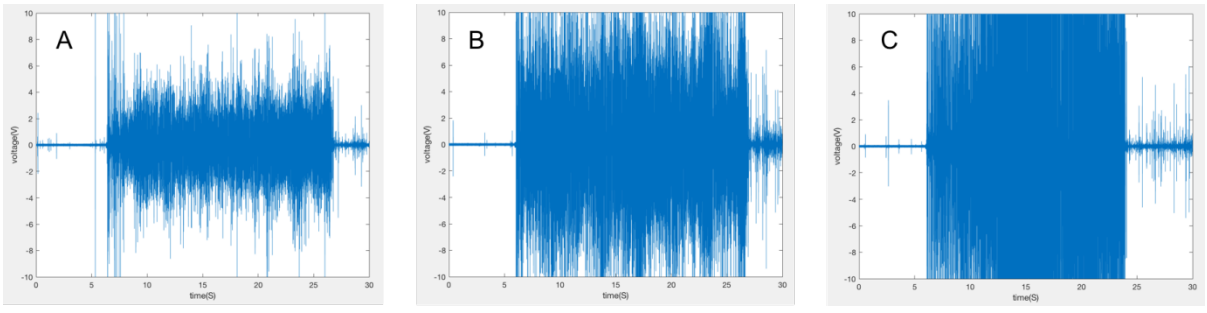

Figure 6-17 Raw data from MAG welding process with EN8 steel

A: Weld ID: 1807. B: Weld ID: 1806. C: Weld ID: 1804

6.3.3.2 De-noising of raw signal from MAG process

Figure 6-18 and 6-19 are the comparisons between raw signals and the filtered signals from the MAG process with CS70 and EN8 steel. The background signal from MAG process is higher than from the TIG process from the observation from the raw signal and the RMS values in Table 6-5. After de-noising, the background noise is reduced by a small percentage according to the RMS results. From the plotted filtered signals, the de-noising results are not obvious. So even after the de-nosing process, the signals are still hard to be used as an index for the detection of defects. Since the MAG is a high noise process, it is possible that during the trial with MAG, the background noise is mixed with other types of noise other than from the welding machine.

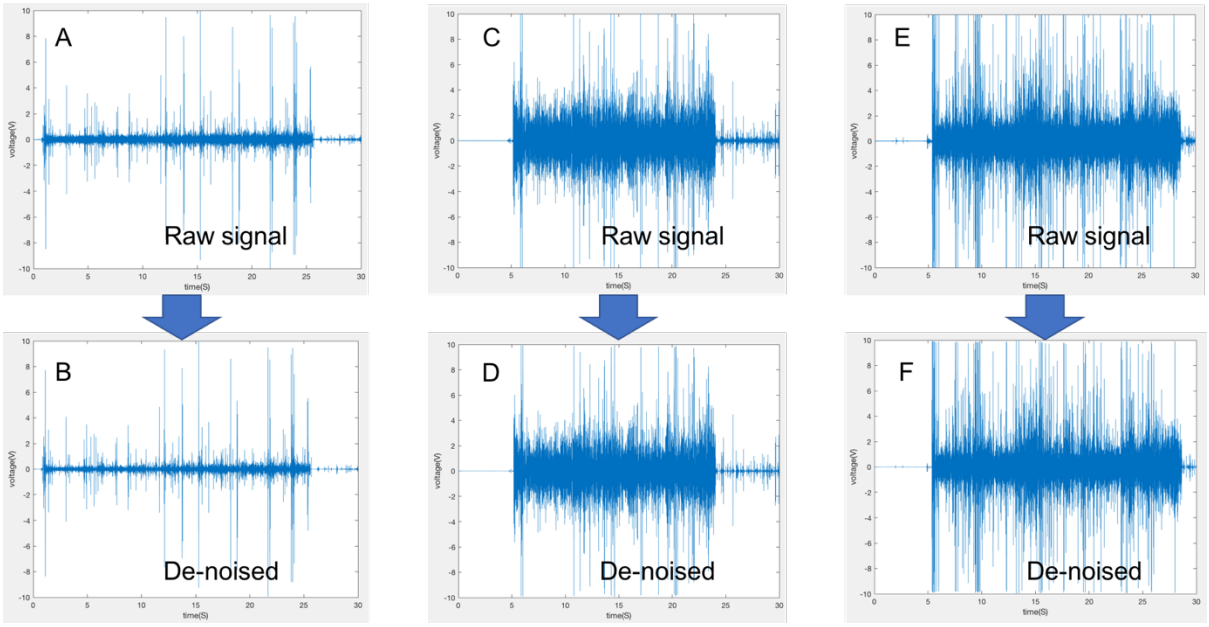

Figure 6-18 Raw signal and the filtered signals from MAG with CS70 steel

A: Weld ID: 1783. C: Weld ID: 1785. D: Weld ID: 1782.

B. De-noised signal (1783) D. De-noised signal (1785) F. De-noised signal (1782)

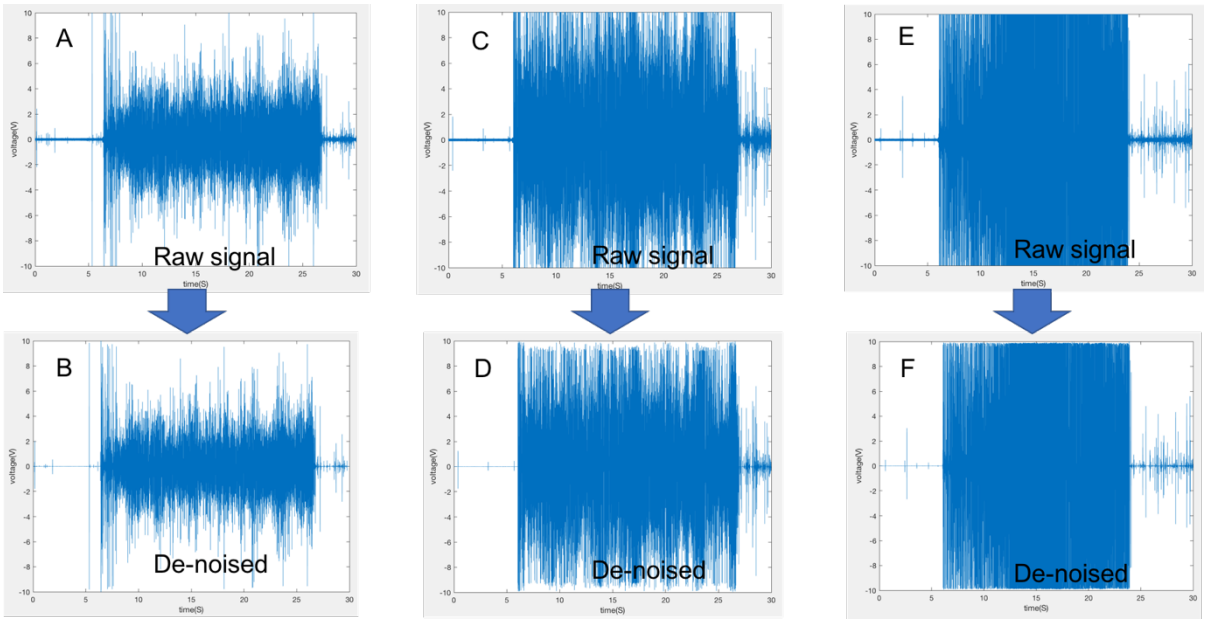

Figure 6-19 Raw signal and the filtered signals from MAG with EN8 steel

A: Weld ID: 1807. C: Weld ID: 1806. D: Weld ID: 1804.

B. De-noised signal (1807) D. De-noised signal (1806) F. De-noised signal (1804)

6.3.3.3 Frequency analysis of signal from MAG process

In this section, the raw signals are processed using Fast Fourier Transform (FFT) and the Power Spectral Density (PSD) values are obtained for detailed frequency analysis.

Figure 6-20 is a frequency comparison between the raw signal and filtered signal with MAG process (trial 1782). Before filtering, there are a few distinguishable frequencies which are marked in Figure 6-20B. After filtering, the marked frequencies are mostly removed. In the raw signal, Figure 6-20C, filtering result is hardly noticeable. However, in the frequency range, the filtering result is obvious. That means with a high spatter, high noise process like MAG process, only a small part of background signal can be filtered out, however, this small part of the signal has noticeable frequencies.

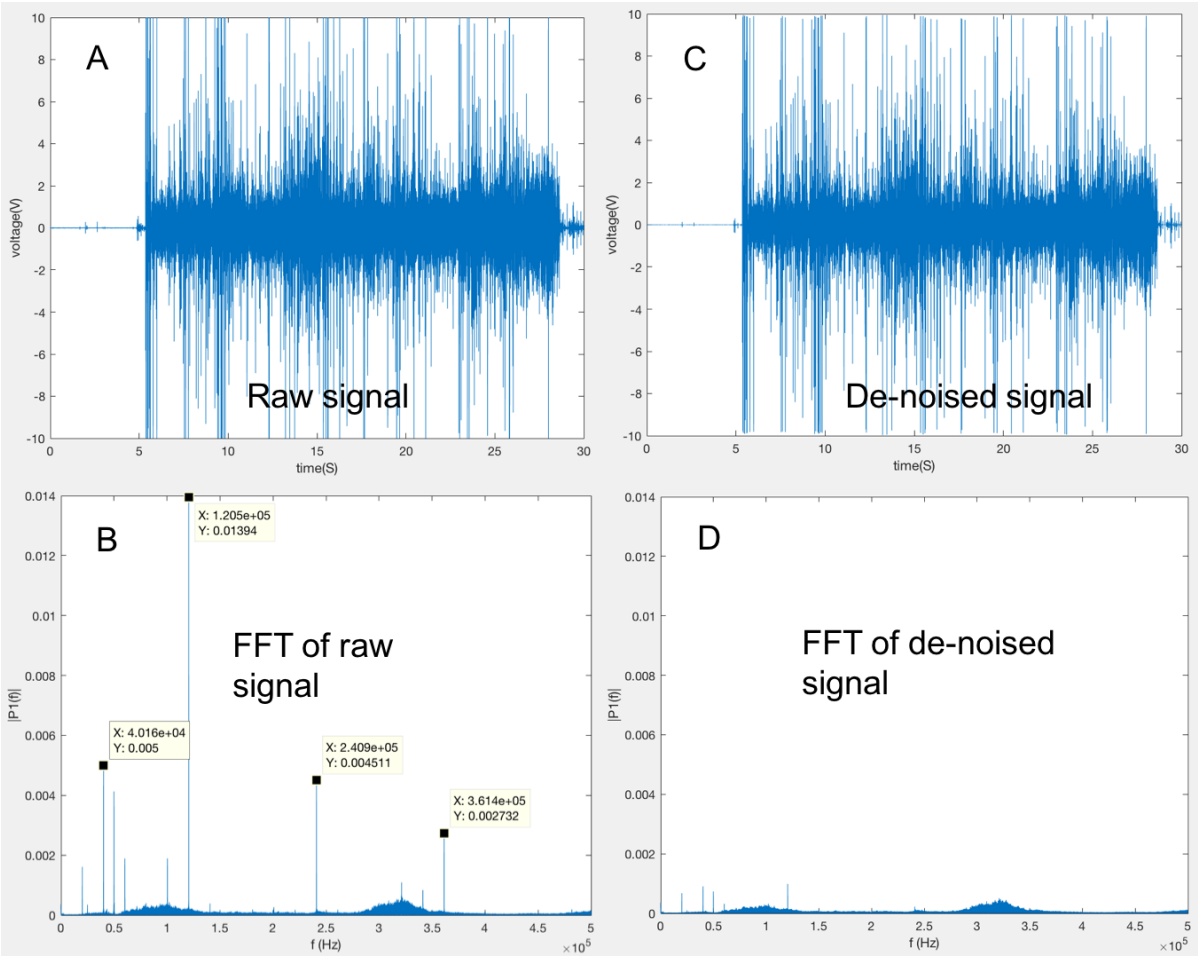

Figure 6-20 Raw and de-noised signals of MAG trial 1782 and FFT results

A. Raw signal from MAG trial 1782. B. FFT result of the raw signal.

C. A de-noised signal from MAG trial 1782. D. FFT result of the de-noised signal.

Figure 6-20 and Figure 6-21 are also frequency comparisons between the raw signal and filtered signal with the MAG welding process (trials 1783 and 1785). The results are very similar to trial 1782. It is also worth noting that apart from the marked frequencies, there are two additional frequency ranges around 100 kHz and 300-350 kHz which are not possible to be filtered out. These two frequency ranges will be discussed in chapter 7.

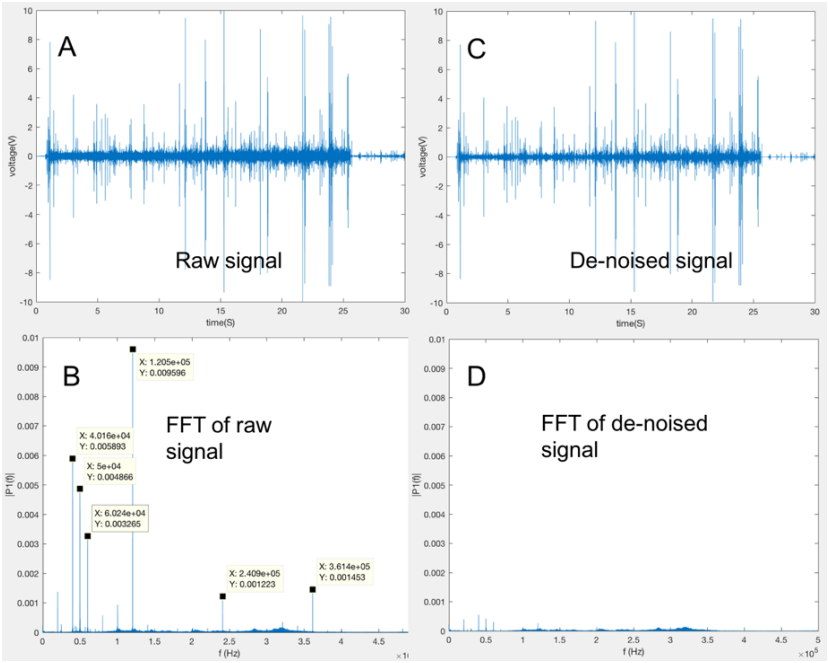

Figure 6-21 Raw and de-noised signals of MAG trial 1783 and FFT results

A. Raw signal from MAG trial 1783. B. FFT result of the raw signal.

C. A de-noised signal from MAG trial 1783. D. FFT result of the de-noised signal.

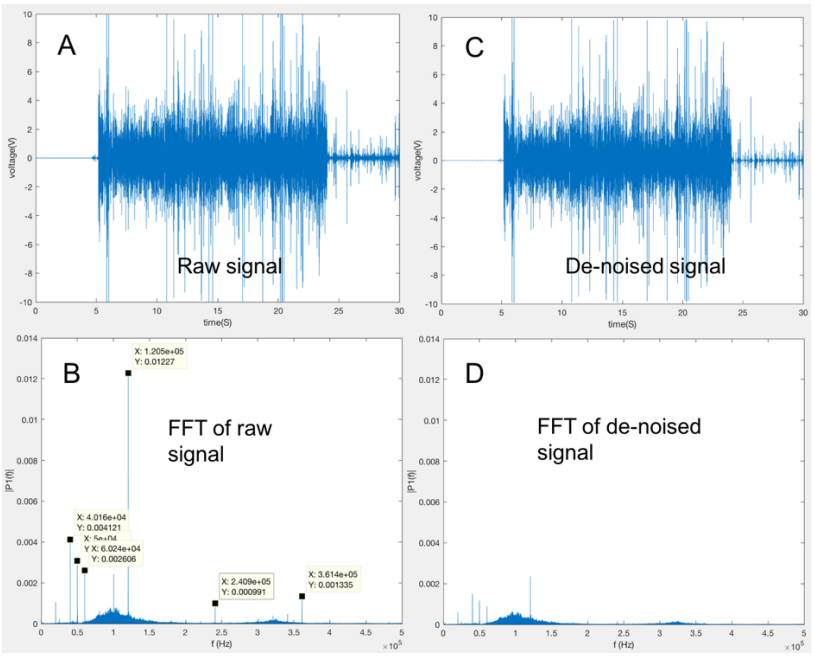

Figure 6-22 Raw and de-noised signals of MAG trial 1785 and FFT results

A. Raw signal from MAG trial 1785. B. FFT result of the raw signal.

C. A de-noised signal from MAG trial 1785. D. FFT result of the de-noised signal.

6.4 Conclusion remarks

This section describes one of the main challenges of AE monitoring technology, the need for source identification, and the models developed in this study to perform this task. The model was tested using data from multiple laboratory experiments. Some important findings and findings in the analysis are summarised as follows:

a. The noise level of the signal from welding largely varies among different processes and material. TIG and CMT process is quiet processes compare to MAG process; With the same process, with more heat input, the level of background signal is higher. Material-wise, different steels have similar background signal level, from the raw signal, Aluminum has a higher level of background signal than steel material.
b. The background is mostly easy to filter out using wavelet transformation. When the background signal is low, the filtering result is obvious in the comparison with the raw signal. However, when the signal is very noisy, the filtering result is hard to observe. However, from the FFT results, no matter the signal is ‘quiet' or ‘noisy', the filtering results are similar and effective since the majority of the frequency related to the background signal are filtered out. In the meanwhile, the discontinuous signal: the spikes in the signal which are possibly associated with the material are preserved.
c. The frequency results show that with different welding processes, there are different frequency features with the background signal. After the de-noising, the frequencies associated with the background is gone. With CMT welding process, in the background signal, a few signature frequencies are observed and successfully filtered out with wavelet transform. With TIG welding process, the signature frequency range mainly locates in around 56 kHz, with different material, the level of the signature frequency range is similar, even with Aluminum material. That means the signature frequency range is from the welding machine and the TIG process itself. MAG

process also has a few noticeable frequency ranges. After the filtering, most of the noted frequencies are filtered out. Even the MAG process is much nosier with the background signal.

Chapter 7

The frequency features for crack-related signals and other types of burst signals

This chapter summarises experimental configuration, results, and subsequent analysis of crack-related signals and other burst signals arising from other sources. Section 7.1 describes the research plan and proposed methods. The experimental setup, instrumentation, and setup are detailed in section 7.2. The results and results are described in section 7.3. Finally, section 7.4 summarises the main findings of the study.

7.1 Approach

In chapter 6, the analysis and filtering of the background signal from different welding processes and the material was carried out. A basic understanding of the characteristics of the continuous background signals was reached. In this chapter, burst signals will be the main focus, which were collected and analysed, that include burst signal from the environment and cracking signal. The burst signal from the environment could cover a wide range of signal sources: the accidental contact with the plates during the recording period, the disturbance in gas and arc etc. In this chapter, a few different types of burst signals from the environment were captured and analysed. For the collection of cracking signal, TIG welding process was applied on high carbon steel CS70 plates to stimulate cracks in the welds. The AE signals were analysed using Fast Fourier Transform (FFT) and Short-Time Fourier Transform (STFT) algorithms. Comparison between the features arising from different sources and observed in the frequency spectra of the acquired AE signals has been carried out. The results demonstrate the possibility of applying the AE technique for monitoring and detecting signals generated from cracking activities by using frequency domain analysis.

7.2 Experiment

7.2.1 Collection of the signal from the environment

The burst signal from the environment has been collected including background noise in the laboratory area, the setup of the AE system is in chapter 5. Noise arising from the gas flow torch movement, arc ignition and mechanical noise which arises from the direct contact with objects and the welding plate were collected. The collection of the AE signals from the environment is achieved by mounting the AE sensor on the side of the parent material and clamped on the welding table. This represents the same condition as during the TIG welding process. The environment noise in the laboratory was recorded using 60 dB gain with the pre-amplifier. The AE signal from the torch moving was collected as the torch moved with a speed of 9.8 cm/min. The AE signal arising from gas flow was recorded using a release rate of Argon gas of 15L/min rate for 5-10s long intervals. The AE signals from arcing sound were collected during the TIG welding process. The AE signal was cropped from the beginning of the signal from welding as that was the arc ignition period.

The direct-contact mechanical noise was simulated based on a) objects dropping and a light hammer knock on the plate which were used to imitate the accidental dropping of an object during the welding process, b) an object sliding on the plate, which imitated the displacement between the plates and fixtures arising from the dilation and contraction of the plates during heating and cooling. The simulation experiment was carried out using a nut dropped from a preselected height and distance from the sensor on the plate and by using a small hammer used to impact the surface of the plate. The sliding signal collection was carried out by a metal plate sliding against the other at a certain distance from the sensor. The experimental configuration parameters are summarised in Table 7-1 below.

Table 7-1 Experiment configuration of the collection of signal from the environment.

Signal type	Data collection condition
Signal from environment	AE sensor attached to the side of the parent material while it is clamped by a fixture. AE sensor for all of the tests below is under the same condition.
Torch moving	Torch moves at 9.8 cm/min.
Arc ignition	The beginning of each welding signal.
Gas purging	Gas flow at 15L/min.
Nut dropping	DIN 934 HEXM5 stainless steel nut drops from 20 cm height and 20 cm far from the sensor.
Hammer knocking	A small hammer lightly taps on the plate 20 cm from the sensor.
Plate sliding	A plate sliding on the plate at 20 cm from the sensor.

7.2.2 Collection of AE signal from the welding process and cracking

The TIG welding settings are listed in Table 7-2, the setup of the TIG welding trial and AE system are in chapter 5. Pass 5, 9, 14 and 18 were welded autogenously, pass 6, 10, 15 and 19 were welded with filler wire, sampled at 1MHz. Recorded welding process duration: about 50 seconds. Recorded cooling time: about 50 seconds. Some of the welds cracked during the recording and some of the welds did not have visible cracks from visual inspection. Photos of the welds are in Figure 7. The defect types are listed in Table 7-2.

Table 7-2 Experimental configuration for TIG welding trials.

ID	Welding condition	Current (A)	Voltage (V)	Travel Speed (cm/min)	Defect
Pass 5	Autogenous	70	12	9.8	Central line crack
Pass 6	Wire	70	12	9.8	Central line crack (cracked two days after)
Pass 9	Autogenous	90	12	9.8	Insufficient penetration
Pass 10	Wire	90	12	9.8	Central line crack
Pass 14	Autogenous	110	12	9.8	Slag
Pass 15	Wire	110	12	9.8	Insufficient penetration
Pass 18	Autogenous	130	12	9.8	Linear cracks
Pass 19	Wire	130	12	9.8	Excessive penetration

7.3 Analysis and discussion

7.3.1 Analysis of environmental and mechanical noise

The raw AE signals from the environment noise of the laboratory, welding table movement and welding gas being released are shown in Figure 7-1. The amplitude of the raw signals from these three sources is very low. The amplitude of signals from background and torch movement is around 0.01 V - 0.02 V, which means the AE signals detected by the sensor are not particularly affected by the background or torch movement noise. For the gas release noise, the recorded signal amplitude is slightly higher but still considered as insignificant when compared with the amplitude of other AE sources. Overall, these three noise sources have little to none

impact on the collected AE signals acquired during the welding process since they have a very low amplitude in comparison with the AE signals arising from other sources.

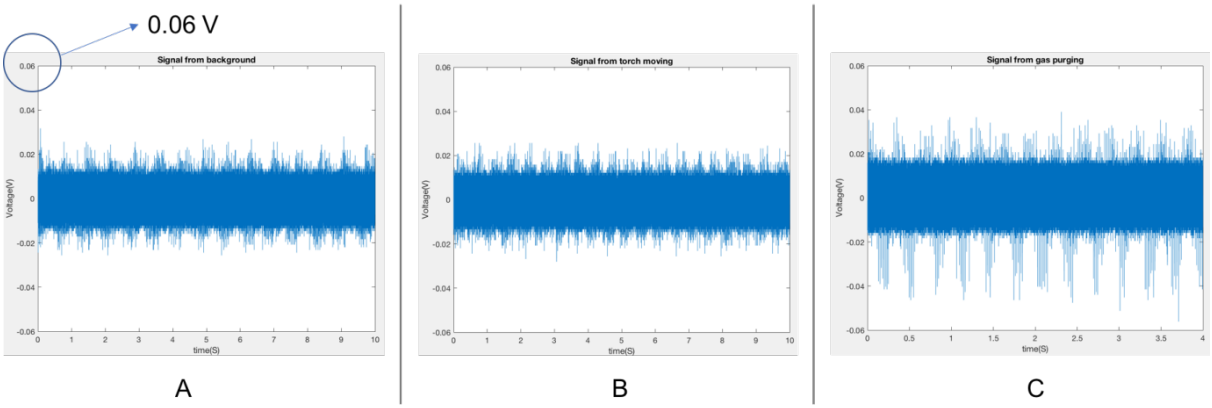

Figure 7-1 Raw signals from various sources.

A. Raw signal from environment.

B. Raw signal from torch moving.

C. Raw signal from gas purging.

The raw AE signals arising from arc ignition and the corresponding FFT results are plotted in Figure 7-2. Figures 7-2A and Figure 7-2B show 0.05 seconds of the AE signals from the beginning of two different welds associated with the arc ignition. The pulses from the arc ignition have an amplitude of 0.5-3V. From the corresponding FFT results, high Power Spectral Density (PSD) value can be observed in the frequency range of 50 kHz -180 kHz.

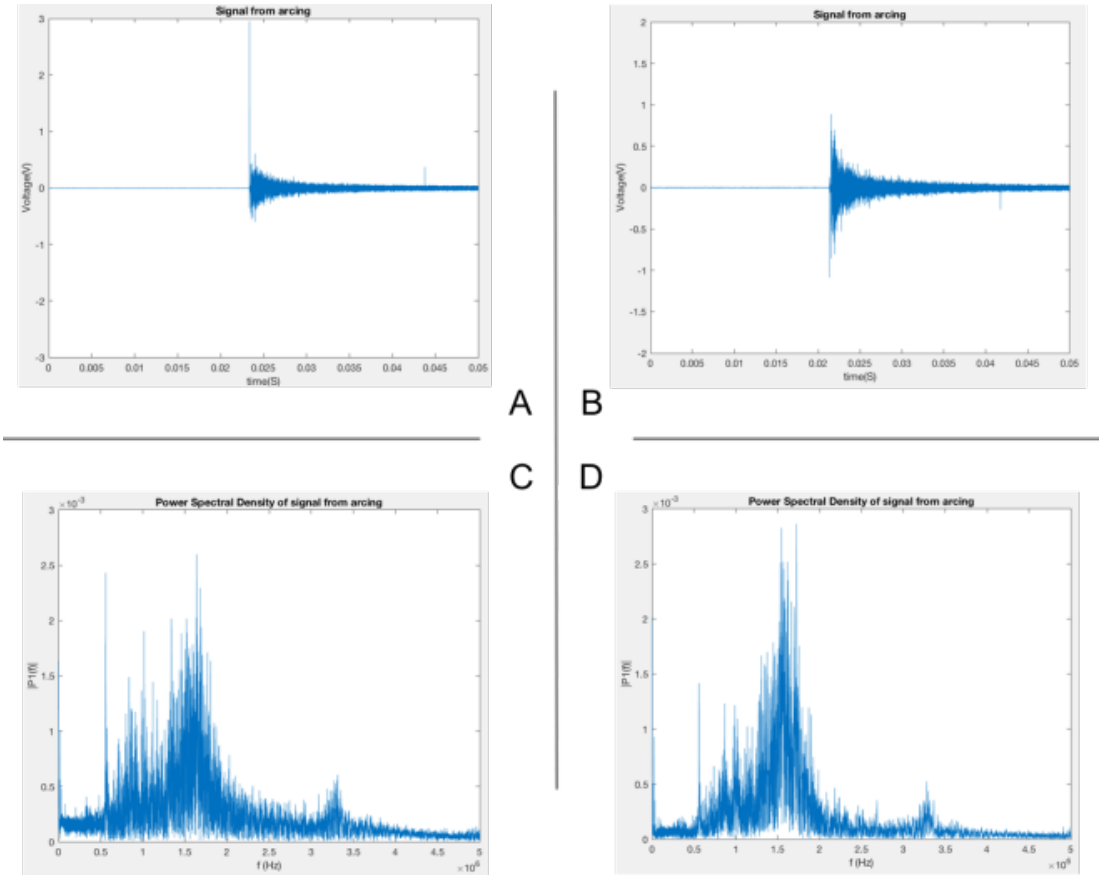

Figure 7-2 Raw signal from arcing and FFT results.

A. and B. Raw signal from arc ignition.

C. and D. The corresponding FFT results of the raw signal in A. and B.

The raw AE signals and FFT results associated with the mechanical noise are plotted in Figure 7-3. The raw AE signals associated with the nut dropping test is shown in Figure 7-3A. In the AE signal, the five nut drops generate 5 respective clusters of AE events. Since the nut bounced randomly after dropping, every cluster of the raw signal is different. The FFT result for nut dropping is shown in Figure 7-3D. A high PSD value is mainly observed in the frequency range of 50 kHz - 180kHz. The raw AE signal from the hammer knocking test is shown in Figure 7-3B. The amplitude of the AE signal from the hammer knocking is lower (under 2 V) and results from the hammer impacts on the plate. The FFT result for the hammer knocking test (Figure5. E) results in a high PSD value which is mainly observed in the frequency range of 50 kHz -

180 kHz. The sliding test generates a similar power spectrum result with a high PSD value observed in the frequency range of 50 kHz – 180 kHz. The power spectrum results from the signal from arc ignition also generate similar high PSD value distribution.

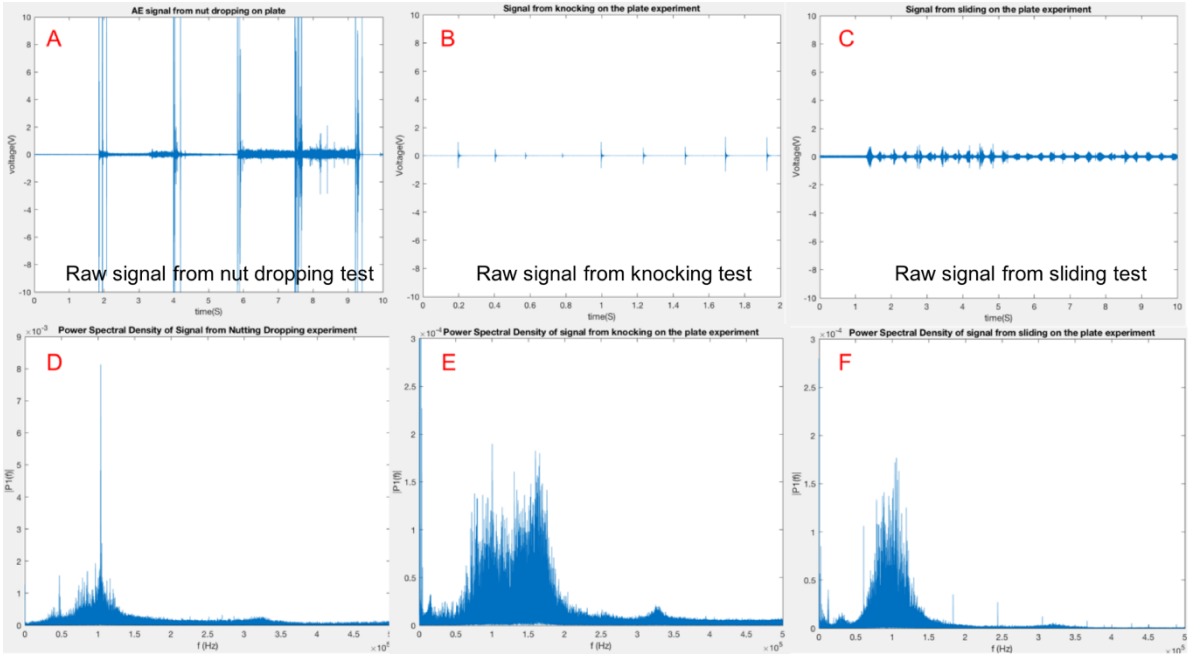

Figure 7-3 Raw signals from various sources and FFT results.

A. Raw signal from nut dropping test.

B. Raw signal from knocking test.

C. Raw signal from sliding test.

D, E and F are the corresponding FFT results.

From the FFT results, the frequency features of the three types of 'mechanical noise' tests are similar. The signal from the nut dropping test has been taken as a representative example for more detailed analysis. Individual AE event (single pulse) has been cropped out as shown in Figure 7-4 C: S1 and S2 are two 0.5 ms of the signal selected from the 10s signal in Figure 7-4 A. The FFT results for S1 and S2 show that high power is also distributed in the frequency range of 50 kHz – 180 kHz with individual AE events. To make a straightforward interpretation

of the relationship between of the AE event and power in the frequency range of 50 kHz - 180kHz, the sum of PSD value of the frequency range 50 kHz – 180 kHz was accumulated for each 0.05ms and plotted over time as shown in figure 7-4 D. From the results shown in figure 7-4 D, a high similarity between the power spectrum in the frequency range of 50 kHz-180 kHz and the AE signal can be observed. This indicates that the power spectrum in the frequency range of 50 kHz - 180 kHz can potentially be used as a method of identifying the mechanical noise effects in the measurement.

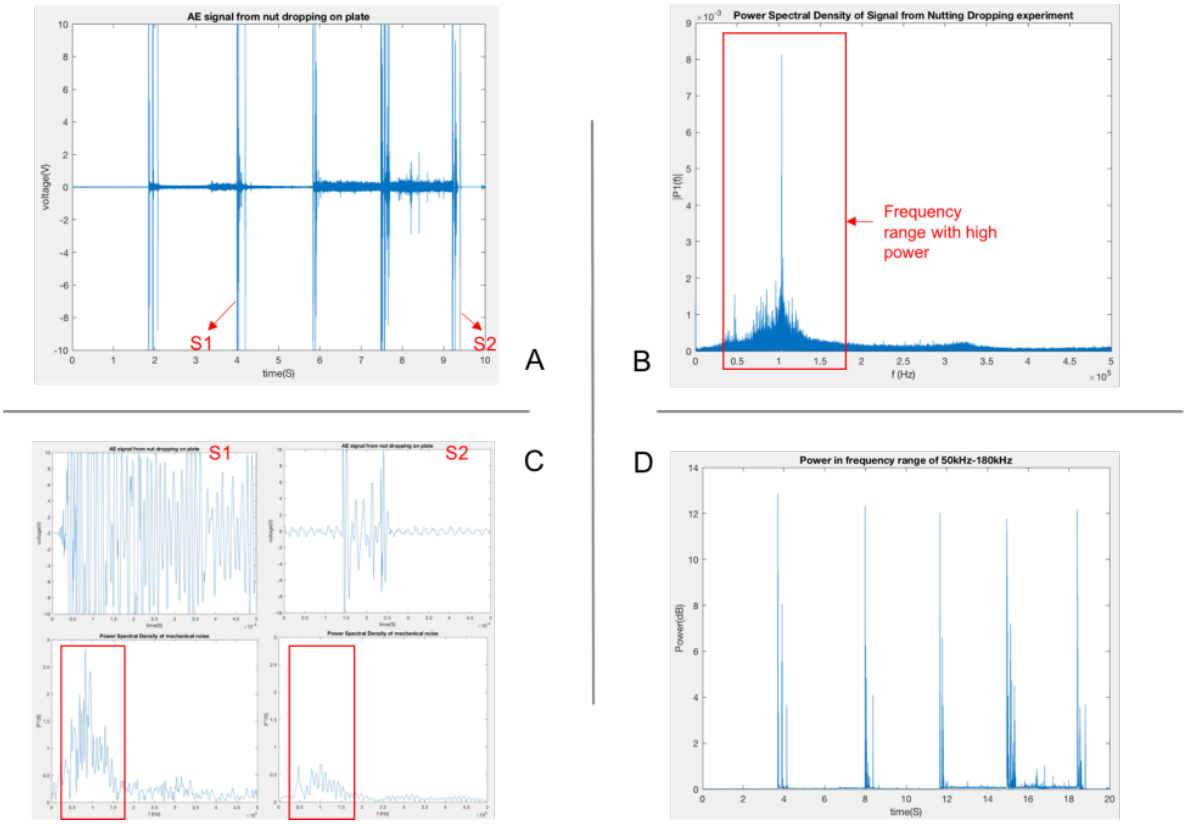

Figure 7-4 Raw signal from nut dropping test, FFT results.

A. Raw signal from nut dropping test.

B. FFT result.

C. Two 0.5ms of the signal selected from the 10s signal in A. and FFT results.

D. Power in the frequency range of 50 kHz-180 kHz over the 10 second time period.

7.3.3 Analysis of AE signal from the welding process and cracking

The types of defects in the welding trial are listed in Table 7-2. Pass 5, 6, 10 and 18 are with cracks in the welds. Figure 7-5 shows a cross-section of a linear crack of trial pass 18. For pass 5, 6 and 10, welds usually start to form small size cracks after welding stopped, eventually developing into a centre-line crack.

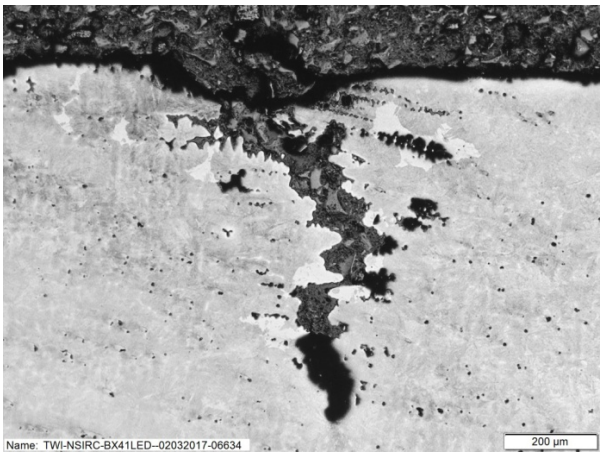

Figure 7-5 The cross section of the linear crack of pass 18.

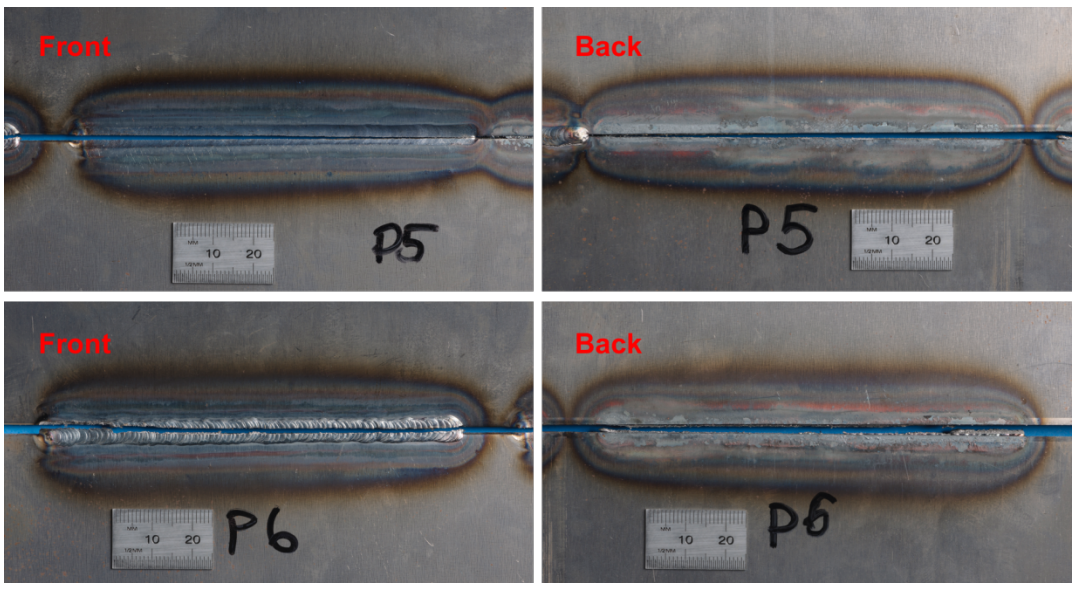

Figure 7-6 Welds with a crack located along the welding beam of pass 5 and 6.

The signal from cracking blends in the signal from the welding process and environment and hence it is difficult to distinguish as shown in Figure 7-7, pass 5: the data acquisition time is 100 seconds long, and the welding period represents the first 30 seconds. The cooling period is closely monitored by listening and visually observing the weld. The intense cracking and the finial centre-line crack happened at the last 20 seconds, as shown in Figure 7-7, pass 5. The clustered AE signals towards the end of the 100 seconds are more likely to be related to cracking in the weld than the beginning of the welding period and the beginning of the cooling period.

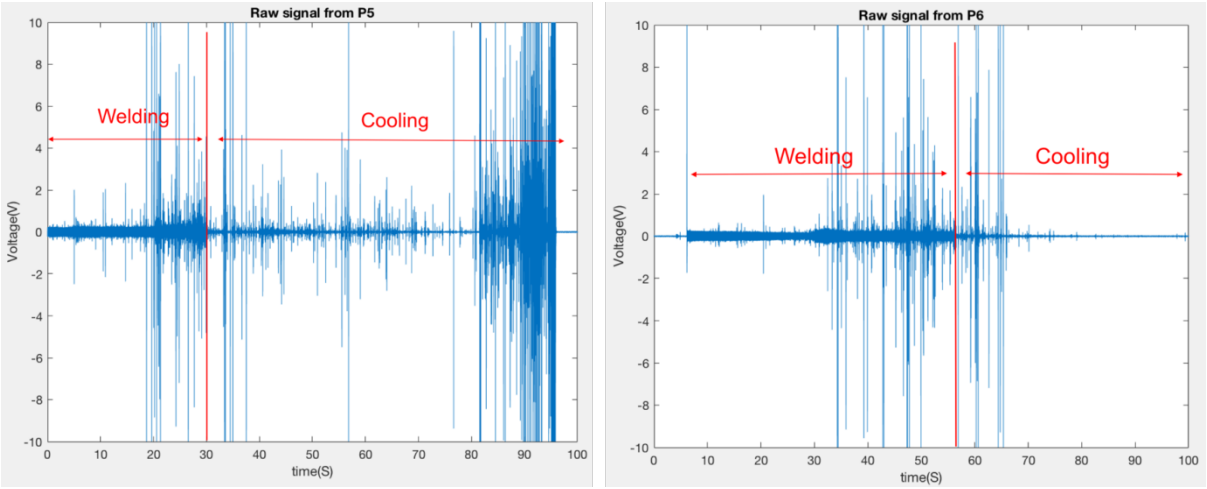

Figure 7-7 Raw signals of pass 5 and 6.

Left: 100 seconds signal of welding and cooling of pass 5

Right: 100 seconds signal of welding and cooling of pass 6

Pass 6 also has a central line cracking as shown in Figure 7-6, however, the central line cracking happened two days after the welding stopped and the final failure did not capture by the AE system. In Figure 7-7 right image: pass 6, the cooling period does not have a period like the last 20 seconds of pass five, which represent the final failure of the welds. However, during the recorded period, small cracks could still happen in the signal of pass 6.

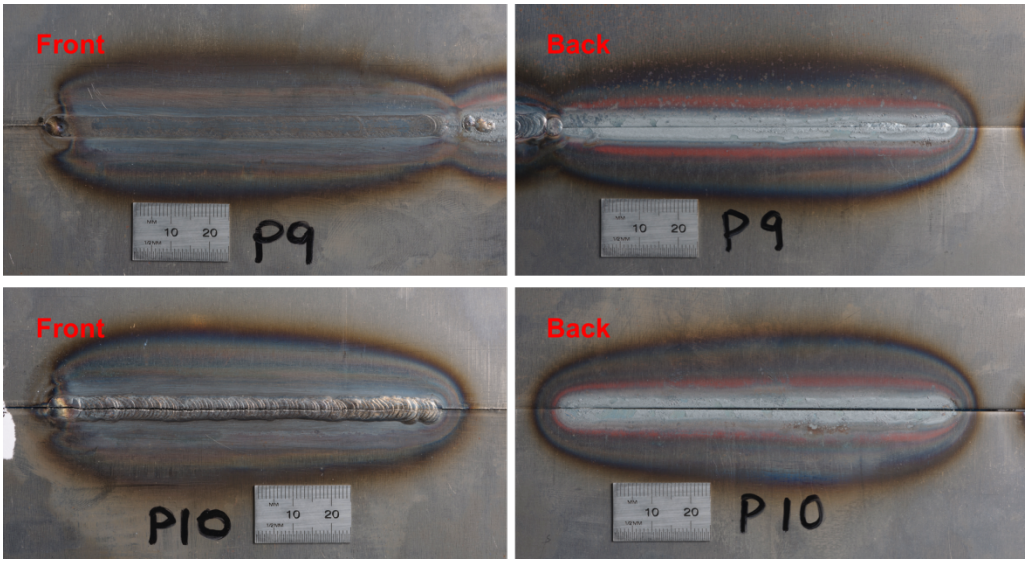

Figure 7-8 Photographs of the weld pass 9 and 10.

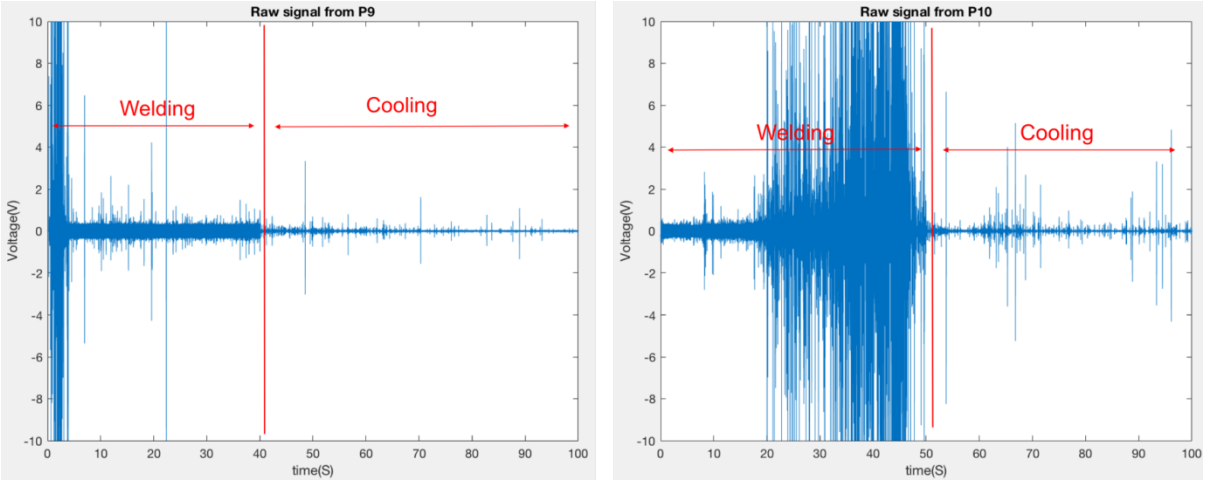

Figure 7-9 Raw signals of pass 9 and 10.

Left: 100 seconds signal of welding and cooling of pass 9

Right: 100 seconds signal of welding and cooling of pass 10

The photograph of pass 9 is in Figure 7-8; it does not have a visible crack on the surface of the welds. From the raw signal of pass 9 in Figure pass 9, there is a clustered high voltage signal at the beginning of the weld, which has more possibility to be mechanical noise. During the cooling period, the signal is quieter than the signal from other passes.

Pass 10 has a central line cracking, as shown in Figure 7-8. However, the central line cracking did not capture by the AE system. In Figure 7-9 right image: pass 10, the cooling period does not have a period like the last 20 seconds of pass five, which represent the final failure of the welds. However, during the recorded period, small cracks could still happen in the signal of pass 10.

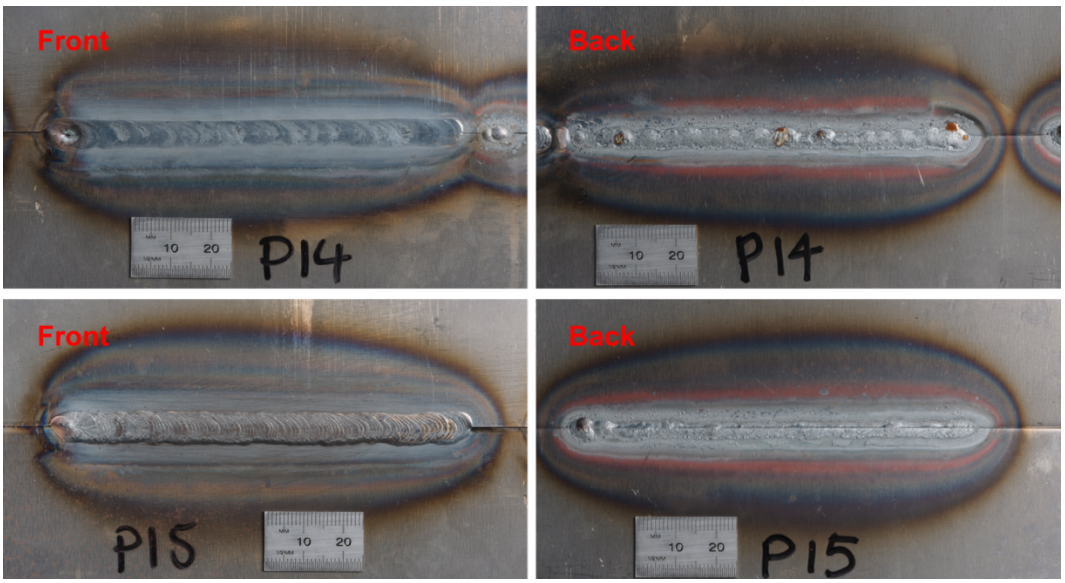

Figure 7-10 Photographs of the weld pass 14 and 15.

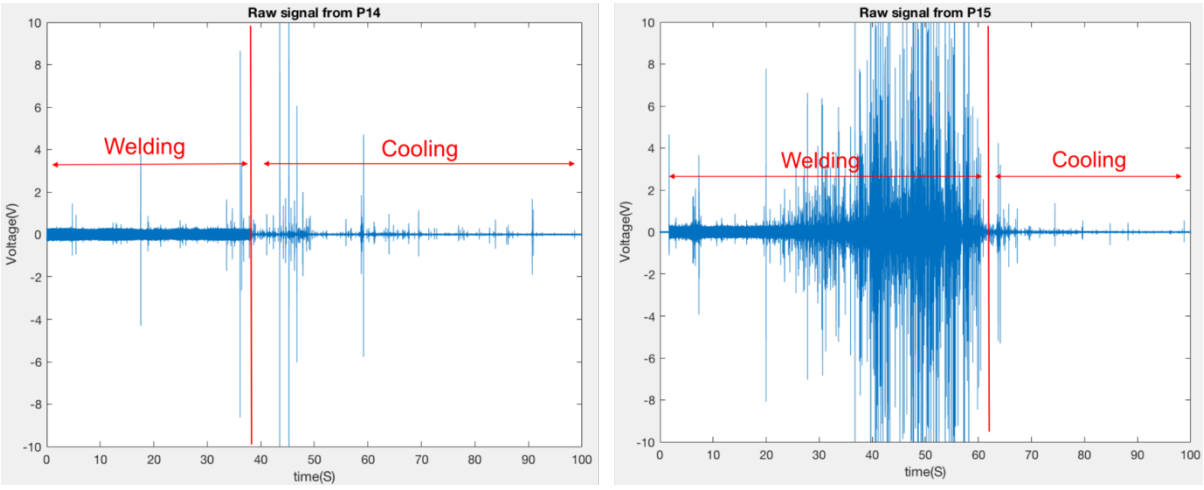

Figure 7-11 Raw signals of pass 14 and 15.

Left: 100 seconds signal of welding and cooling of pass 14

Right: 100 seconds signal of welding and cooling of pass 15

The photograph of pass 14 is in Figure 7-10; it does not have a visible crack on the surface of the welds. From the raw signal of pass 14 in Figure 7-11, overall, the signal is quieter than the signal from other passes. The photo of pass 15 is in Figure 7-10; it also does not have a visible crack on the surface of the welds. From the raw signal of pass 14 in Figure 7-11, during the welding period, the signal is much nosier than signals from other passes. Even under the surface, there might still be cracks, but it is hard to distinguish cracking signal from the noisy signal from the welding period of pass 15 since it is unclear what types of burst signals in during the welding period.

The pass 18 has a few linear cracks in the weld, as shown in Figure 7-12. The cracking signals can be found in the burst signal in the raw signal of pass 18 in Figure 7-13 left the image. For pass 19, both the weld in Figure 7-12 and the raw signal in Figure 7-13 are similar to pass 15.

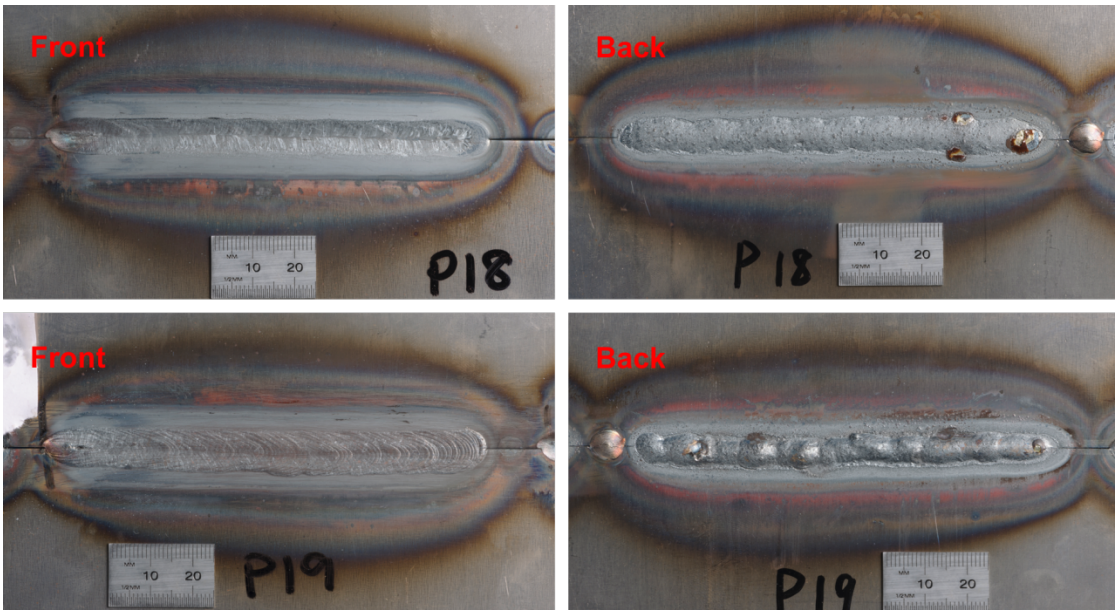

Figure 7-12 Photographs of the weld pass 18 and 19.

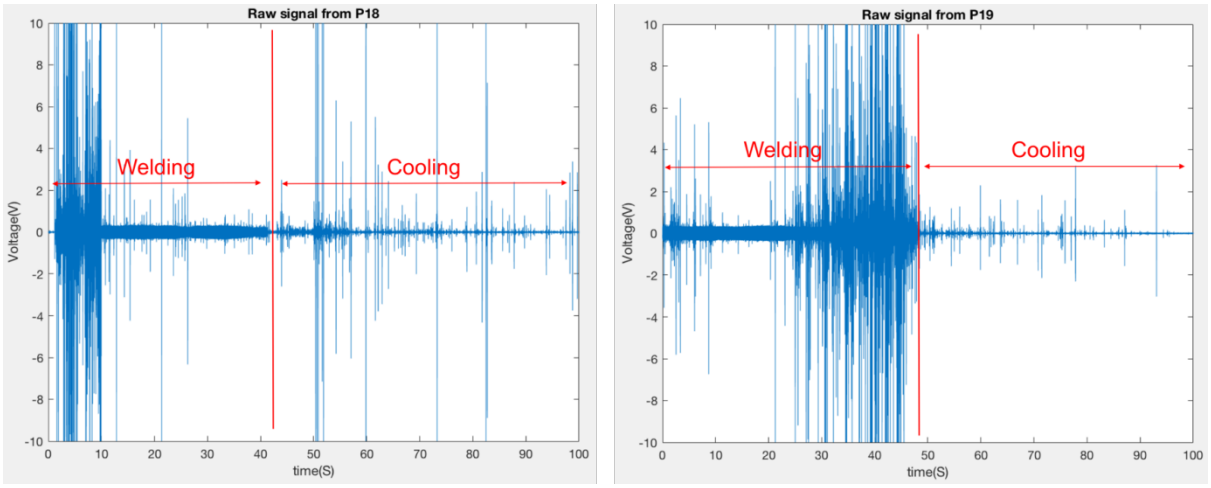

Figure 7-13 Raw signals of pass 18 and 19.

Left: 100 seconds signal of welding and cooling of pass 18

Right: 100 seconds signal of welding and cooling of pass 19

Pass 5 is the best choice for the study of cracking signal out of the passes above. The first 10 seconds of the signal and the FFT result of it are shown in Figure 7-14. Figure 7-14B and the filtered FFT result shows that in the first 10 seconds, the signal is mostly from the TIG welding process itself. The last 10 seconds of the signal, which is presented in Figure 7-15 A, the period has the major crack happened. The FFT result is shown in Figure 7-15 B. The PSD value of the last 10 seconds associated with cracking has two main high power parts: at a lower frequency range of 50 kHz - 180kHz and a higher frequency range of 250 kHz – 380 kHz. Comparing with the high PSD frequency range of the signal from the mechanical test, the frequency range 250 kHz – 380 kHz has a high possibility to be associated with the cracking events occurring in the weld.

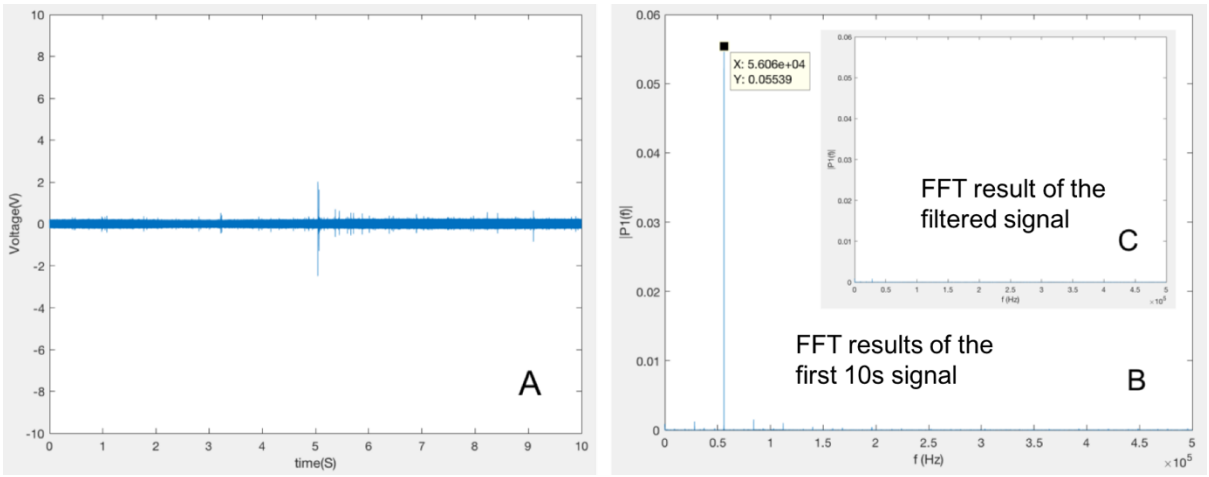

Figure 7-14 First 10 seconds recording of the trial pass 5, FFT result and filtered FFT result.

A. First 10 seconds recording of the trial pass 5

B. FFT results of the first 10s signal

C. FFT result of the filtered signal

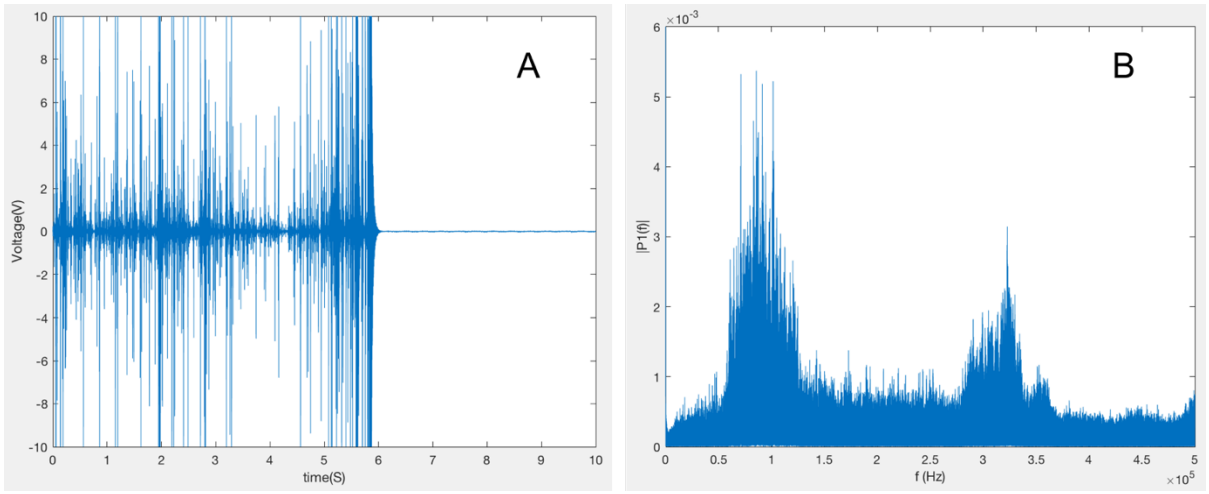

Figure 7-15 Last 10 seconds of the signal of the pass 5 and the FFT result.

A. Last 10 seconds recording of the signal of the trial pass 5

B. FFT results of the last 10s signal

Figure 7-16 is a series of 0.01 second of signals that separated from the last 10 seconds recording of the signal of the trial pass 5. The corresponding RMS values of the short signal are listed in Table 7-3. Figure 7-16 A and Figure 7-16 C are the spikes with smaller voltage

and the relevant FFT results in Figure 7-16 B and Figure 7-16 D show very low values of PSD. In the Figure 7-16 E and Figure 7-16 G are the higher level of spikes, there are two noticeable frequency ranges: 50 kHz - 180kHz and 250 kHz – 380 kHz that shows in Figure 7-16 F and H.

For Figure 7-16 I, K, and M are continuous signals from an extensive cracking period. Figure 7-16 J, L and N are the corresponding FFT results. In these three signals, there is a pattern can be observed that the longer the 'cracking' signal last (the higher is the RMS value), the higher the values of the PSD in the frequency range of 50 kHz - 180kHz. In Figure 7-16 P, which is the FFT results of the ending part of the 'cracking' signal, the higher frequency range which is from 250 kHz- 380 kHz, part disappeared, the 50 kHz – 180 kHz remained.

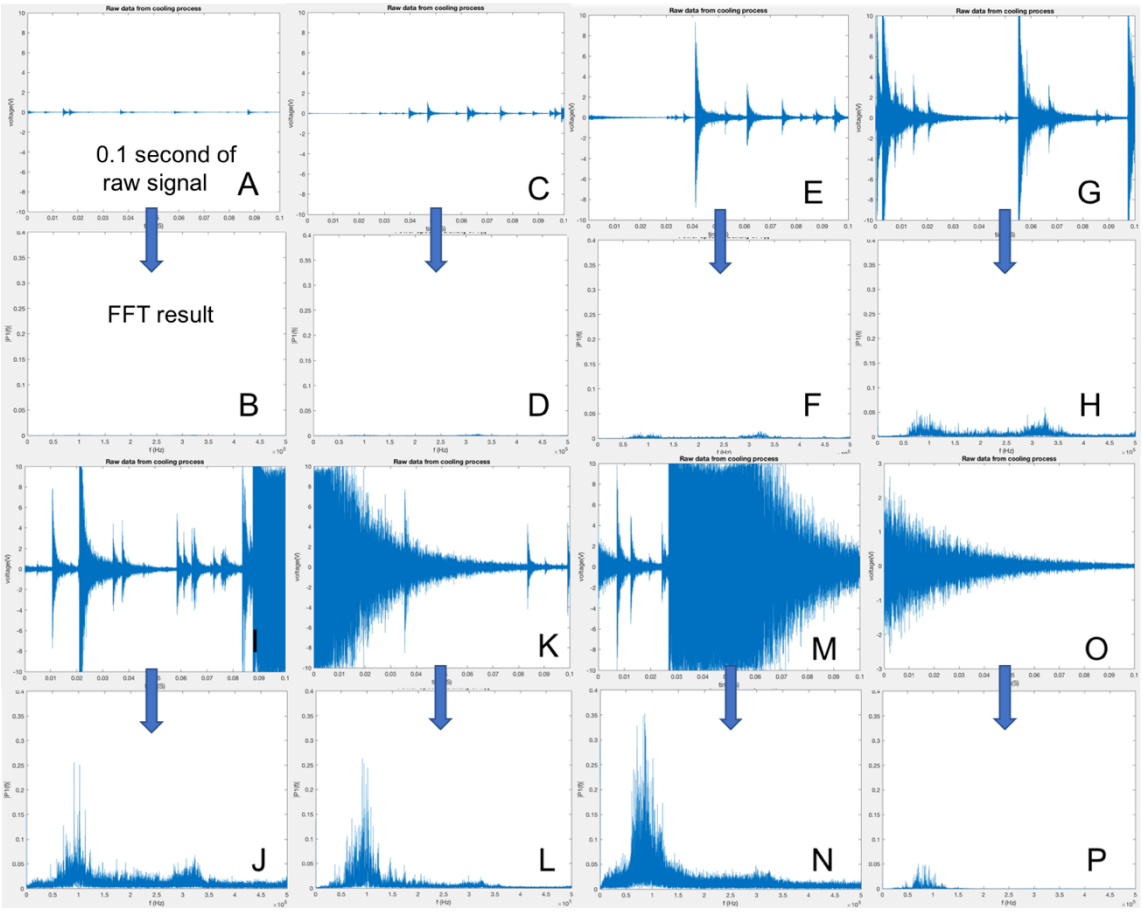

Figure 7-16 A series of 0.01 second of signals that separated from the last 10 seconds recording of the signal of pass 5.

Table 3-3 The RMS values of the individual spikes in Figure 7-16.

A	From 94.2 to 94.3 second.	RMS=0.0239
C	From 94.3 to 94.4 second.	RMS=0.0659
E	From 94.9 to 95.0 second.	RMS=0.3286
G	From 95.7 to 95.8 second.	RMS=1.0968
I	From 95.5 to 95.6 second.	RMS=2.7707
K	From 95.6 to 95.7 second.	RMS=2.3277
M	From 95.8 to 95.9 second.	RMS=4.2861
O	From 95.9 to 96.0 second.	RMS=0.2859

One event which lasts around 0.1 second has been taken as an example for more detail analysis, as shown in Figure 7-17. Figure 7-17A is the plot of one of the AE events occurring in the last 10 seconds. From the raw signal, no significant difference can be observed from the mechanical testing signal. From the FFT of the 0.01-second signal, two high PSD frequency range can be found: a lower frequency part in the range of 50kHz - 180kHz and a higher frequency part in the range of 250 kHz -380 kHz. The spectrogram of the 0.1 second of the signal is shown in Figure 7-17C. The frequency range of 250 kHz-380 kHz has a higher PSD value in the beginning but attenuates faster than the PSD in a frequency range of 50 kHz -180 kHz. A more explicit interpretation of this trend is shown in Figure 7-17D in which the FFT result associated with the 0.5ms of the signal in the period marked as 1-9 in Figure 7-17A are presented. This trend indicates that the PSD in the two frequency ranges is both closely related to the occurrence of cracking activity. The different behaviour of the PSD value can potentially be used to identify the part of the AE signal related to the cracking formation.

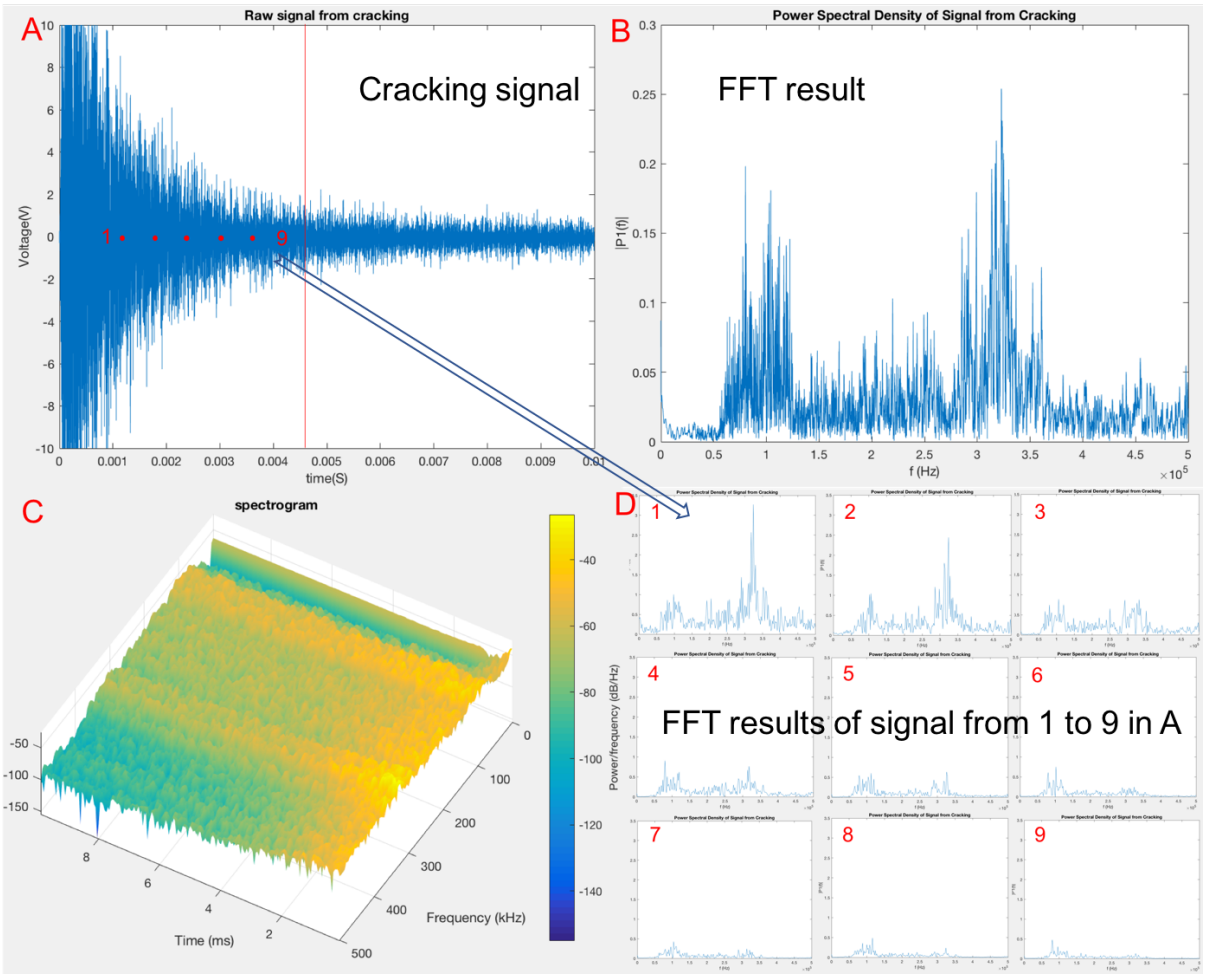

Figure 7-17 Detail analysis of a cracking signal.

A. 0.01s of cracking signal.

B. FFT result of the 0.01s of the signal.

C. Spectrogram

D. FFT results of the 0.5ms of the signal in the period marked as 1-9 in A.

Figure 7-18 and Figure 7-19 are another two examples of crack-related signals analysis. The change through time in the two frequency ranges occurs at 50 kHz – 180 kHz and 250 kHz - 380 kHz. The results are similar to those seen in Figure 7-17. In both Figure 7-18 and 7-19, in the right image 1-9 initially the higher frequency of 250 kHz - 380 kHz has higher PSD values, but then the values decline through a time fast. In the end, the PSD values in the lower frequency range 50 kHz – 180 kHz are higher than in the range of 250 kHz-380 kHz.

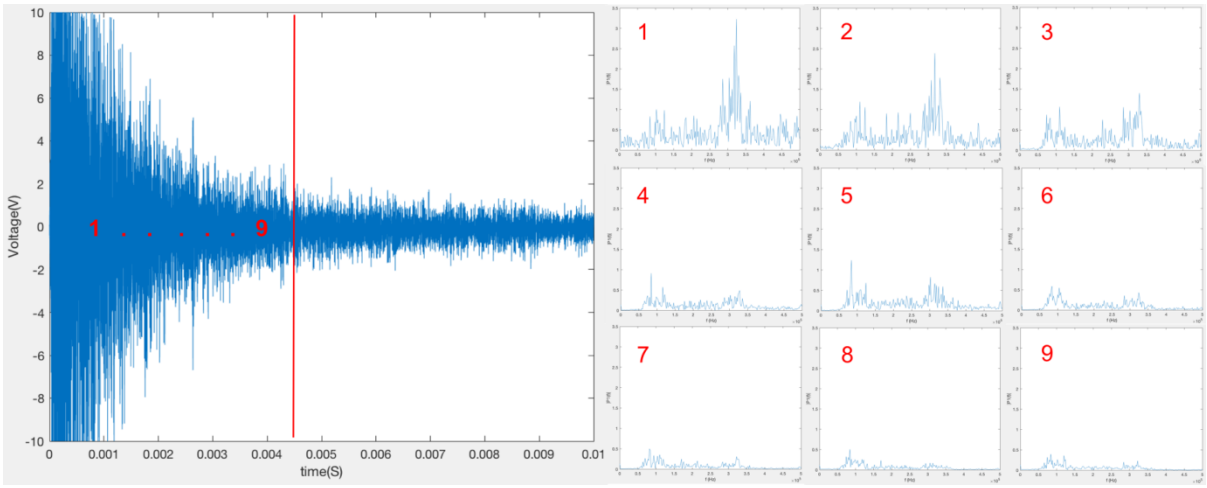

Figure 7-18 Detail analysis of a cracking signal.

A. 0.01s of cracking signal.

B. FFT results of the 0.5ms of the signal in the period marked as 1-9 in A.

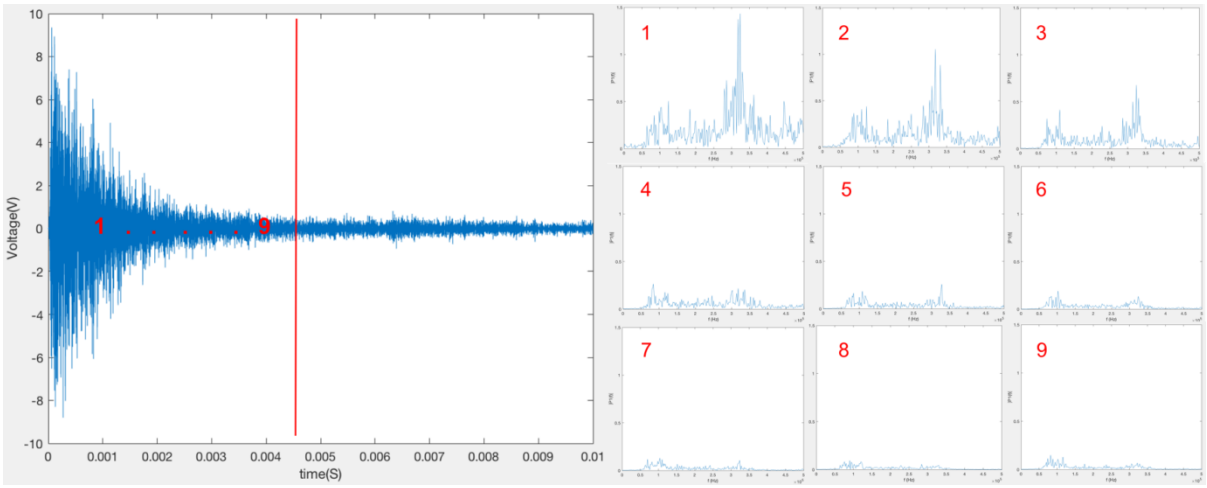

Figure 7-19 Detail analysis of a cracking signal.

A. 0.01s of cracking signal.

B. FFT results of the 0.5ms of the signal in the period marked as 1-9 in A.

7.4 Conclusion remarks

In this chapter, the different types of discontinuous signals collected and analysed have been discussed That includes background signal, torch moving, arc ignition, gas purging, nut dropping, hammer knocking and plate sliding. The cracking-related signals from TIG process with CS70 material are also collected and analysed. The cracking-related signals and other signals arising from background sources are compared. The main findings from the analysis of the results obtained are listed below.

a. From the frequency analysis of the impact-arising signals, the high PSD value is mostly observed in the frequency range of 50 kHz – 180 kHz, which is the same as the arc ignition signal. Other signals from the surrounding environment such as laboratory noise, gas release noise and torch movement noise are rather insignificant.
b. The frequency features associated with cracking in the signal are observed in the frequency range of 250 kHz – 380 kHz and 50 kHz – 180 kHz. From the further analysis of the available results, the PSD value in the higher frequency range is typically higher than in the lower frequency range for the features associated with cracking.
c. The difference is more distinct at the beginning of the recorded AE event. As the higher frequency signal tends to attenuate faster than the lower frequency, the difference becomes smaller over time. The two frequency ranges 250 kHz – 380 kHz and 50 kHz – 180 kHz are essential for the separation of the different AE sources and the detection of the cracking in welds.

To conclude, the mechanical-related signal has the signature frequency range of 50kHz-180kHz. For cracking-related signal, the signature frequency range is 250 kHz – 380 kHz and 50 kHz – 180 kHz. The pattern in changes of PSD value in different frequency range could potentially be used for the identification of cracking and prediction of welding quality.

Chapter 8

Real time monitoring

This chapter describes the methods used to determine whether the results obtained in chapter 7 of chapter 6 can be used to detect weld cracking, experimental design, results, and subsequent analysis. Section 8.1 describes the research plan and proposed methods. Section 8.2 details the experimental setup, equipment and settings. The results are discussed in Section 8.3. Finally, Section 8.4 summarises the main findings of the study.

8.1 Approach

In chapter 6 and 7, the frequency features in different AE source in terms of Power Spectral Density distribution, wave modes and arriving time, few conclusions have been reached: Including:

a) From the raw signal, the unwanted noise from the welding process has very distinctive frequency and it is easy to filter out using discrete wavelet transformation.
b) From the frequency analysis results of the mechanical signals, the high PSD value is mostly observed in the frequency range of 50 kHz – 180 kHz.
c) The frequency features associated with cracking in the signal are observed in the frequency range of 250 kHz – 380 kHz and 50 kHz – 180 kHz.
d) The difference is more distinct at the beginning of the recorded AE event. As the higher frequency signal tends to attenuate faster than the lower frequency, the difference becomes smaller over time.

In this chapter, the analysis of results from chapter 6 and 7 has been used for the development of the real-time monitoring methodology. TIG welding with CS70 steel and MAG welding with CS70, EN8 trials with different levels of defects were carried out. The first method for the detection of a cracking signal is Cross-correlation analysis. Cross-correlation analysis calculates the similarity of two series as a function of the time-lag shift. In signal processing,

it reflects the various frequency components held in common between the two signals. This technique is based on the concept that signals generated by the same source have consistent spectral characteristics. A short but sufficiently long part of the signal which is related to cracking is selected as a template. Then the similarity is calculated between the raw signals obtained and the template. The second method for the detection of a cracking signal is a customised pattern recognition algorism to accommodate the frequency features of the cracking signal. These two real-time analysis approaches used are discussed and compared. The collected signals from the TIG and MAG processes are processed using both approaches and results are compared. The TIG trials were inspected using visual inspection, LPI and radiographic inspection. The accuracy of the results and possibilities for improvement are discussed as well.

8.2 Experiments and characterisation

8.2.1 TIG trial and characterization

The TIG trials were performed on the CS70 steel plate. The welds 1A to 9A and 1B to 10B are 2-3 cm short welds, with current 130 A, voltage 12 V and travel speed 9.8cm/min. All of these welds were performed autogenously.

Table 8-1 is the radiographic inspection results for the trials. The detected defects include isolated porosities, clustered porosities and branch cracking. For individual trials, radiographic inspection results will be discussed individually.

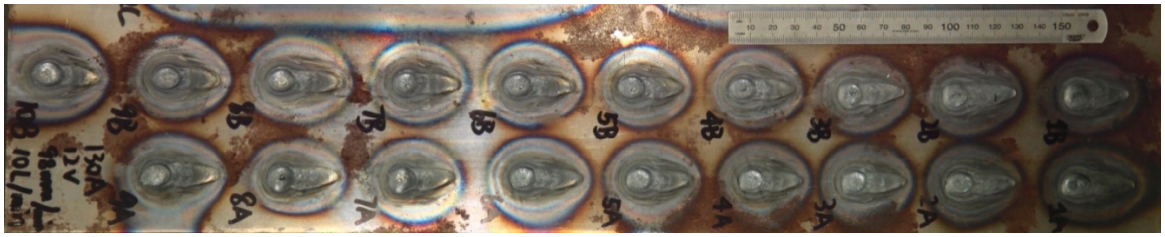

Figure 8-1 Photograph of the CS70 plate.

Table 8-1 Radiographic inspection results.

RESULTS	Acceptance criteria: Note particular indications, but don't need specific sizing or assessment.		
Radiograph identity	Weld/Sample identity	Accepted/ Rejected	Comments
C0383	MI 1461 A-B	N/A	Isolated porosity, cluster porosity and branch cracking noted.
C0384	MI 1461 B-C	N/A	Isolated porosity, cluster porosity and branch cracking noted.

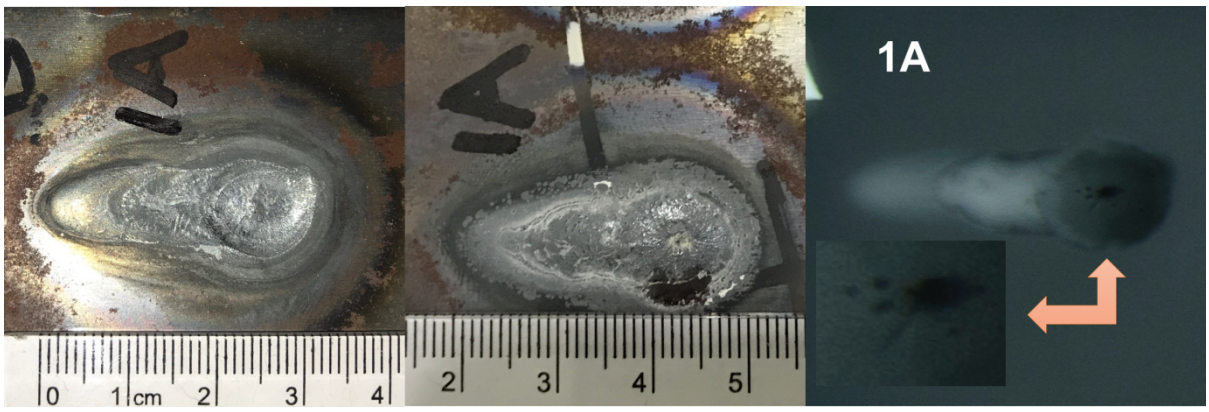

Figure 8-2 Photos of weld cap/ root of trial 1A and radiographic inspection result.

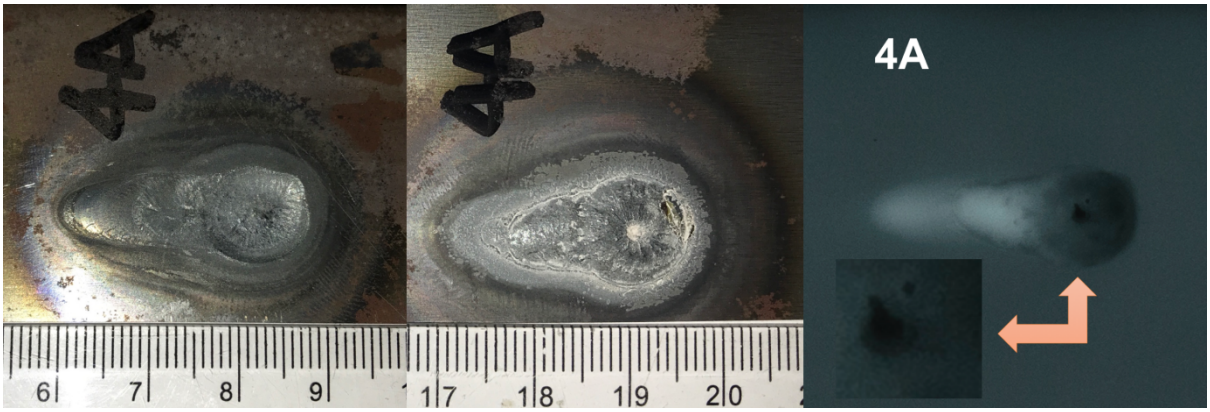

Figure 8-3 Photos of weld cap/ root of trial 4A and radiographic inspection result.

The photographs of the welds are in Figure 8-2 to 8-12. From weld cap of 1A trial in Figure 8-2, cracking can be observed. In 1A weld root, there are porosities present at the end of the weld. From the radiographic inspection result, linear cracking and porosities can be observed. In Table 8-1 and Table 8-2, from the LPI, 1 mm linear cracking and porosities are noted.

From weld cap of 4A trial in Figure 8-3, no obvious cracking can be observed. In 4A weld root, there are porosities at the end of the weld. From the radiographic inspection result, linear cracking and porosities can be observed at the end of the weld. In Table 8-1 and Table 8-2, from the LPI, 2 mm linear crack and porosities are noted.

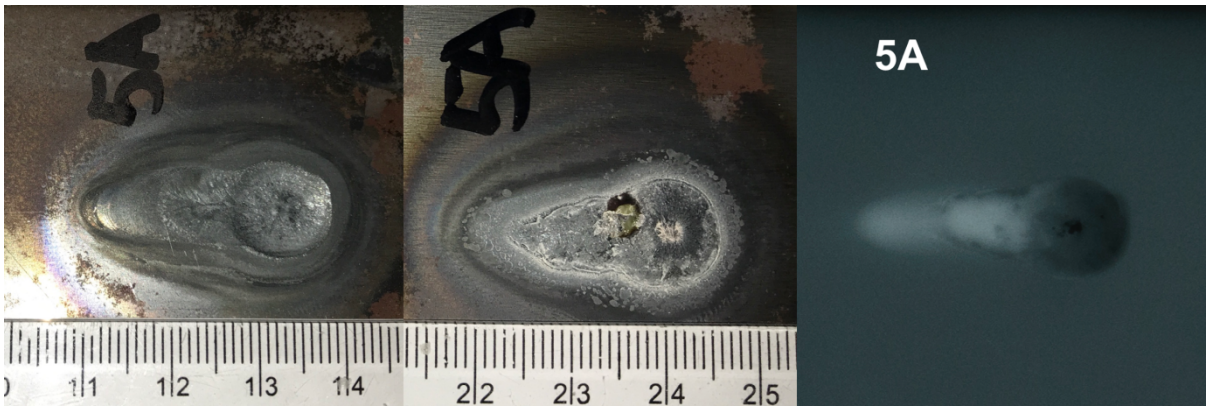

Figure 8-4 Photos of weld cap/ root of trial 5A and radiographic inspection result.

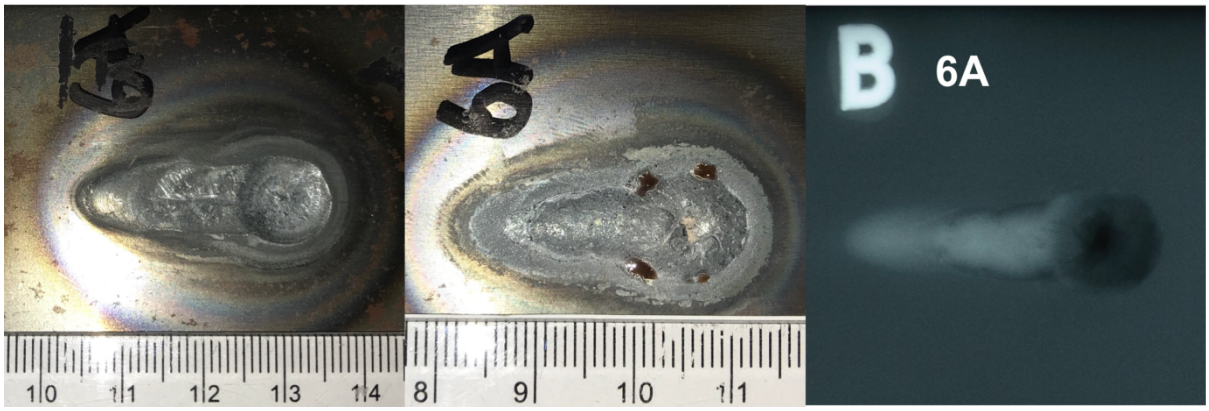

Figure 8-5 Photographs of weld cap/ root of trial 6A and radiographic inspection result.

In Figure 8-4 trial 5A, there are no noticeable cracks can be seen. On the root of 5A, porosities can also be observed. From the radiographic inspection result, linear cracks can be seen, from the LPI results, there are no cracks noted, means the cracks are not on the surface.

In Figure 8-5 trial 6A, there is no noticeable cracking which can be seen. On the root of 6A, porosities can also be observed. From the radiographic inspection result and LPI result, also no noticeable cracking can be seen.

From weld cap of 8A trial in Figure 8-6, a crack can be observed. In 4A weld root, there are porosities at the end of the weld. From the radiographic inspection result, crater cracking and porosities can be observed at the end of the weld. In Table 8-1 and Table 8-2, from the LPI, porosities are noted.

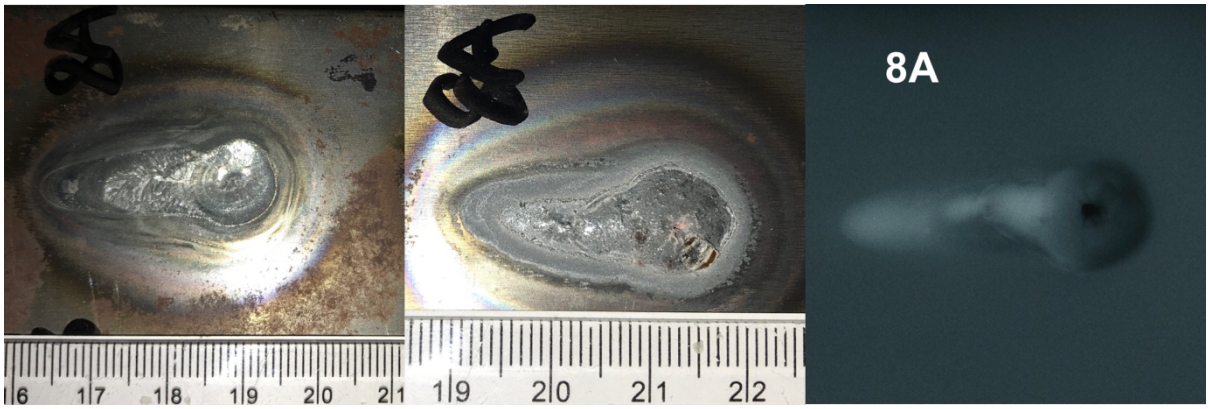

Figure 8-6 Photographs of weld cap/ root of trial 8A and radiographic inspection result.

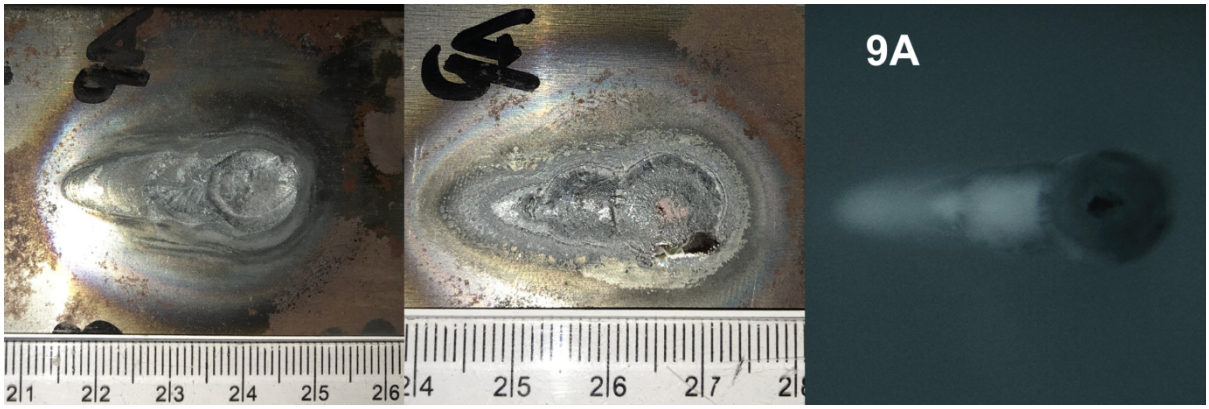

Figure 8-7 Photographs of weld cap/ root of trial 9A and radiographic inspection result.

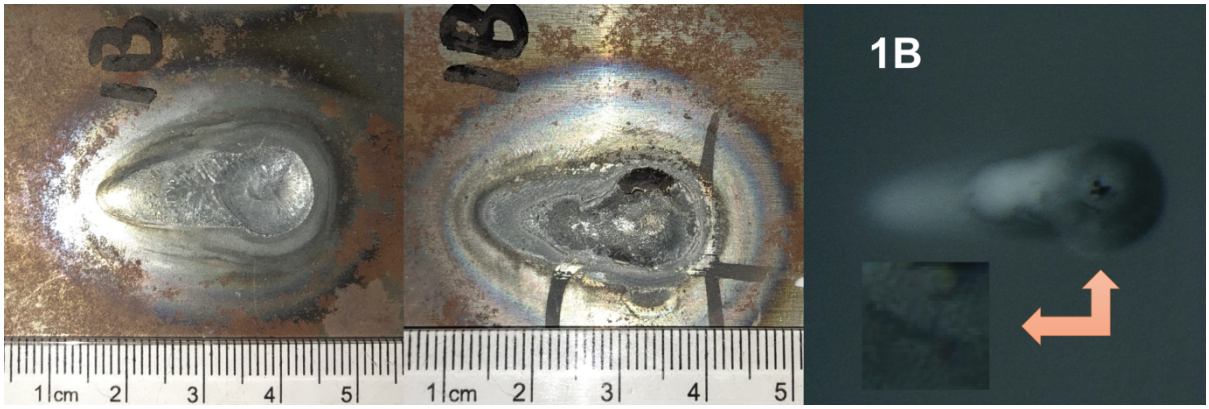

Figure 8-8 Photos of weld cap/ root of trial 1B and radiographic inspection result.

In Figure 8-7 trial 9A, no noticeable cracks can be seen. In the root of 9A, porosities can also be observed. From the radiographic inspection result and LPI result, also no noticeable cracks can be seen.

From the inspection of the weld cap of 1B trial in Figure 8-8, cracking can be observed. In 1B weld root, there are porosities at the end of the weld. From the radiographic inspection result, linear cracking and porosities can be observed. In Table 8-1 and Table 8-2, from the LPI, 5 mm linear crack and porosities are noted.

From weld cap of 2B trial in Figure 8-9, large size cracks can be observed. In 2B weld root, there are porosities at the end of the weld. From the radiographic inspection result, crater cracking and porosities can be observed. In Table 8-1 and Table 8-2, from the LPI, crater cracking and porosities are noted.

From weld cap of 4B trial in Figure 8-10, cracks can be observed; In 4B weld root. There is also porosity at the end of the weld. From the radiographic inspection result, a crater crack and porosities can be observed. In Table 8-1 and Table 8-2, from the LPI, a crater crack and porosities are noted.

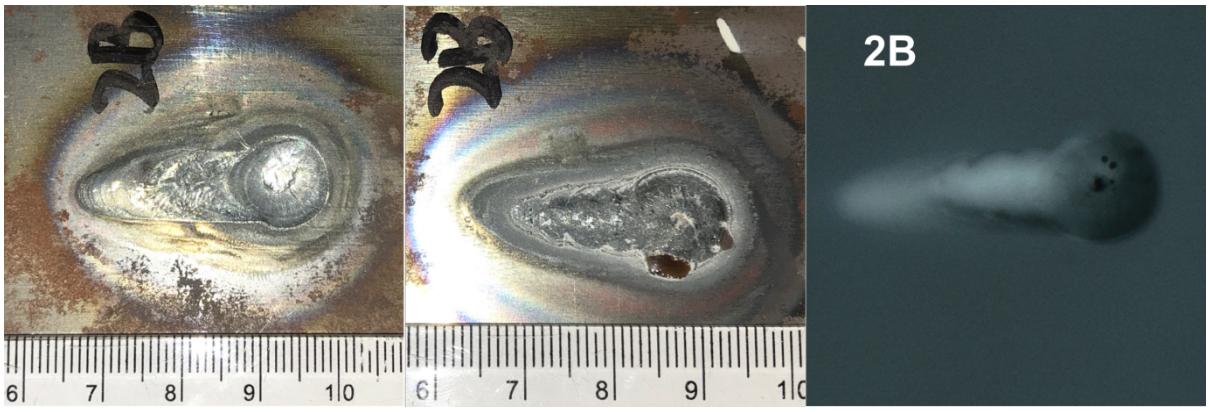

Figure 8-9 Photos of weld cap/ root of trial 2B and radiographic inspection result.

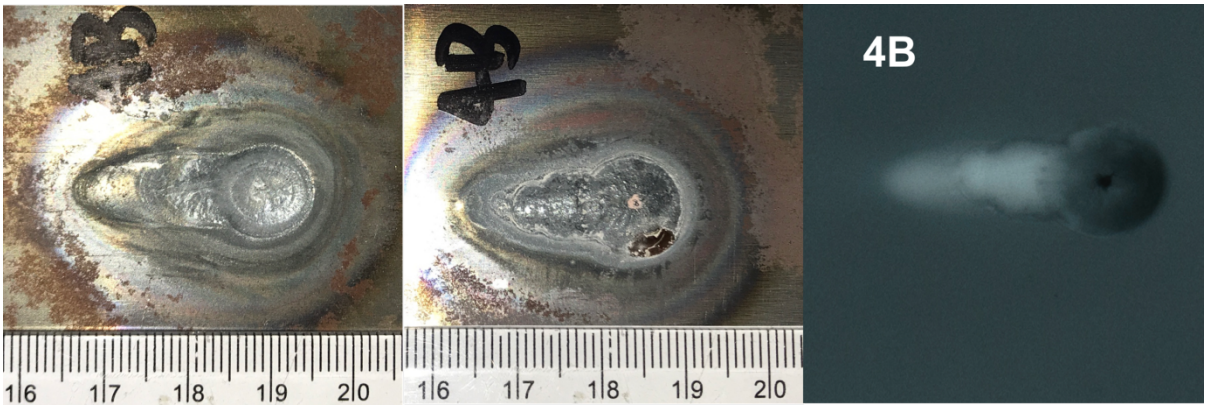

Figure 8-10 Photos of weld cap/ root of trial 4B and radiographic inspection result.

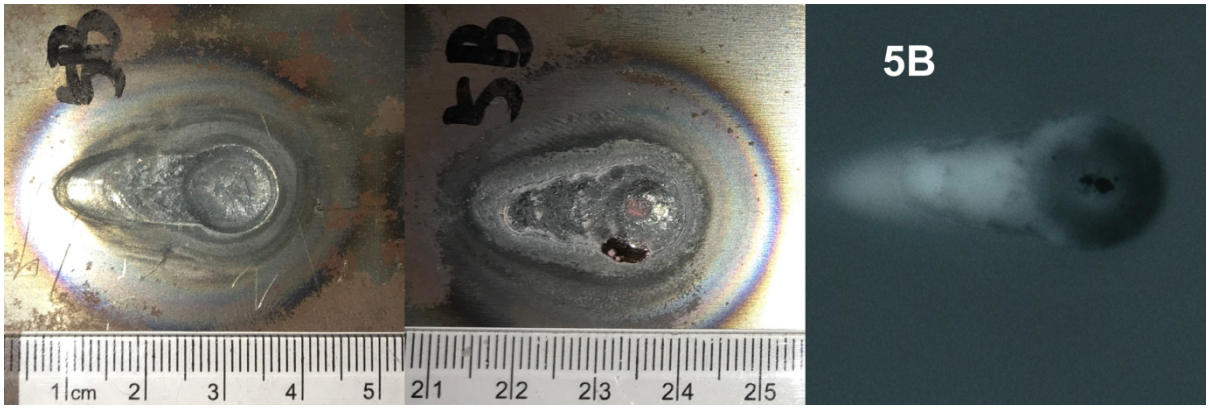

Figure 8-11 Photos of weld cap/ root of trial 5B and radiographic inspection result.

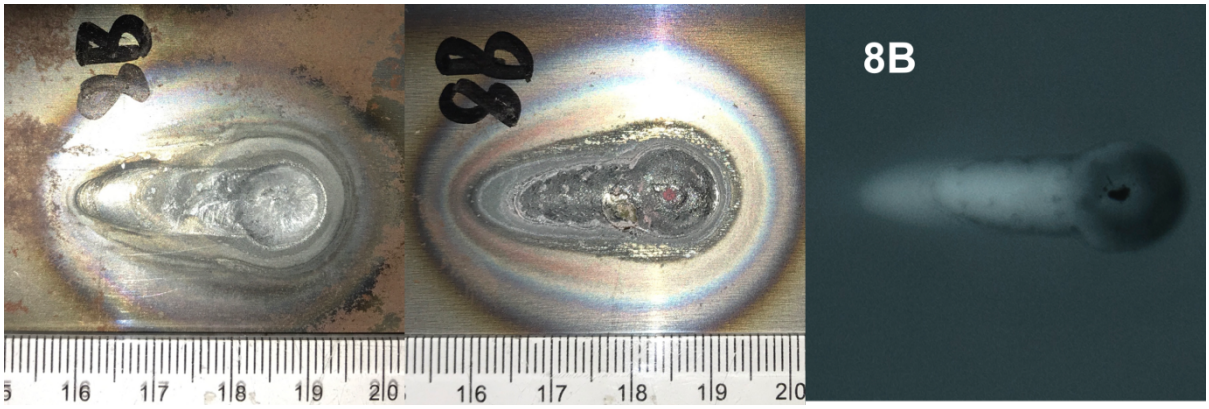

Figure 8-12 Photos of weld cap/ root of trial 8B and radiographic inspection result.

From weld cap of 5B trial in Figure 8-11, large size cracks can be observed; In 5B weld root, there is porosity at the end of the weld. From the radiographic inspection result, crater crack and porosities can be observed. In Table 8-1 and Table 8-2, from the LPI, crater crack and porosities are noted.

From weld cap of 8B trial in Figure 8-12, cracks can be observed; In 8B weld root, there is porosity at the end of the weld. From the radiographic inspection result, crater crack and porosities can be observed. In Table 8-1 and Table 8-2, from the LPI, crater crack and porosities are noted. The results of the defects in the trials are summed in Table 8-4.

Table 8-2 Liquid Penetrant Inspection result (weld cap).

RESULTS	Acceptance criteria: note all indications found.
Surface	Accepted Rejected
100% of weld cap	N/A

Location Comments
1A- Linear crack in the Stop start, 1mm in length. 1B- Linear crack in the Stop start, 5mm in length. 2B- Crater crack in the Stop start, 1mmØ. 3B- Crater crack in the Stop start, 5mmØ. 4B- Crater crack in the Stop start, 4mmØ. 4A- Linear crack in the Stop start, 2mm in length. 5B- Crater crack in the Stop start, 4mmØ. 6B- Crater crack in the Stop start, 1mmØ. 7B- Crater crack in the Stop start, 2mmØ. 7A- Crater crack in the Stop start, 4mmØ. 8A- Surface pore in the Stop start, 3mmØ. 9B- Linear crack in the Stop start, 4mm in length. 1C- Surface pore in the Stop start, 1mmØ. 2C- Surface pore in the Stop start, 1mmØ.

Table 8-3 Liquid Penetrant Inspection result (weld root).

RESULTS	Acceptance criteria: note all indications found.
Surface	Accepted Rejected
100% of weld root	N/A

Location Comments
1A- Surface pore in the Stop start, 2mmØ. Slag noted, 6mm in length. 1B- Surface pore in the Stop start, 1mmØ. 2A- Surface pore in the Stop start, 2mm Ø. Slag noted, 6mm in length. 2B- Surface pore in the Stop start, 1mm Ø. 3A- Surface pore in the Stop start, 1mm Ø. 3B- Surface pore in the Stop start, 1mm Ø. 4A- Stop start noted. 4B- Surface pore in the Stop start, 1mm Ø. Slag noted, 6mm in length. 5A- Surface pore in the Stop start, 1mm Ø. 5B- Slag noted, 6mm in length. 6A- Surface pore in the Stop start, 6mm Ø. 8A- Surface pore in the Stop start, 1mm Ø. Slag noted, 3mm in length. 9A- Surface pore in the Stop start, 2mm Ø. 10B- Surface pore in the Stop start, 1mm Ø. 2C- Slag noted, 10mm in length.

Table 8-4 IDs of the welds and defects.

AE data	ID	Defects
1431	1A	Linear crack and surface pore.
1435	4A	Linear crack.
1436	5A	Linear cracks
1437	6A	Surface pore.
1440	8A	Crater crack, surface pore and slag.
1441	9A	Surface pore.
1442	1B	Linear crack and surface pore.
1443	2B	Crater crack and surface pore.
1446	4B	Crater crack, surface pore and slag.
1447	5B	Crater crack and slag.
1450	9B	Linear crack and surface pore.

8.2.2 MAG welding trial

The trials were produced in TWI Middleborough. The principle of MAG welding is explained in chapter 5. The materials used in the trials include CS70 carbon steel, EN8 steel. The experiment configurations are listed in Table 8-5. The signal was collected with 1M Hz.

Table 8-5 Experiment configurations of MAG trials.

ID	Material	Thickness (mm)	Current (A)	Voltage (V)	WFS (m/min)	TS (cm/min)
1782	CS70	3	166	19	6.37	41
1783	CS70	3	168	19	6.37	41
1785	CS70	3	160	21	6.37	41
1804	EN8	3	154	15.5	5.91	59
1806	EN8	3	152	16.5	6.22	59
1807	EN8	3	153	16.5	5.5	59

8.3 Development of the analysing method

8.3.1 Correlation analysis

Cross-correlation analysis calculates the similarity of two series as a function of the time-lag shift. In signal processing, it reflects the various frequency components held in common between the two signals. This technique is based on the concept that signals generated by the same source have consistent spectral characteristics.

A short period of a signal which is related to cracking is selected as a template, then calculates the similarity between raw signal and the template.

The cracking-related signals discussed in chapter 7 are the potential templates for the detection of cracking activity. For the current analysis, a 0.005 s signal has been used as the template. This template is from a period during which cracking happened, as shown in Figure 8-13. The area that circled in Figure 8-13 is most likely to contain the cracking signal, which is a suitable period for selecting the template.

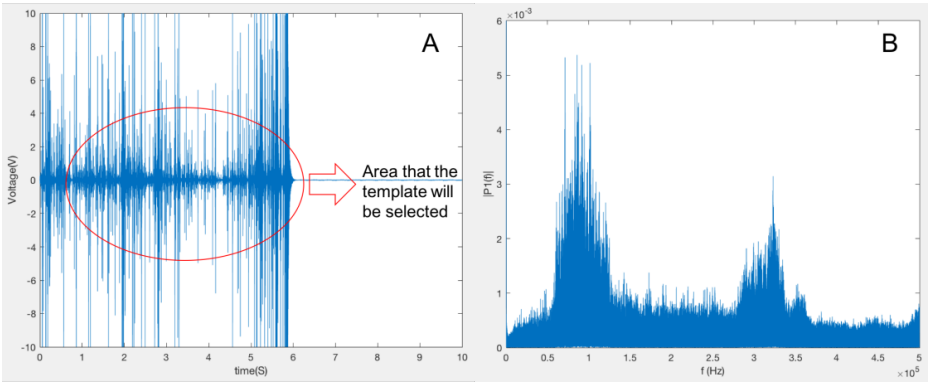

Figure 8-13 The selection of template.

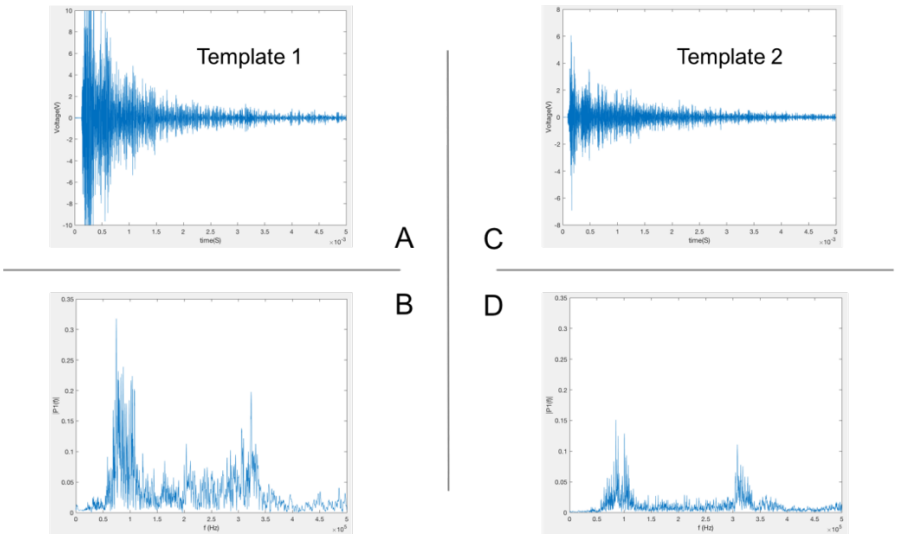

Figure 8-14 Selected templated and FFT results.

A and C two templates that selected from the circled area in Figure 8-13. B and D are the corresponding FFT results.

The FFT results of the templates are shown in Figure 8-14 B and D: typical frequency distribution of signals related to cracking. A 0.005-second-long time period related to the crack propagation has been selected from the raw signal as a template. From the results detailed in chapter 7, within the 0.005 second time-period, the frequency also changes through time. However, the 0.005 second time-period can represent the whole cracking signal, so this period is selected for the cross-correlation analysis.

Figure 8-15A and Figure 8-15D are raw signals from welding processes, Figure 8-15B and Figure 8-15E are the corresponding cross-correlation result using template 1. Figure 8-15C and Figure 8-15F are cross-correlation result using template 2. In raw welding signal in Figure 8-15A is quieter compared to the raw welding signal in Figure 8-15D. In Figure 8-15D, towards the end of the signal, there are two big spikes. In the cross-correlation results in Figure 8-15B and Figure 8-15C, there are three spikes in the plot. However, the similarities are very low compared to the results in Figure 8-15E and Figure 8-15F. The results based on the two templates are very similar except for the similarity index obtained. The reason for this difference is because the overall PSD value of template 1 is higher than template 2. However, the frequency distributions of the two templates are very similar, so the results from the two templates look similar.

Figure 8-16A and Figure 8-16D show the raw signals from cooling processes, Figure 8-16B and Figure 8-16E are the corresponding cross-correlation result using template 1. Figure 8-16C and Figure 8-16F show the cross-correlation result using template 2. From the results from both cooling signals, indicate a big spike in similarity, which suggests the occurrence of cracking activity. The results for the two templates are similar with both signals arising from cooling except that the similarity values are different. The results show that the two templates

could both work as a template for cross-correlation analysis. Template 1 is used as a template for the rest of the processing in this chapter.

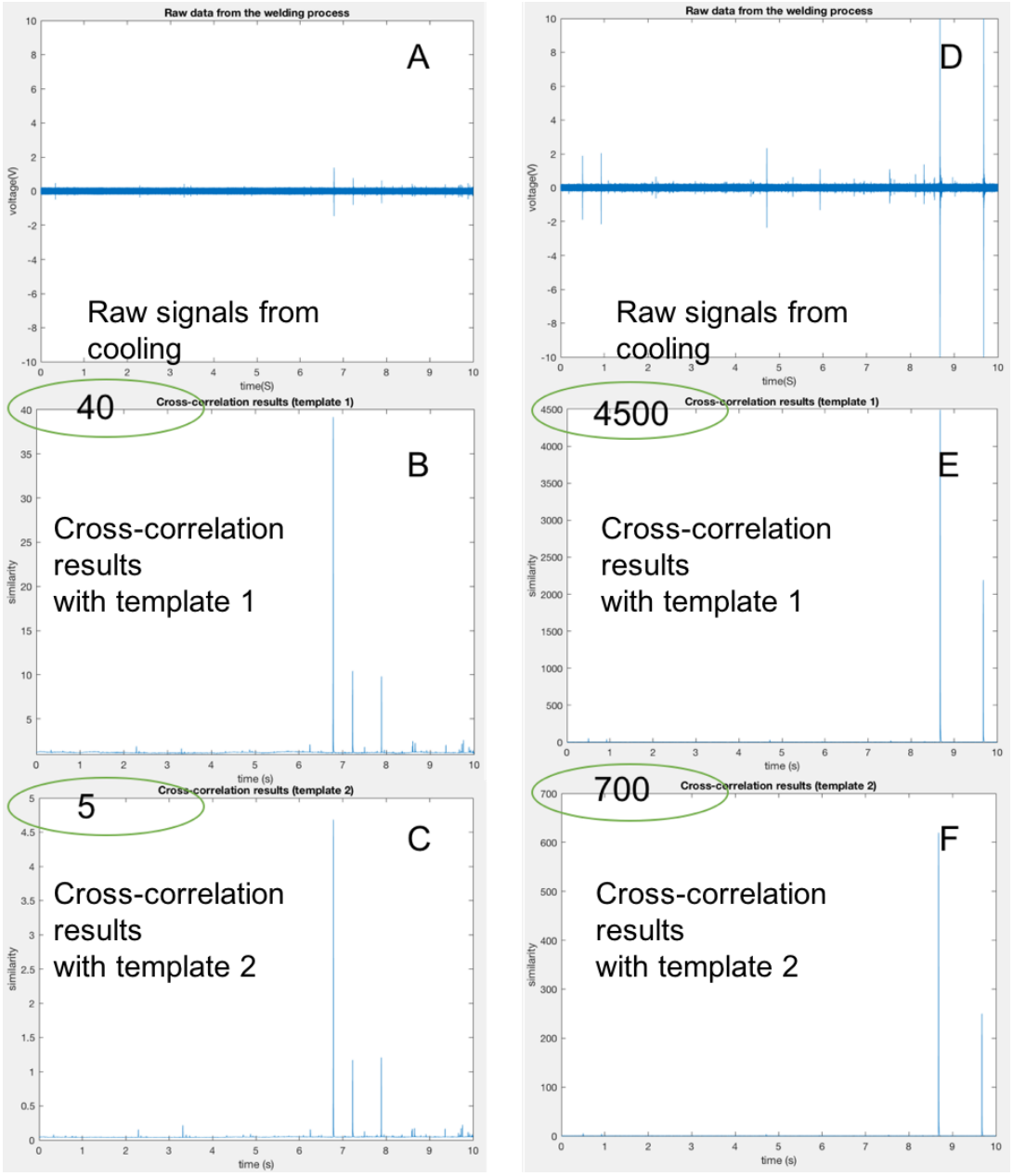

Figure 8-15 The cross-correlation result welding process.

A and D: raw signals from welding processes.

B and E: Cross-correlation results with template 1.

C and F: Cross-correlation results with template 2.

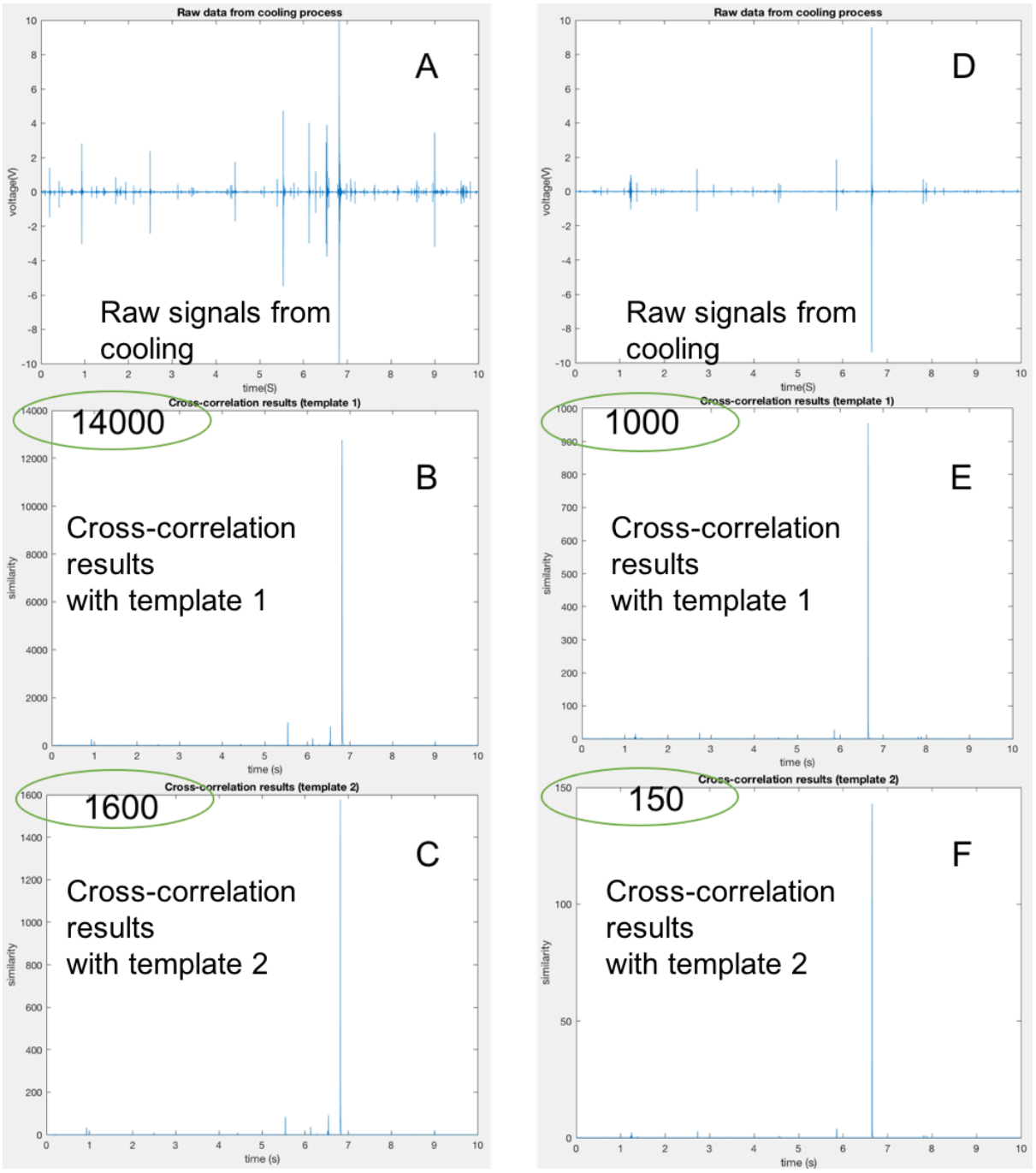

Figure 8-16 The cross-correlation result from cooling processes.

A and D: Raw signals from cooling processes.

B and E: Cross-correlation results with template 1.

C and F: Cross-correlation results with template 2.

8.3.2 Pattern recognition analysis

The pattern recognition algorithm has been employed to accommodate the frequency features of the cracking signal, frequency distribution of cracking signal and mechanical signal. The Power Spectral Density of cracking AE signal and mechanical AE signal from knocking on the plate is shown in the Figure below. For the signal from cracking, high power of frequency mainly located in two parts. For the mechanical noise, high power mainly located in one part: lower frequency (50-200kHz).

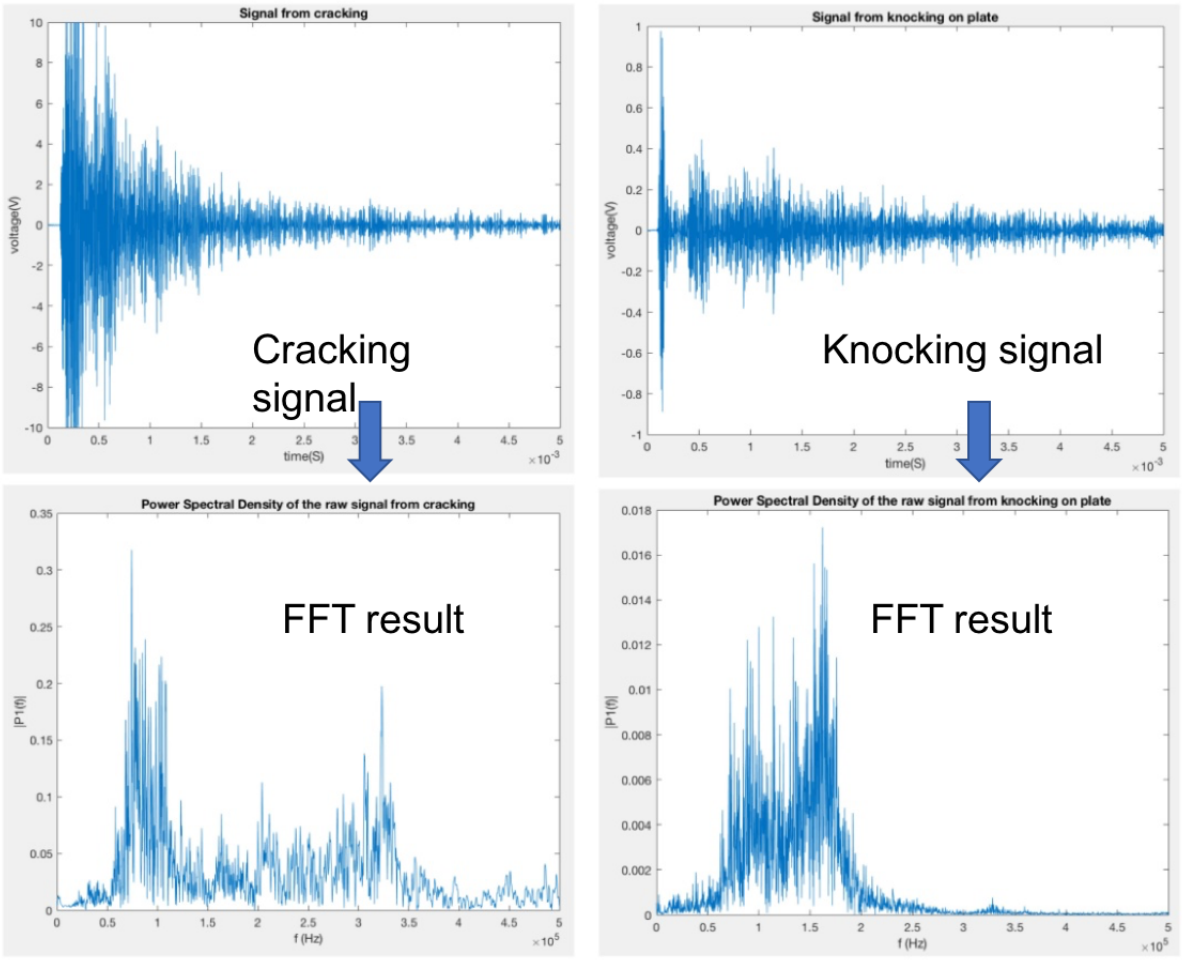

Figure 8-17 Signals of cracking and knocking on plate.

Left two images: Raw signal of cracking and its FFT.

Right two images: Raw signal of knocking on the plate and its FFT.

From the previous results, it has been found out that for the cracking signal, the higher frequency part of the signal arrives slightly before the lower frequency part (different wave mode has different travel speed in the material); the lower frequency part attenuates slower than the higher frequency part. However, with mechanical noise, there is no distinctive difference in arriving time.

Given the provided cracking signal template, the cracking-related signal will have a positive spike first, following a negative value. The mechanical noise and other AE activities will give a negative value only.

The algorism consists of mainly three parts. The first part is to take 500 points of data (0.5ms), the second part is to calculate the FFT of the 500 points of signal, which can get the power distribution of the frequency range from 0-500kHz. Then the third part is to calculate the difference in power between the frequency range of 250kHz-380kHz and 50kHz-180kHz. Then the next 500 points in the signal will be calculated in the same way until the end of the process. The mechanical AE signal will only have a negative value, the cracking-related signal will have a positive spike first, following a negative value. The algorism is written by the frequency feature of the cracking signal. Figure 8-18 is an illustration of the algorism.

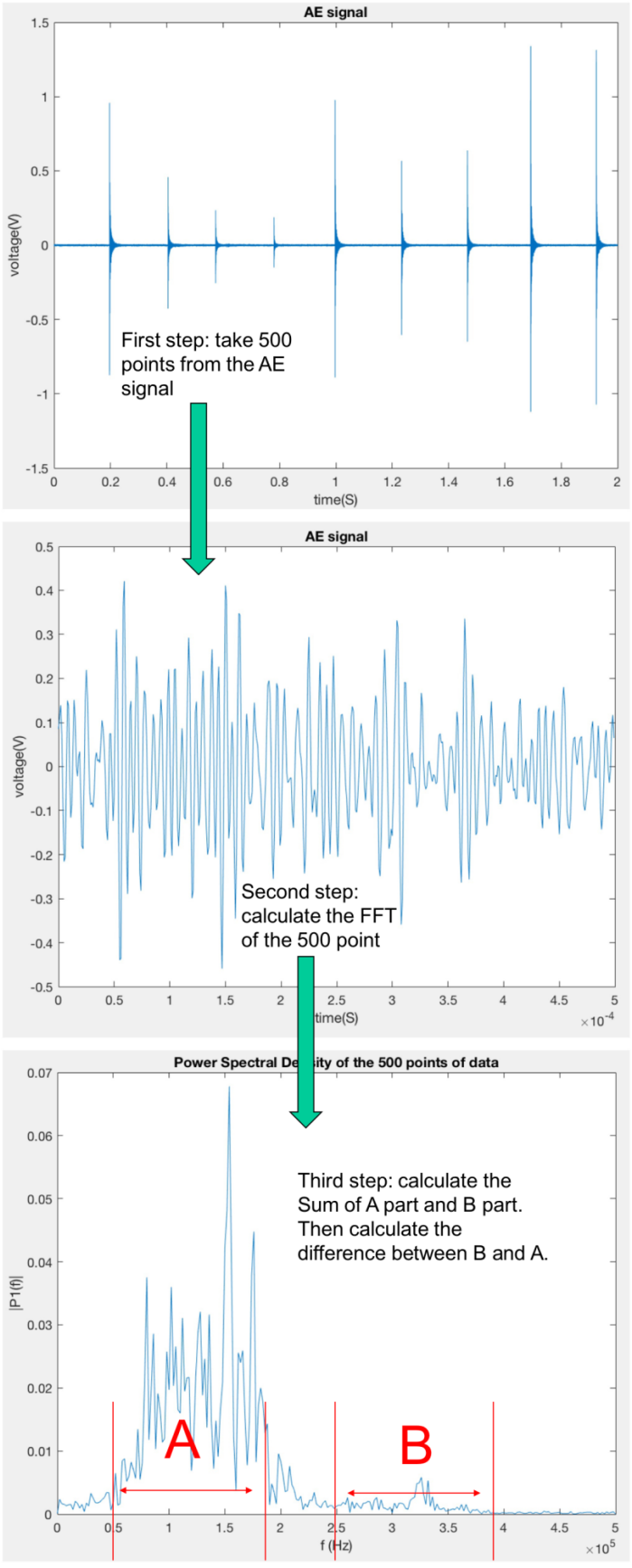

Figure 8-18 Illustration of the Pattern recognition analysis algorism.

Results of Cross-correlation and pattern recognition analysis of AE mechanical signal are plotted in Figure 8-19.

Action like knocking on the plate is one of the methods to test the AE system before collecting the signal from welding. It normally lasts 2-10s. In Figure, 8-19A and Figure 8-19D are the raw signals: the mechanical AE signals from knocking on the plate. The cross-correlation results from using one of the cracking templates are shown in Figure 8-19B and Figure 8-19E. This gives a very low level of similarity compared to the results with the plate with cracking. The pattern recognition analysis results are shown in Figure 8-19C and Figure 8-19F. the results only give negative peaks to the AE event in the signal, which meet the expectation according to the frequency features with the mechanical AE signal.

The results of the pattern recognition analysis of signals from the welding process are in Figure 8-20. Figure 8-20A is a raw signal from the welding process, which is very quiet, the PR result show low to none similarity thus it is unlikely that the weld cracked. The Figure 8-20C is raw signal from welding process, with two big spikes towards the end of the signal, the PR results in Figure 8-20D give two positive similarity corresponding to the spikes in the raw signal. However, the first one is larger than the second, thus the first positive similarity is more likely to associated with cracking.

The results of the pattern recognition analysis of signals from cooling are in Figure 8-20. Figure 8-20E and Figure 8-20G are the raw signals from material cooling after welding. The PR results in Figure 8-20F and Figure 8-20H both have positive similarity, with suggest cracking activities happened during the cooling process. Even the signals are from a cracked weld, it is hard to know which part of the signal is the cracking part thus hard to test if the algorism is working. A new set of tests are performed with a shorter period which can help to locate the time of the cracking, so it can help to test the effectiveness of cross-correlation and PR analysis.

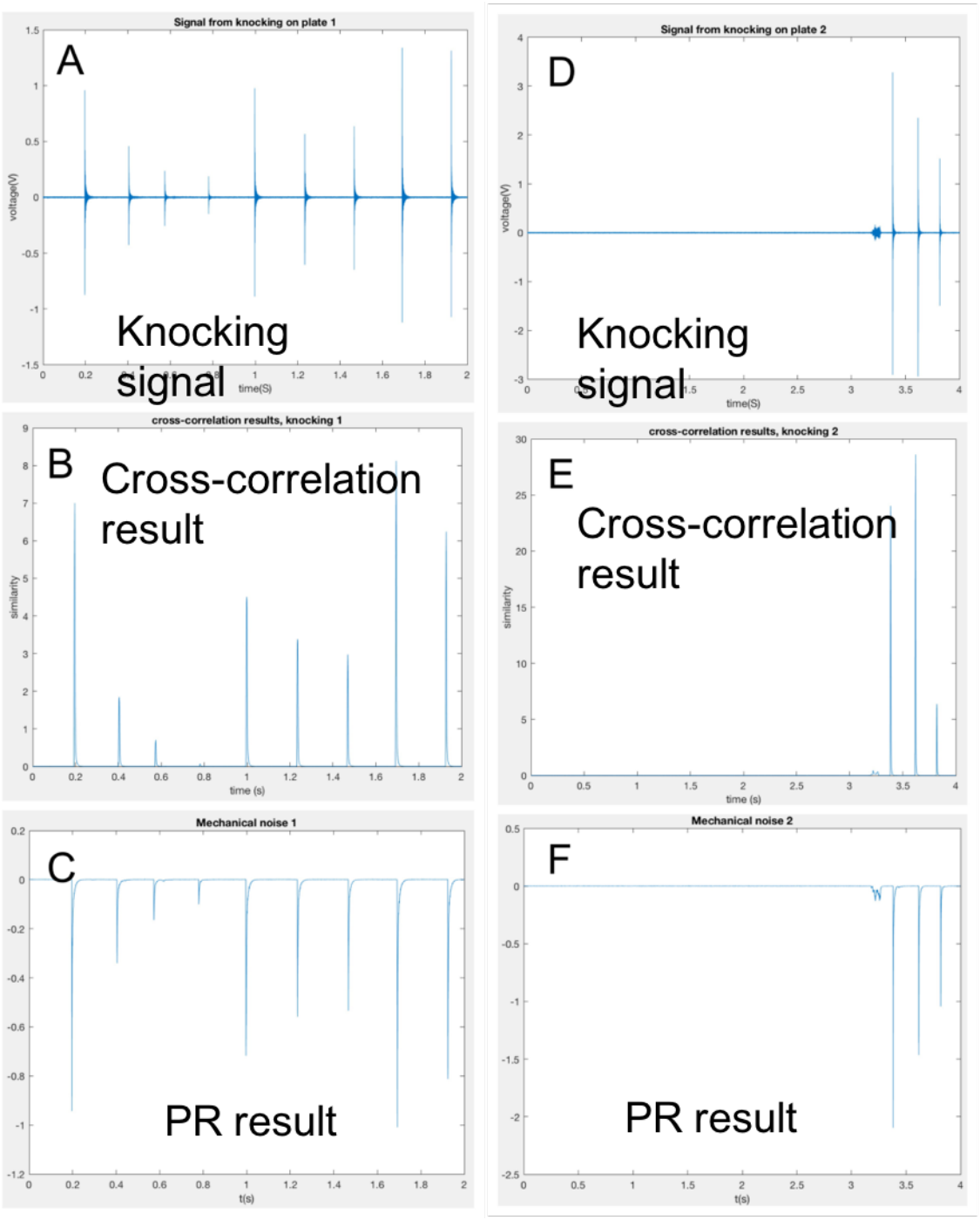

Figure 8-19 Results of Cross-correlation and pattern recognition analysis of AE mechanical signal.

A: Signal from knocking on the plate 1.
B: Cross-correlation results of A using the template in Figure 3.
C: PR result of A
D: Signal from knocking on the plate 2.
E: Cross-correlation results of D using the template in Figure 3.
F: PR result of D

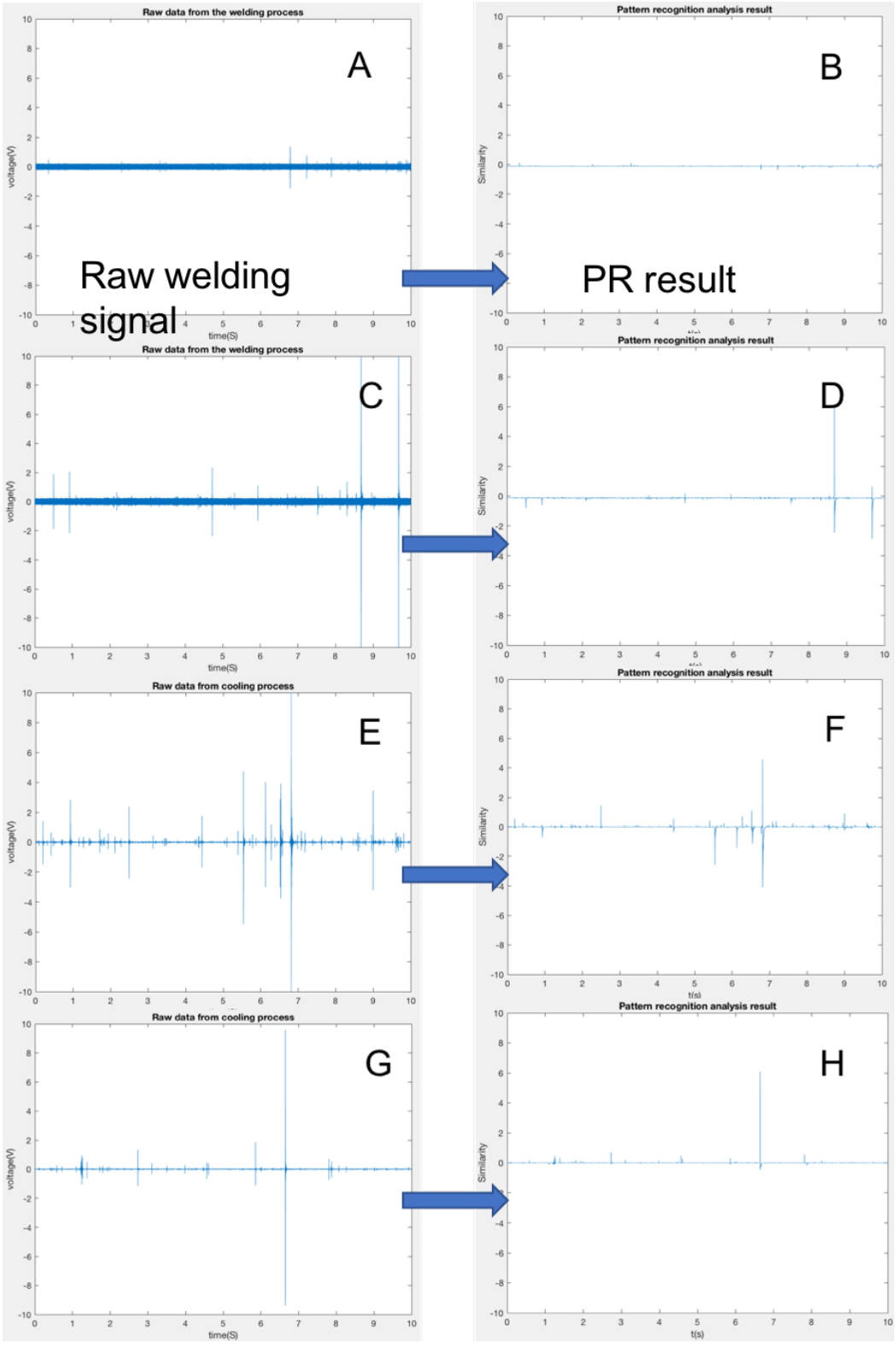

Figure 8-20 Results of pattern recognition analysis of signals from AE welding and cooling.

A and B: signals from welding process. B and D: PR results of A and B.

E and D: signals from Cooling. F and H: PR results of E and D.

8.3.3 CS70 Processing results

The AE measurements acquired during welding of carbon steel have been selected to perform the analysis. The photos of the welds are shown in Figure 8-1 to Figure 8-12. In some of the welds, there are visible cracks at the end of the welding pools. The welds are around 3 cm each. The raw signal consists of four important areas as marked in 8-21A:

1. Initial spikes: the spikes in the signal at the beginning of the welding process is most likely related to the noise from arc initiating. In the correlating result, after comparing them with the template, the similarity of the initial spikes with the template is low. The PR result shows only negative Figure at the beginning of the welding process. Both results show that it is unlikely the initial spikes are related to cracking or material related activities.
2. During the welding process. Rarely any big spikes can be observed in during the welding process. This is possibly due to the length of the welding period is very short, the welds have not reached the temperature when the cracking activities normally happen. It gives no similarity in both analysis methods.
3. 10-20 seconds after the welding process stopped. Nearly towards the end of the welds, intensive spikes can be found. This can give the cross-correlation results dense high peaks. However, with the PR results shows that not all of the spikes in the raw signal are related to cracking or material related activities. Most of the spikes give negative Figure, during this period, one or two positive peaks can be observed.
4. Some point during the cooling period, the cross-correlation results gave high similarities in some welds during the cooling process. The PR results during the cooling period can give high positive results in some welds like in 1A. This could be a strong indication of cracking activity.

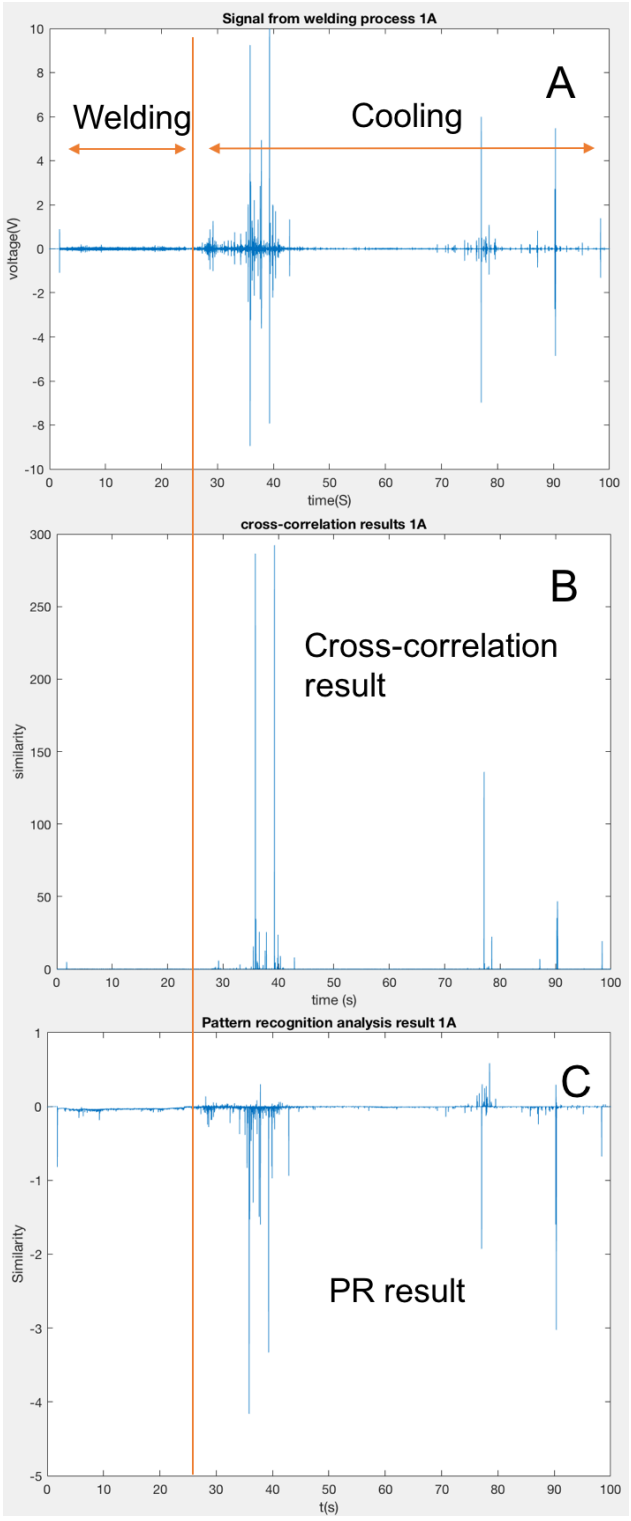

Figure 8-21 The raw data, Cross-correlation and PR results of trials 1A.

A and D: raw siganls from trial 1A

B and E: Cross-correlation results for 1A

C and F: PR results for 1A

From Table 8-4, trial 1A has cracks in the weld. The raw signal of trail 1A is plotted in Figure 8-21A, the raw signal has clustered spikes, which are not all associated with cracking in welds. From the cross-correlation results of 1A in Figure 8-21B, there are two parts in the results has a high similarity: 30-40s and 75-95s. The similarity of the first part is higher than the second part. For the PR result of 1A in Figure 8-21 C, two parts have positive results: around 40s and 75-95s. The highest similarity appears around 80s, which means the cracking happened 40s and 80s in the raw signal. From the results in 1A, the cross-correlation results and the pattern recognition results have similar detection results.

From Table 8-4, trial 4A and 5A have cracks in the weld. The raw signals of trial 4A and 5A are plotted in Figure 8-22A and Figure 8-22D, the raw signals have clustered spikes, from the cross-correlation results of 1A in Figure 8-21B, the high similarities appear the same time as the clustered spikes. For the PR result of 4A in Figure 8-22 C, the first positive similarity appears at 10-20 s after the welding stop which is the area 3 in trial 1. Compare to the first high similarity area in the cross-correlation result, some of the spikes in the cross-correlation result are excluded and defined as a mechanical signal. The PR result for 5A in Figure 22F, the spikes in the raw signal in 30-40s are defined as a mostly mechanical signal, however, in the cross-correlation result, it gives high similarity to the same spikes. The results are similar to 8A in Figure 8-23D, Figure 8-23E and Figure 8-23F. The results from both cross-correlation and PR results both indicate that there is cracking during the recording, which matches the results in Table 8-4. However, these two methods will sometimes give different results.

From Table 8-4, trial 6 does not contain cracks. However the cross-correlation and PR results in Figure 8-23B and Figure 8-23C it is suggested that there is a signal similar to cracking in the raw signal collected in Figure 8-23A. There might be two explanations for this. Firstly, there are smaller size cracks which are not on the surface of the welds which is under the

detection sensitivity or overlapped with the porosity in the Radiographic Inspection results. Secondly, both methods are not accurate enough in this particular case and need to be improved.

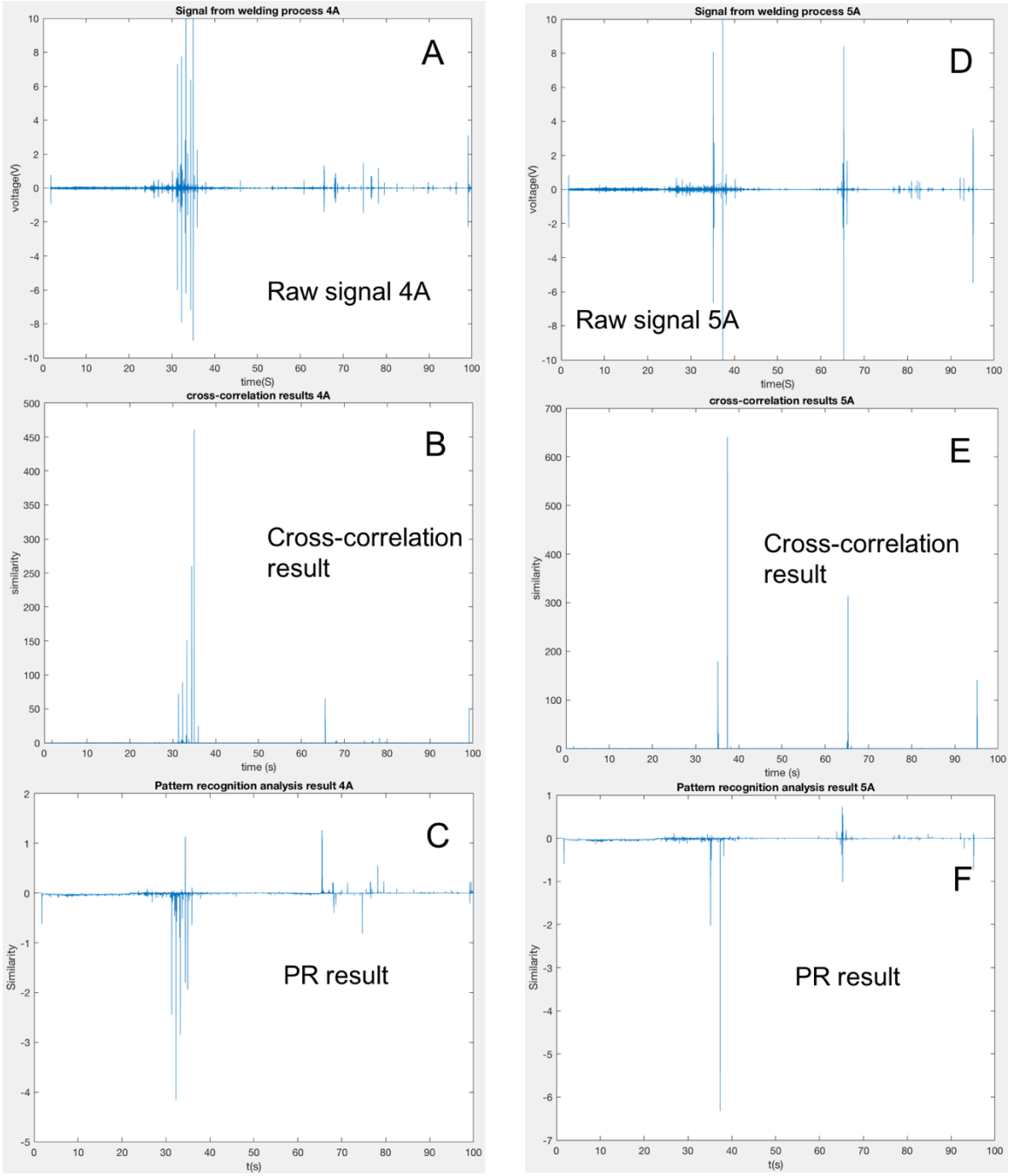

Figure 8-22 The raw data, cross-correlation and PR results of 4A, 5A.

A and D: raw siganls from trial 4A and 5A

B and E: Cross-correlation results for 4A and 5A

C and F: PR results for 4A and 5A

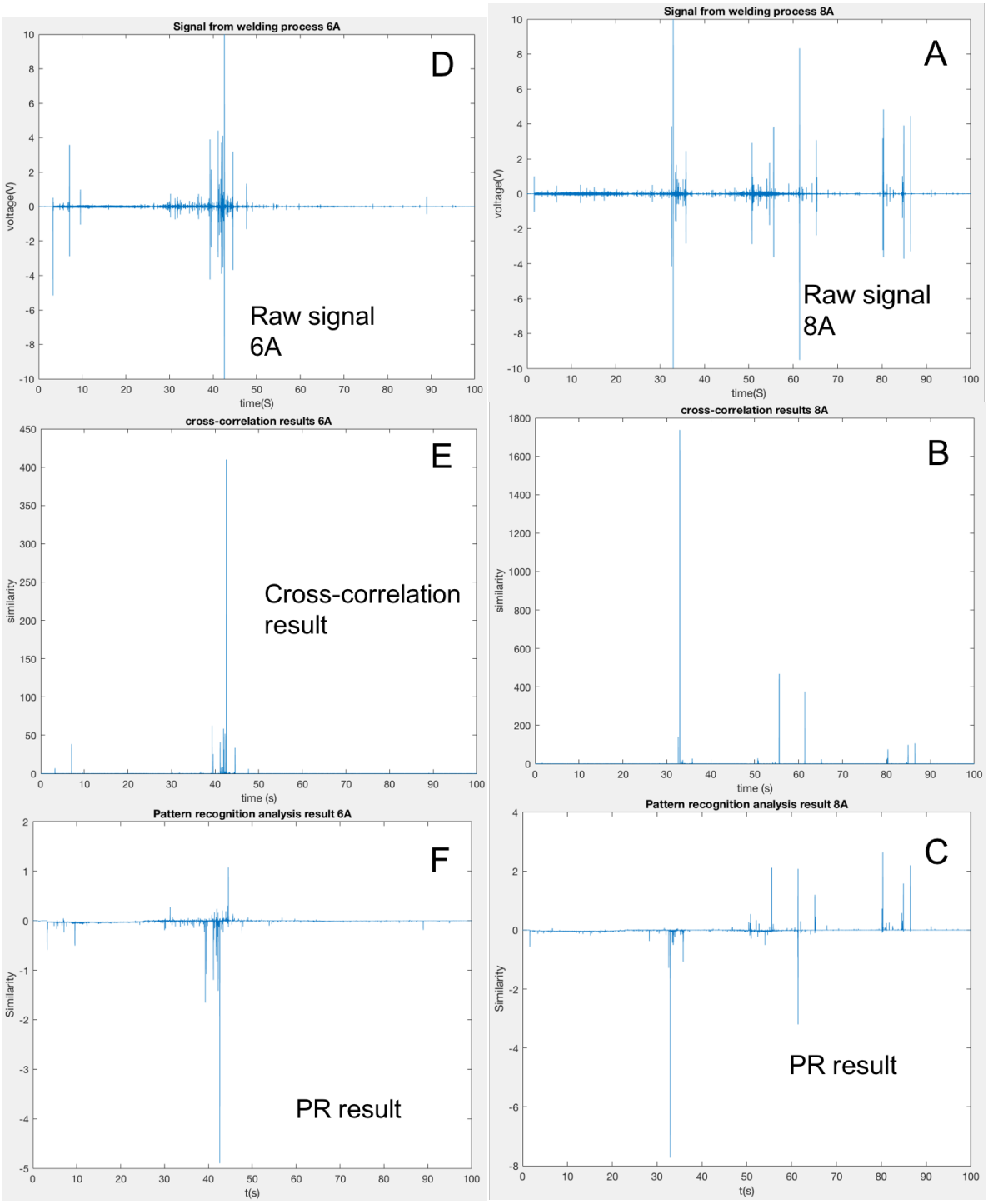

Figure 8-23 The raw data, cross-correlation and PR results of 6A, 8A.

A and D: raw siganls from trial 6A and 8A

B and E: Cross-correlation results for 6A and 8A

C and F: PR results for 6A and 8A

In Table 8-1, trial 9A does not have cracks. The raw signal in Figure 8-24A shows that the spikes are mostly in the area that 10-20s after the welding stopped which is area 3 in the trial 1A. In the cross-correlation analysis result in Figure 8-24B, high similarities are also distributed in the same area: 5-10s after the welding stopped. However, in the PR result in Figure 8-24C, there is almost no positive similarity in the plot, which indicates no cracks in the trials. In the result of 9A, the result of PR analysis is more accurate that the cross-correlation analysis.

In Table 8-1, trials 1B, 2B, 4B, 5B and 8B all has cracks in the weld. Their raw signals are plotted in the Figures 8-24, Figure 25 and Figure 26. The raw signals exhibit clustered spikes. The results from both cross-correlation and PR results indicate the occurrence of cracking. This matches the results in Table 8-4. However, these two methods will sometimes give different results.

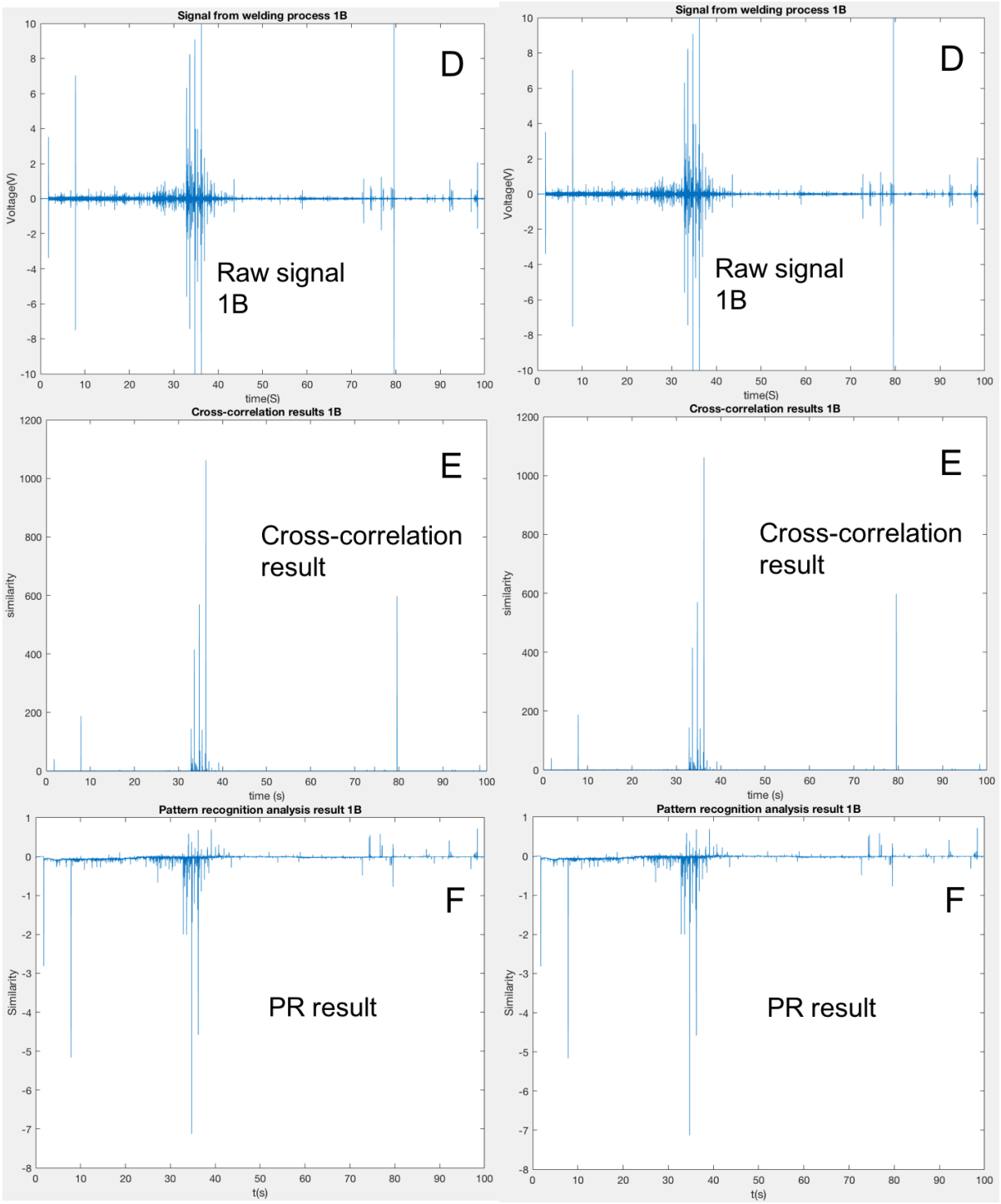

Figure 8-24 The raw data, cross-correlation and PR results of 9A, 1B.

A and D: raw siganls from trial 9A and 1B

B and E: Cross-correlation results for 9A and 1B

C and F: PR results for 9A and 1B

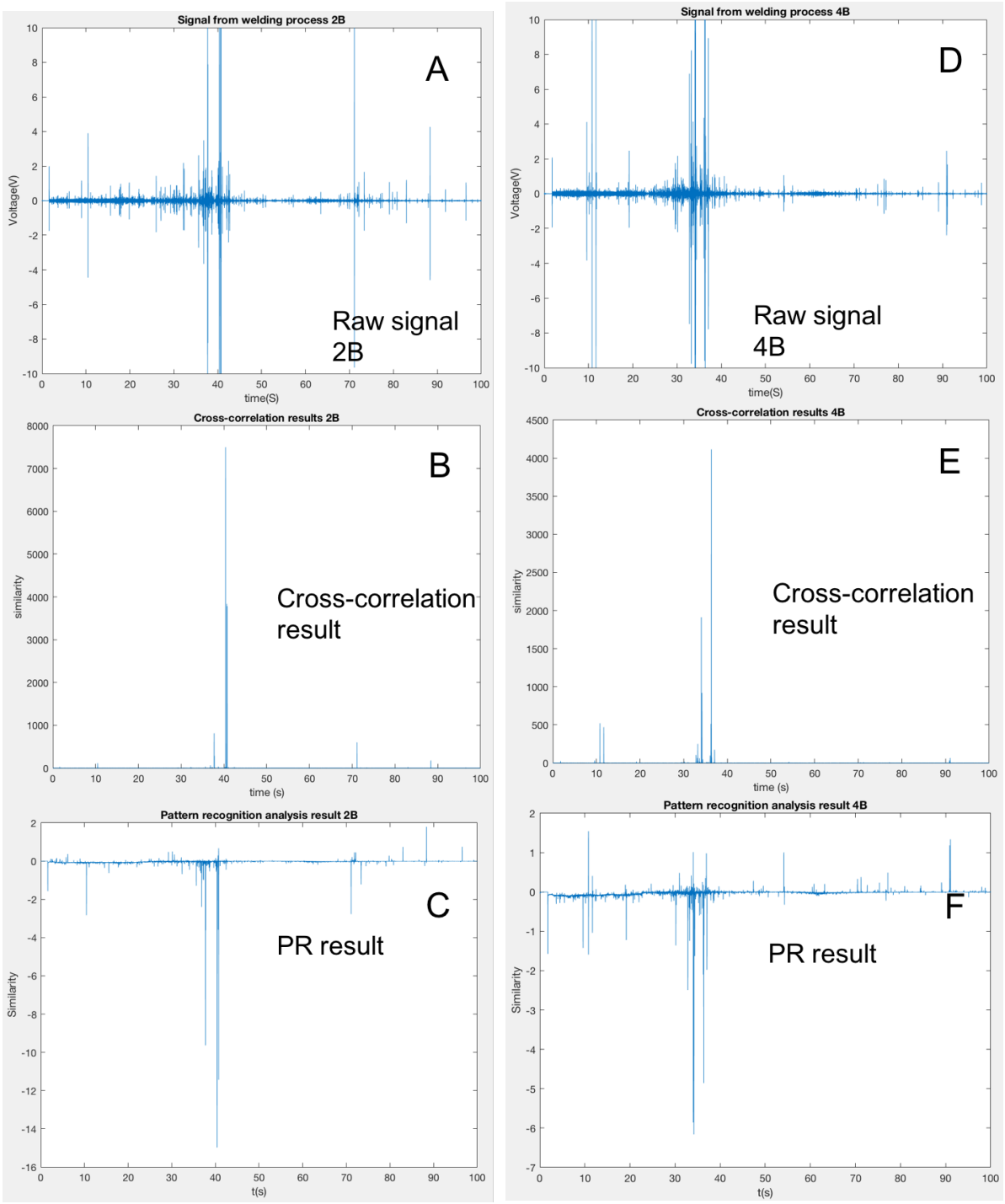

Figure 8-25 The raw data, cross-correlation and PR results of 2B, 4B.

A and D: raw siganls from trial 2B and 4B

B and E: Cross-correlation results for 2B and 4B

C and F: PR results for 2B and 4B

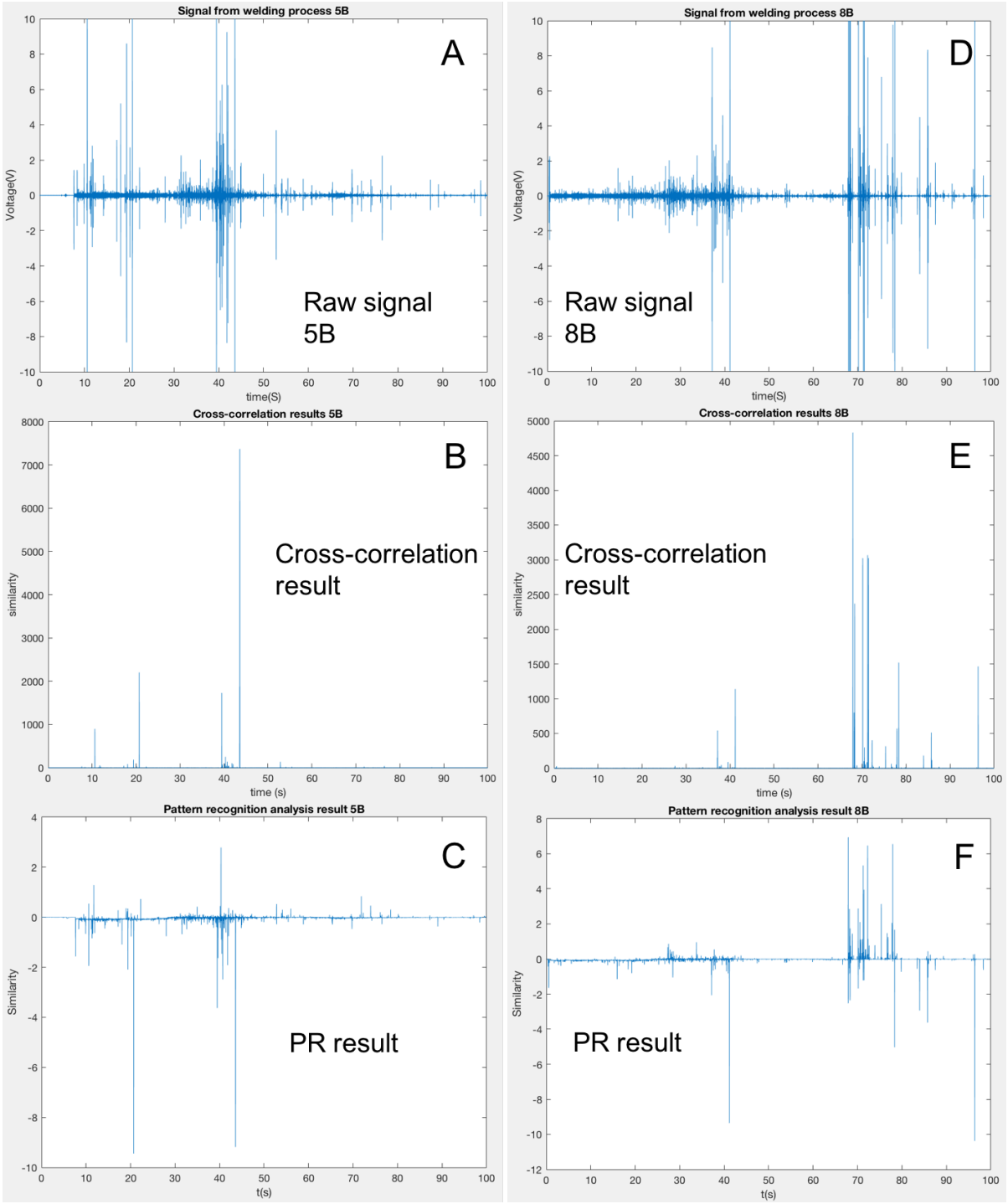

Figure 8-26 The raw data, cross-correlation and PR results of 5B, 8B.

A and D: raw siganls from trial 5B and 8B

B and E: Cross-correlation results for 5B and 8B

C and F: PR results for 5B and 8B

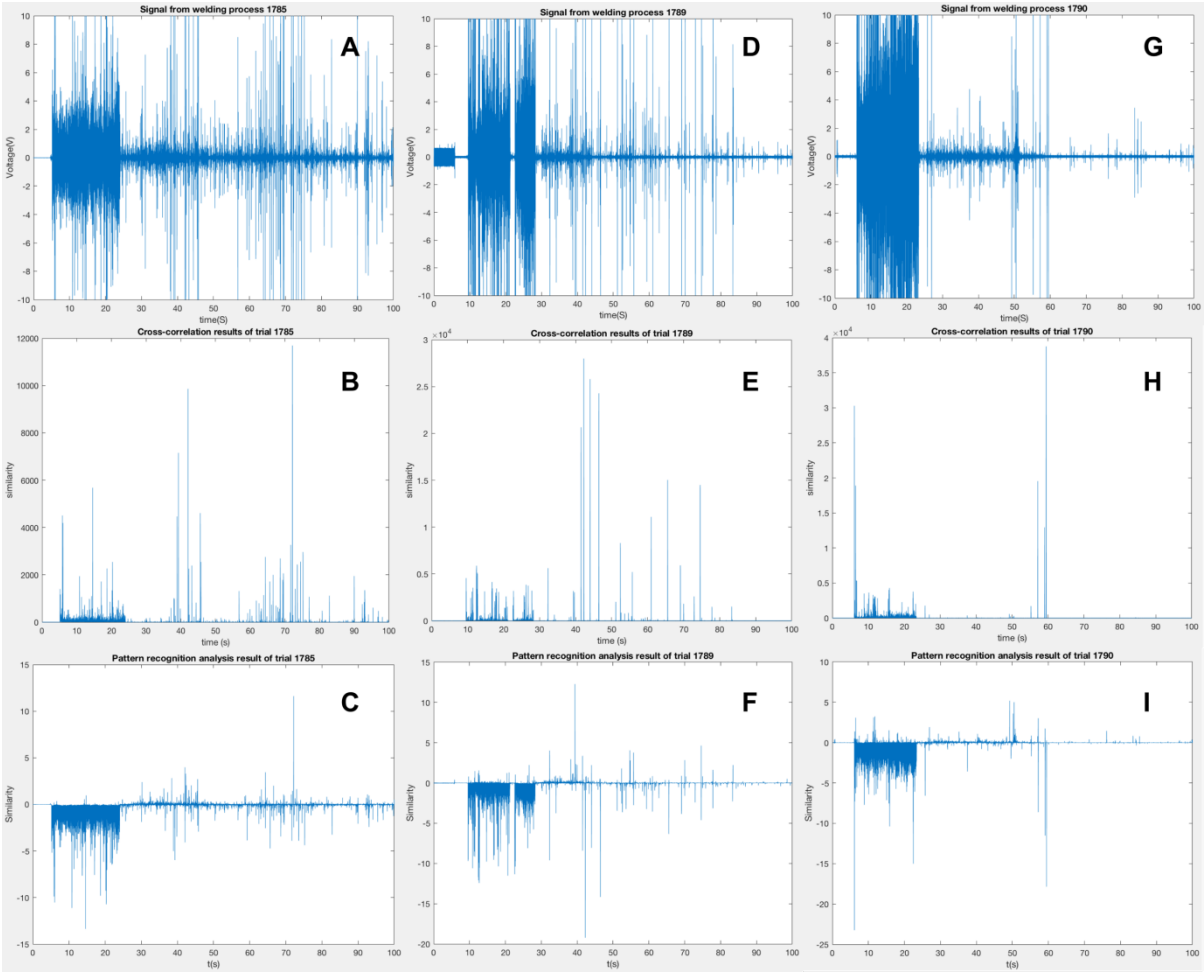

Figure 8-27 The raw data, cross-correlation and PR results of trial 1785, 1789 and 1790.

A, D and G: raw siganls from trial 1785, 1789 and 1790

B, E and H: Cross-correlation results 1785, 1789 and 1790

C, F and I: PR results for 1785, 1789 and 1790

Figure 8-27 are the raw data, cross-correlation and PR results of trial 1785, 1789 and 1790. The raw signals in Figure 8-27A, Figure 8-27D and Figure 8-27G are very noisy. The filtering process of the signal obtained from the MAG welding process in chapter 6 does not always give a good result,. However, both the cross-correlation and the PR results have some noticeable parts. During the welding period, even the welding signal from MAG process is noisy, the cross-correlation results show low similarity value for the welding process. The PR

results in Figure 8-27C, Figure 8-27F and Figure 8-27I are showing mostly negative similarities, which means the spikes during the welding process are mostly mechanical noise.

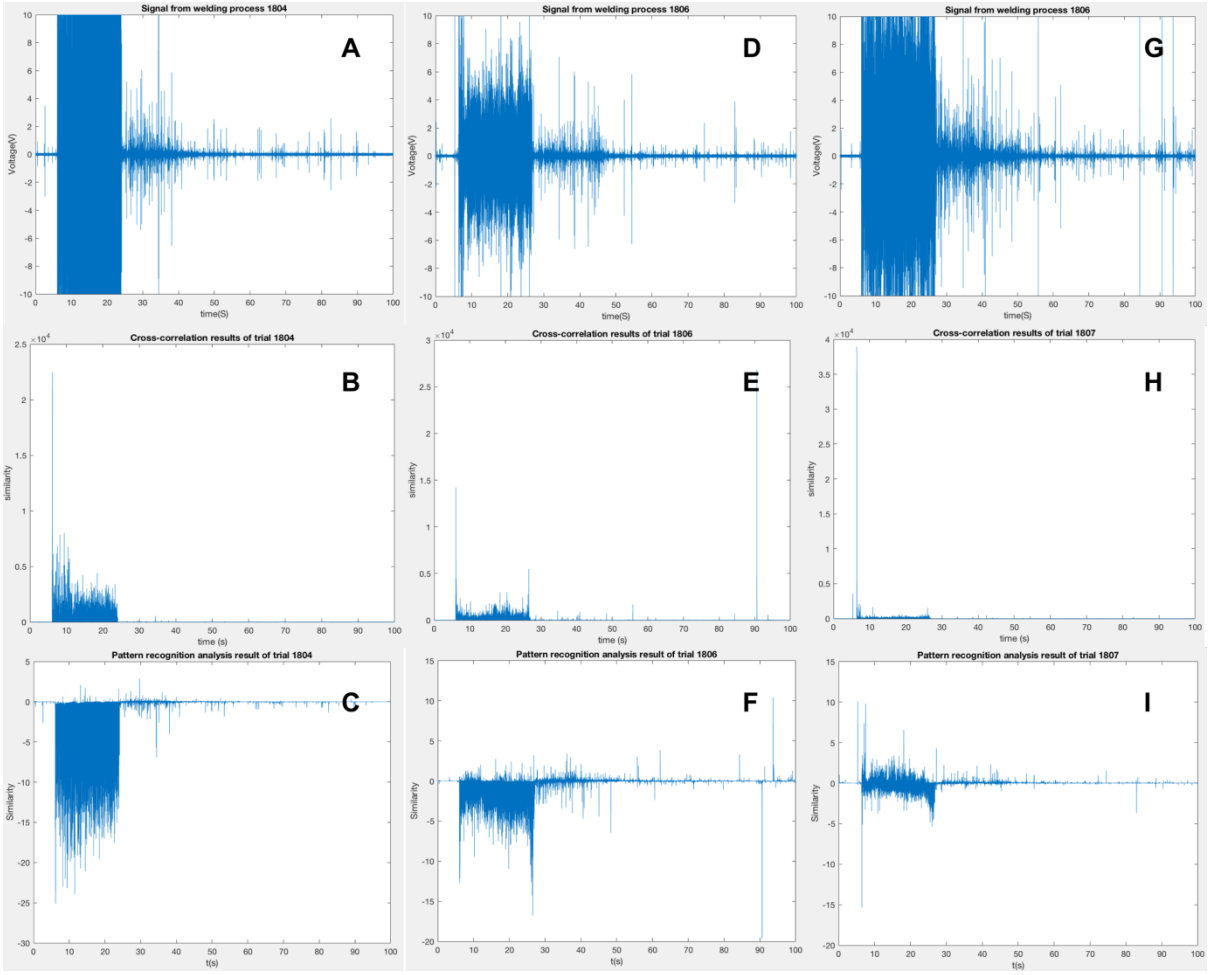

Figure 8-28 The raw data, cross-correlation and PR results of trial 1804, 1806 and 1807.

A, D and G: raw siganls from trial 1804, 1806 and 1807

B, E and H: Cross-correlation results 1804, 1806 and 1807

C, F and I: PR results for 1804, 1806 and 1807

8.4 Conclusion remarks

The following summarise some of the important findings and findings of the analysis.

a. The results of both cross-correlation and pattern recognition analysis both give similarities to the potential cracks. The cross-correlation will show lower similarity to mechanical signal while show higher similarity to cracking-related signal. The PR analysis will give negative results to mechanical signal and positive results in cracking related signal.
b. For the CS70 steel results, all of the cracks in the trials are given similarities by both methods. There are two trials: 6A and 9A are without cracks. Both methods suggest that 6A has cracks, Cross-correlation analysis give similarity to 9A, PR analysis suggests that 9A does not have cracks.
c. From the results from MAG trial, both results have the potential to discriminate the mechanical signal and signal related to cracking, even with high noise level process without filtering.
d. For cross-correlation analysis, the key is the template used. The other key is to find an appropriate threshold for the cracking signal. The usual use of the Cross-correlation is to normalise the results to 0 to 1 then set the threshold.
e. For Pattern Recognition analysis, the accuracy for the detection of cracking is higher. It is owing to the design of the algorism; it is written based on the difference in the frequencies of cracking signal and mechanical signal. It has the potential to be used as a tool for the development of a real-time AE monitoring system.

Chapter 9

Conclusions and recommendations for future work

9.1 Conclusions

Condition monitoring is one of the key methods for the industry to lower maintenance costs, maximise production output and increase the lifespan of equipment and structures. Welding condition monitoring requires the innovative replacement of welding NDT inspection techniques. This study has looked into the development of a novel AE monitoring system for the detection of crack-related signals arising during the welding process as part of the development of a multi-sensory welding monitoring system by TWI. The work towards the development of a novel AE system intelligently combining different signal processing methods investigated within this study has been split into three stages. These three stages were discussed in chapter 6, chapter 7 and chapter 8. The main results of the experimental work, data analysis and model development for each major problem haven been listed at the end of each chapter. The following comments are to summarise all the findings:

a) From the literature review, it is obvious that complication dispersive nature of AE waves and the noisy nature of the welding process, the signal discrimination is the key to cracking detection for this project. From the past literature, some has studied the frequency features of cracking signal, but there is not a comprehensive comparison of the cracking signal and other sources of signals from the processes, and there is no evidence that the results from the past can contribute to an AE monitoring system.
b) The noise level of the signal from welding largely varies among different processes and material. Each process has its signature frequencies. The filtering results also vary among processes and material. From the results, it is difficult to take advantage of the raw signal for the detection of the cracking in welding.
c) The different kind of discontinuous signals is collected and analysed. That includes background signal, torch moving, arc ignition, gas purging, nut dropping, hammer knocking and plate sliding. The cracking signals from TIG process are also collected

and analysed. The cracking signals and other signals from the background are compared. The differences in the frequency range of the signal from different sources will be used as the tool in the development of the algorisms for detection of cracking signal.

d) Two methods that have the potential to be used in a real-time monitoring system: Cross-correlation and Pattern Recognition were developed. Both methods are developed under the frequency features of the signals from different sources. Both methods are applied to the signal from trial and positive results are received. Both of the methods are still needed to be adjusted and to be integrated into a real-time monitoring system.

As final comments, the overall results of this study are useful for developing tools that intelligently combine multiple signal processing and analysis methods to identify the cause of damage accurately and to distinguish between different causes. These findings are believed to make AE technology more promising for weld monitoring applications.

9.2 Future work

The integration of the results arising from this study to the application of the techniques proposed for real-life monitoring purposes should be the main focus of future work. Some recommendations for future work are presented:

a) The two processing methods: Cross-correlation and Pattern Recognition analysis both need to be improved due to the need for more accurate detection results. This could be done by altering the parameters in the algorisms or use a better template for cracking detection.

b) The methods could be integrated into a monitoring system, which can collect and process the signal from arc welding in real-time. This will require an improved system from the perspective of hardware, software and advanced data processing

techniques.

c) Source localisation by using more than one sensor also needs to be studied, which this project did not include. This could be a part of the monitoring system.

Although several tests were planned and some were carried out, it is not possible to carry out all due to time constraints and accessibility to different processes. There is a need to study different levels of system dependence. A more complex database system is needed along with a computer with a more powerful processing capability.

References

1. Palmer, W.G., Effects of Welding on Health IV. Safety and Health Committee American Welding Society, 1982: p. 1-10.
2. Shiotani, T., Parameter Analysis. In: Grosse C., Ohtsu M. (eds) Acoustic Emission Testing. Springer, Berlin, Heidelberg, 2008.
3. Wadley, H.N.G., Scruby, C.B.S., Cooling rate effects on acoustic emissionmicrostructure relationships in ferritic steels. Journal Of Materials Science, 1991. 26: p. 5777-5792.
4. Karlsson, L., Crack Detection in Welding Process using Acoustic Emission. Mälardalen University, Master thesis, 2010.
5. Apasov, A. M. and Apasov, A. A., Acoustic emission diagnostics of faulty fusion in welding. in Strategic Technology (IFOST), 2012 7th International Forum on. 2012.
6. Charunetratsameea, S., et al., Feasibility study of acoustic emission monitoring of hot cracking in GTAW weld. Key Engineering Materials, 2013. 545: p. 236-240.
7. M. Wevers, K.L., Applications of acoustic emission for SHM: A review. In: Boller C, Chang FK, Fujino Y, eds. Encyclopedia of structural health monitoring: John Wiley & Sons, Ltd., 2009.
8. Wevers, M., Applications of acoustic emission for SHM: A review. In: Boller C, Chang FK, Fujino Y, eds. Encyclopedia of structural health monitoring: John Wiley & Sons, Ltd., 2009.
9. Jing, Y. and Yu, L., Ship welding defect analysis and quality control. Applied Mechanics and Materials, 2013. 365-366: p. 1229-1234.
10. Weman, K. and Lindén, G., ESAB and AGA, Facts about MIG/ MAG welding. ESAB Welding Equipment AB. MIG welding guide. Woodhead Publishing Limited, 2006.

11. Ponomarev, V. and Slivinsky, A., Welding arc and MIG/MAG welding transfer. Kiev, 2003.
12. Houldcroft, P. and John, R., Welding and cutting. Woodhead Publishing Limited 1988.
13. Houldcroft, P., Submerged arc welding. Woodhead Publishing Limited, 1990.
14. Muncaster, P., A practical guide to TIG (GTA) welding. Woodhead Publishing Limited, 1991.
15. Lucas, W., TIG and plasma welding. Woodhead Publishing Limited, 1990.
16. TWI, A general review of geometric shape imperfections - types and causes. Technical Knowledge Job Knowledge 67.
17. TWI, Defects/imperfections in welds - slag inclusions. Job Knowledge 43. Connect, 1999.
18. TWI, Defects/imperfections - incomplete root fusion or penetration. Technical Knowledge Job Knowledge. 40.
19. TWI, Defects/imperfections in welds – porosity. Technical Knowledge Job Knowledge 42.
20. Lippold, Hot Cracking, Welding Metallurgy and Weldability. 2014.
21. Lippold, Solid-State Cracking, Welding Metallurgy and Weldability,. 2014.
22. Kazasidis, M., Investigation of metal cored arc welded FCA (Fatigue Crack Arrester) steel in terms of microstructure, toughness and tensile properties. . Thesis from Trinity College Dublin, 2008.
23. Lippold, Hydrogen-Induced Cracking, Welding Metallurgy and Weldability. 2014.
24. ISO 5817, Welding — Fusion-welded joints in steel, nickel, titanium and their alloys (beam welding excluded) — Quality levels for imperfections. The International Organization for Standardization, 2003. 5817: 2014.

25. Welder's visual inspection handbook. 2013. [cited; Available from: https://supplier.huntingtoningalls.com/sourcing/docs/NNS_Technical_Documents/Welders_Visual_Inspection_Handbook-2013_WEB.pdf]
26. Radiography Testing - NDT Inspection TWI NDT Techniques, [cited; Available from: https://www.twi-global.com/what-we-do/services-and-support/asset-management/non-destructive-testing/ndt-techniques/radiography-testing]
27. EIS, Radiography Inspection. 2013, [cited; Available from: http://eisl.ie/radiography-inspection/]
28. Liquid Penetrant and Magnetic Particle Testing at Level 2. Manual for the Syllabi, Contained in IAEA-TECDOC-628, "Training Guidelines in Non-destructive Testing Techniques" 2000.
29. Betz, C.E., Principles of Magnetic Particle Testing American Society for Nondestructive Testing, 1985: p. 234.
30. Panchal, V., Pumps and valves: NDT flaw detection. World Pumps, 2014. 2014(5): p. 34-40.
31. Kolahan, A. and Zolfaghari, F., Reliability and sensitivity of visible liquid penetrant NDT for inspection of welded components. Materials Testing, 2017. 59(3): p. 290-294
32. Birks, A. S. and Green Jr, R. E., Ultrasonic testing, 2nd ed. Columbus, OH. American Society for Nondestructive Testing, 1991.
33. Hennigar, T., Wright, M., Eddy Current Testing Technology. 2012.
34. Buckley, J.M., An Introduction to Eddy Current Testing Theory and Technology. 2015.
35. Sadek, H.M., NDE technologies for the examination of heat exchangers and boiler tubes – principles, advantages and limitations. 2006. 48.

36. Wang, X., Three-dimensional vision-based sensing of GTAW: a review. The International Journal of Advanced Manufacturing Technology, 2014. 72(1-4): p. 333-345.

37. Cayo, E.H. et al., A Non-Intrusive GMA Welding Process Quality Monitoring System Using Acoustic Sensing. Sensors (Basel, Switzerland), 2009. 9(9): p. 7150-7166.

38. Grad, L., et al., Feasibility study of acoustic signals for on-line monitoring in short circuit gas metal arc welding. International Journal of Machine Tools and Manufacture, 2004. 44(5): p. 555-561.

39. Erdmann-Jesnitzer, F., Feustel, E. and Rehfeldt, D., Akustische Untersuchungen am Schweislichtbogen. Schw. und Schn, 1967. 19(3): p. 95–100.

40. Sánchez Roca, A., et al., Stability analysis of the gas metal arc welding process based on acoustic emission technique. Welding International, 2009. 23(3): p. 173-180.

41. Shujuan, B., et al. Characteristic analysis and pattern recognition of Arc sound under typical penetration status in MIG welding. in Information and Automation (ICIA), 2010 IEEE International Conference on. 2010.

42. Pal, K., Bhattacharya, S. and Pal, S.K., Investigation on arc sound and metal transfer modes for on-line monitoring in pulsed gas metal arc welding. Journal of Materials Processing Technology, 2010. 210(10): p. 1397-1410.

43. Pal, K. and Pal, S.K., Monitoring of Weld Penetration Using Arc Acoustics. Materials & Manufacturing Processes, 2011. 26(5): p. 684-693.

44. Lv, N., et al., Automatic measuring and processing system of audio sensing for real-time arc height control of pulsed GTAW. Sensor Review, 2014. 34(1): p. 51-66.

45. Lv, N., et al., Research on detection of welding penetration state during robotic GTAW process based on audible arc sound. Industrial Robot: An International Journal, 2013. 40(5): p. 474-493.

46. SERVO-ROBOT, i-CUBE: Universal Robot Sensor, 2013, [cited; Available from: http://servorobot.com/i-cube-universal-robot-sensor/]

47. TWI, Measurement of Arc Welding Parameters. Job knowledge. 139.

48. Zhang, Z., et al., Feature extraction and modeling of welding quality monitoring in pulsed gas touch argon welding based on arc voltage signal. Journal of Shanghai Jiaotong University (Science), 2014. 19(1): p. 11-16.

49. Adolfsson, S., Ericson, K. and Grennberg, A., Automatic detection of burn-through in GMA welding using a parametric model. Mechanical Systems and Signal Processing, 1996. 10(5): p. 633-657.

50. Simpson, S.W., WeldPrint™ – real time quality monitoring in automated welding applications. The University of Sydney, 2014.

51. Simpson, S.W., Signature images for arc welding fault detection. Science and Technology of Welding and Joining, 2007. 12(6): p. 481-486.

52. Simpson, S.W., Weld Quality Measurement. Patent WO 098/45078, 1998.

53. Li, X. and Simpson, S. W., Parametric approach to positional fault detection in short arc welding. Science and Technology of Welding and Joining, 2009. 14(2): p. 146-151.

54. Verhaeghe, G. and Melton, G., An investigation of the use of transient arc data to detect process deviations. TWI Industrial Member Report Summary 701/2000, 2000.

55. Shinoda, T., Nishikawa, H. and Shimizu, T., The development of data processing algorithms and assessment of arc stability as affected by the titanium content of GMAW [GMA welding] wires during metal transfer. Computer Technology in Welding. Proceedings, Sixth International Conference, Lanaken, Belgium, 1996.

56. Hermans, M. and Ouden, O. D., Process Behavior and Stability in Short Circuit Gas Metal Arc Welding. Welding Journal, 1999. 78: p. 137-141.

57. Adolfsson, S., Bahrami, A., Bolmsjö, G.and Claesson, I., On-Line Quality Monitoring in Short Circuit Gas Metal Arc Welding. Welding Journal, 1999. 78: p. 59-72.

58. Kim, J. W. and Na, S. J., A Study on Prediction of Welding Current in Gas Metal arc Welding Part 1: Modelling of Welding Current in Response to Change of Tip-to-Workpiece Distance. Proceedings of the Institution of Mechanical Engineers, Part B: Journal of Engineering Manufacture, 1991. 205(1): p. 59-63.

59. Kim, J. W. and Na, S. J., A Study on Prediction of Welding Current in Gas Metal arc Welding Part 2: Experimental Modelling of Relationship Between Welding Current and Tip-to-Workpiece Distance and its Application to Weld Seam Tracking System. Proceedings of the Institution of Mechanical Engineers, Part B: Journal of Engineering Manufacture, 1991. 205(1): p. 64-69.

60. Wong, Y.R. and Ling, S.F., Novel classification method of metal transfer modes in gas metal arc welding by real time input electrical impedance. Science and Technology of Welding and Joining, 2014. 19(3): p. 224-230.

61. Prasad, K., et al., Drop transfer mode prediction in pulse GMAW of aluminum using statistical model. Journal of Materials Processing Technology 2008. 201(1-3): p. 5.2-5.6.

62. Alfaro, S.C.A. and Cayo, E.H., Sensoring Fusion Data from the Optic and Acoustic Emissions of Electric Arcs in the GMAW-S Process for Welding Quality Assessment. Sensors (Basel, Switzerland), 2012. 12(6): p. 6953-6966.

63. Cayo, E.H. and Alfaro, S.C.A., Real-time assessment of the stability of metal transfer in GMAW-S process based on arc emissions. Welding&Meterial Testing 2012(2): p. 21-24.

64. Barborak, D., et al. Through-arc process monitoring: techniques for control of automated gas metal arc welding. in Robotics and Automation, 1999. Proceedings. 1999 IEEE International Conference on. 1999.

65. Wei, E., et al., Detection of Weld Surface Porosity by Statistical Analysis of Arc Current in Gas Metal Arc Welding. Journal of Manufacturing Processes, 2001. 3(1): p. 50-59.

66. Cook, G.E., Robotic Arc Welding: Research in Sensory Feedback Control. Industrial Electronics, IEEE Transactions on, 1983. IE-30(3): p. 252-268.

67. Christner, B.K., Lovell, R. and Campbell, M., Developing a GTAW penetration control system for the Titan IV programe. Weld Met Fabr, 1998. 66(4): p. 33-38.

68. Nixon J.H., Underwater repair technology. Woodhead, Cambridge, 2000: p. 41-43.

69. Zhang, Z., et al., Online welding quality monitoring based on feature extraction of arc voltage signal. The International Journal of Advanced Manufacturing Technology, 2014. 70(9-12): p. 1661-1671.

70. Xu, Y., et al., The acquisition and processing of real-time information for height tracking of robotic GTAW process by arc sensor. The International Journal of Advanced Manufacturing Technology, 2013. 65(5-8): p. 1031-1043.

71. Pal, S., Pal, S.K.S. and Arun K., Artificial neural network modeling of weld joint strength prediction of a pulsed metal inert gas welding process using arc signals. Journal of Materials Processing Technology, 2008. 202(1–3): p. 464-474.

72. Chen, B. and S. Chen, Multi‐sensor information fusion in pulsed GTAW based on fuzzy measure and fuzzy integral. Assembly Automation, 2010. 30(3): p. 276-285.

73. Jae Seon, K., et al. A robust method for vision-based seam tracking in robotic arc welding. in Intelligent Control, 1995., Proceedings of the 1995 IEEE International Symposium on. 1995.

74. Luo, H. and Chen, X., Laser visual sensing for seam tracking in robotic arc welding of titanium alloys. The International Journal of Advanced Manufacturing Technology, 2005. 26(9-10): p. 1012-1017.

75. Schwemmer, D., Beattie, B. and Wahlen, P., Advanced Technologies for Tandem SAW Narrow Groove Applications. Welding Journal, 2011: p. 32-37.

76. Servo-Robot, Power-scan: Compact weld bead inspect system, 2014. [cited; Avalible from: http://servorobot.com/arc-weld-inspection/]

77. Kuo, H.C. and Wu, L.J., An image tracking system for welded seams using fuzzy logic. Journal of Materials Processing Technology, 2002. 120(1–3): p. 169-185.

78. Shen, H., et al., Arc welding robot system with seam tracking and weld pool control based on passive vision. The International Journal of Advanced Manufacturing Technology, 2008. 39(7-8): p. 669-678.

79. Ge, J., et al., A vision-based algorithm for seam detection in a PAW process for large-diameter stainless steel pipes. The International Journal of Advanced Manufacturing Technology, 2005. 26(9): p. 1006-1011.

80. Ye, Z., et al., Passive vision based seam tracking system for pulse-MAG welding. The International Journal of Advanced Manufacturing Technology, 2013. 67(9-12): p. 1987-1996.

81. Wikle, H.C., et al., Survey of infrared sensing techniques for welding process monitoring and control. Journal of the Chinese Institute of Engineers, 1998. 21(6): p. 645-657.

82. Alfaro, S.C.A. and Franco, F.D., Exploring Infrared Sensoring for Real Time Welding Defects Monitoring in GTAW. Sensors (Basel, Switzerland), 2010. 10(6): p. 5962-5974.

83. Vasudevan, M., et al., Real-Time Monitoring of Weld Pool during GTAW using Infra-Red Thermography and analysis of Infra-Red thermal images. Welding in the World, 2011. 55(7-8): p. 83-89.

84. Chokkalingham, S., Chandrasekhar, N. and Vasudevan, M. Predicting the depth of penetration and weld bead width from the infra red thermal image of the weld pool using artificial neural network modeling. Journal of Intelligent Manufacturing, 2012. 23(5): p. 1995-2001.

85. Sreedhar, U., et al., Automatic defect identification using thermal image analysis for online weld quality monitoring. Journal of Materials Processing Technology, 2012. 212(7): p. 1557-1566.

86. Fidali, M. and Jamrozik, W., Diagnostic method of welding process based on fused infrared and vision images. Infrared Physics & Technology, 2013. 61: p. 241-253.

87. Mirapeix, J., et al., Spectroscopic analysis of the plasma continuum radiation for on-line arc-welding defect detection. Journal of Physics D: Applied Physics, 2008. 41(13): p. 135202.

88. Mirapeix, J., et al., Use of the Plasma Spectrum RMS Signal for Arc-Welding Diagnostics. Sensors (Basel, Switzerland), 2009. 9(7): p. 5263-5276.

89. Llinas, J. and Hall D.L., An introduction to multi-sensor data fusion. in Circuits and Systems, 1998. ISCAS '98. Proceedings of the 1998 IEEE International Symposium on. 1998.

90. Wang, G., Review of "Mathematical Techniques in Multisensor Data Fusion" by David L. Hall and Sonya A. H. McMullen. BioMedical Engineering OnLine, 2005. 4: p. 23-23.

91. Yan, L., et al. Study on multi-sensor data fusion for the wheeled mobile robot. in Intelligent Control and Automation, 2004. WCICA 2004. Fifth World Congress on. 2004.

92. Xu, L.J., Chen, Y.Z. and Cui, P.Y., Improvement of D-S evidential theory in multisensor data fusion system. in Intelligent Control and Automation, 2004. WCICA 2004. Fifth World Congress on. 2004.

93. Wan. W.J. and Fraser, D., Multisource data fusion with multiple self-organizing maps. Geoscience and Remote Sensing, IEEE Transactions on, 1999. 37(3): p. 1344-1349.

94. Russo, F. and Ramponi, G., Fuzzy methods for multisensor data fusion. Instrumentation and Measurement, IEEE Transactions on, 1994. 43(2): p. 288-294.

95. Chanussot, J., Mauris, G. and Lambert, P., Fuzzy fusion techniques for linear features detection in multitemporal SAR images. Geoscience and Remote Sensing, IEEE Transactions on, 1999. 37(3): p. 1292-1305.

96. Cullen, J.D., et al., Multisensor fusion for on line monitoring of the quality of spot welding in automotive industry. Measurement, 2008. 41(4): p. 412-423.

97. Teodiano Freire, B., Calderon, L., Martin, J. M. and Ceres, R., Ultrasonic sensors and arc welding-a noisy mix. Sensor Review, 1996. 16(3): p. 26-32.

98. Christian, U. and Ohtsu, G.M., Acoustic emission testing 2008: p. 3-9.

99. Gmbh, V.S., AE Testing Fundamentals,Equipment, Applications. Journal of Nondestructive Testing(Germany), 2002.

100. Pollock, A.A., Acoustic Emission Inspection. Princeton Junction, 1989.

101. Rose, J.R., Ultrasonic waves in solid media. Cambridge, UK: Cambridge University Press 1999.

102. Finlayson, R.D., Luzio, M.A., Miller, R. and Pollock A.A., Continuous health monitoring of graphite epoxy motorcases (GEM). CINDE Journal, 2003: p. 15-24.

103. Holford, K.M. and Lark, R.J., Acoustic emission testing of bridges. In: Fu G, ed. Inspection and monitoring techniques for bridges and civil structures. . Cambridge, England: Woodhead Publishing Limited and CRC 2005: p. 183-215.

104. Lozev, M.G., Clemena, G.G., Duke, J.C., Sison, M.F. and Horne. M.R., Acoustic emission monitoring of steel bridge members. Virginia transportation research council, 1997.

105. Grosse C. and Linzer L., Signal-Based AE Analysis. In: Grosse C., Ohtsu M. (eds) Acoustic Emission Testing. Springer, Berlin, Heidelberg, 2008.

106. Physical Acoustics Corporation. PCI-2 based AE system User's manual. Physical Acoustics Corporation, 2007.

107. Shigeshi, M. and Colombo, S., et al., Acoustic emission to assess and monitor the integrity of bridges. Construction and building materials, 2001. 15: p. 35-49.

108. Huang, M., et al., Using acoustic emission in fatigue and fracture materials research. JOM, 1998. 50(11).

109. Grosse, C.U. and Linzer, L.M., Signal-based AE analysis. In: Grosse CU, Ohtsu M, eds. Acoustic Emission Testing: Springer-Verlag 2008.

110. Vallen, H., AE testing fundamentals, equipment, applications. NDTnet., 2002. 7(09).

111. Romrell, D.M., Acoustic Emission Weld Monitoring of Nuclear Components. Welding Research Supplement, 1973: p. 81-87.

112. Hopwood II, T. and Havens J.H., Acoustic Emission Monitoring Of Weldments. American Society for Testing Materials, 1978.

113. Ranganayakulu S. V., Shiva Raju J., Kuchedludu A. and Ramesh Kumar B., Acoustic Emission Studies on Weld Bead Defects in Nuclear Grade SS 316L Materials. Open Journal of Acoustics, 2014.

114. Rodgers, J.M., Morgan, B.C. and Tilley, R.M. Acoustic emission monitoring for inspection of seam-welded hot reheat piping in fossil power plants. SPIE Conference on Nondestructive Evaluation Techniques for Aging Infrastructure & Manufacturing, 1996. 2947.

115. Ser'eznov, A.N., et al., Acoustic-emission study of the possibilities of localizing flaws of a welded joint during cooling. Russian Journal of Nondestructive Testing, 2009. 45(5): p. 310-316.

116. Van Bohemen, S. M. C., Hermans, M. J. M. and Den Ouden, G., Monitoring of martensite formation during welding by means of acoustic emission. Journal of Physics D: Applied Physics, 2001. 34(22): p. 3312.

117. Kikuta, Y., Araki, T., Chihara, H, and Iwamoto, H., Practical application of acoustic emission detecting for welding process (Report2). J. Japan Welding Society, 1983. 1: p. 450-455.

118. Kikuta, Y., Araki, T., Chihara, H, and Iwamoto, H., Practical application of acoustic emission detecting for welding process (Report3). J. Japan Welding Society, 1983. 1: p. 455-461.

119. Apasov, A.M. and Apasov, A.A., Examination of acoustic emission in welding of austenitic steels. Welding International, 2001. 15(6): p. 466-472.

120. Chen, C., Kovacevic, R. and Jandgric, D., Wavelet transform analysis of acoustic emission in monitoring friction stir welding of 6061 aluminum. International Journal of Machine Tools and Manufacture, 2003. 43(13): p. 1383-1390.

121. Charunetratsameea, S., et al., Feasibility study of acoustic emission monitoring of hot cracking in GTAW weld. Key Engineering Materials, 2013. 545: p. 236-240.

122. Ozevin, D., Greve, D.W., Oppenheim, I.J. and Pessiki, S., Resonant Type MEMS Transducers Excited by Two Acoustic Emission Simulation Techniques. Smart Structures and Materials, 2004: p. 239-43.

123. Golaski, L., Gebski, P. and Ono, K., Diagnostics of reinforced concrete bridges by acoustic emission. Journal of acoustic emission, 2002. 20: p. 83-98.

124. Gorman, M.R., Some connections between AE testing of large structures and small samples. . Nondestructive testing and evaluation, 1998. 14.

125. Physical Acoustics Corporation. [cited; Available from: http://www.pacndt.com/index.aspx?go=products&focus=Sensors.htm

126. Mathworks, MATLAB Users Guide. Natick, 2009.

127. Yoon, D.J., Weiss, W.J. and Shah. S.P., Assessing damage in corroded reinforced concrete usign acoustic emission. . Journal of engineering mechanics, 2000. 126(3).

128. Qi, G., Barhorst, A., Hashemi, J. and Kamala, G., Discrete wavelet decomposition of acoustic emission signals from carbon-fiber-reinforced composites. Composites Science and Technology, 1997. 57: p. 389-403.

129. Qi, G., Wavelet-based AE characterization of composite materials. NDT&E International, 2000. 33(3):: p. 133-44.

130. Grosse, C.U., Reinhardt, H.W., Motz, M. and B.H. Kroplin., Signal conditioning in acoustic emission analysis using wavelets. . NDTnet., 2002. 7(9).

131. Grosse, C.U., Finck, F., Kurz, J.H. and Reinhardt. H.W., Improvements of AE technique using wavelet algorithms, coherence functions and automatic data analysis. Construction and building Materials. , 2004. 18(3): p. 203-213.

132. Reda Taha, M.M., Noureldin, A., Lucero, J.L. and Baca, T.J., Wavelet transform for structural health monitoring: a compendium of uses and features. Structural health monitoring., 2006. 5(3): p. 267-295.

133. Bailey, N., et al., Welding Steels Without Hydrogen Cracking (Second Edition (Revised)). Woodhead Publishing Series in Welding and Other Joining Technologies, 2004. Chapter 3 - Selecting values for graphical presentation: p. 33-45.

134. Dautov, Ç.P., Özerdemb, M.S., Introduction to Wavelets and their applications in signal denoising. Journal of Science and Technology, 2017: p. 1–10.

135. Misiti, M., Misiti, Y., Oppenheim, G., Poggi, J., Wavelet Toolbox TM 4 User ' s Guide. The MathWorks Inc, 2009.

Appendices

Appendix A: Data spreadsheet

The spreadsheet below is the parameter settings, IDs of the samples and IDs of different types of data acquired in the experiment.

Note: WFS is wire feed speed of the welding process.

AE data/ Sampling rate	VISION data	AMV data	Date	ID	Description	Material/ Thickness (mm)	Current (A)	Voltage (V)	Travel speed (mm/s)	WFS (mm/s)
46/ 500k	N/A	N/A	23.05.2016	N/A	CMT	s304				
49/ 500k	N/A	N/A	23.05.2016	N/A	CMT	s304				
50/ 500k	N/A	N/A	23.05.2016	N/A	CMT	s304				
51/ 500k	N/A	N/A	23.05.2016	N/A	CMT	s304				
N/A	160705-113121-50mmLens w.s.154cm.m	N/A	05.07.2016	N/A	CMT	s304				
N/A	160705-113736-50mmLens w.s.140cm.m	N/A	05.07.2016	N/A	CMT	s304				
N/A	160705-114214-50mmLens w.s.75cm.m	N/A	05.07.2016	N/A	CMT	s304				
N/A	160705-114635-50mmLens w.s.33.4cm.m	N/A	05.07.2016	N/A	CMT	s304				
N/A	160705-114925-50mmLens w.s.16cm.m	N/A	05.07.2016	N/A	CMT	s304				
N/A	160705-115916-50mmLens stationary	N/A	05.07.2016	N/A	CMT	s304				
N/A	160705-121115-50mmLens added slug	N/A	05.07.2016	N/A	CMT	s304				
N/A	160705-121434-50mmLens added slug	N/A	05.07.2016	N/A	CMT	s304				
N/A	160705-121542-50mmLens added slug	N/A	05.07.2016	N/A	CMT	s304				
N/A	160705-150529-50mmLens 250A 22V	N/A	05.07.2016	N/A	CMT	s304				
N/A	160705-150850-50mmLens 250A 22V w.s.lev8	N/A	05.07.2016	N/A	CMT	s304				
N/A	160705-151210-50mmLens 150A 17.2V w.s.lev8	N/A	05.07.2016	N/A	CMT	s304				
N/A	160705-151311-50mmLens 150A 17.2V w.s.lev8	N/A	05.07.2016	N/A	CMT	s304				
N/A	160705-160043-50mmLens 100A 12V w.s.lev.15	N/A	05.07.2016	N/A	CMT	s304				
55/500k	N/A	N/A	06.07.2016	N/A	BG	s304				
56-66/500k	N/A	N/A	06.07.2016	N/A	CMT	s304				
67-71/500k	N/A	N/A	06.07.2016	N/A	CMT	s304				
72-73/500k	N/A	N/A	06.07.2016	N/A	BG	s304				

84/500k	N/A	N/A	07.07.2016	N/A	CMT, applied water	s304	
85-86/500k	160707-111307-50mmLens 200A w.s.11.5cm.m + no shielding gas	N/A	07.07.2016	N/A	TIG	s304	200
87-93/500k	160707-111524-50mmLens 200A w.s.11.5cm.m + no shielding gas	N/A	07.07.2016	N/A	TIG	s304	200
94-97/500k	160707-111731-50mmLens 200A w.s.11.5cm.m + Effys glue	N/A	07.07.2016	N/A	TIG	s304	200
98-100/500k	160707-114507-50mmLens 200A w.s.33.4cm.m	N/A	07.07.2016	N/A	TIG	s304	200
101-102/500k	160707-114735-50mmLens 150A w.s.33.4cm.m	N/A	07.07.2016	N/A	TIG	s304	150
104-106/500k	160707-142854-50mmLens 150A w.s.Lev31 No Joint	N/A	07.07.2016	N/A	TIG	s304	150
107-108/500k	160707-143316-50mmLens 200A w.s.19cm.m	N/A	07.07.2016	N/A	TIG	s304	200
109-110/500k	160707-143851-50mmLens 150A w.s.19cm.m No Joint	N/A	07.07.2016	N/A	TIG	s304	150
112-114/500k	160707-144657-50mmLens 150A w.s.19cm.m	N/A	07.07.2016	N/A	TIG	s304	150
116-119/500k	160707-151317-50mmLens 200A w.s.19cm.m try joining	N/A	07.07.2016	N/A	TIG	s304	200
120-123/500k	160707-152834-50mmLens 250A w.s.50cm.m try joining	N/A	07.07.2016	N/A	TIG	s304	250
124-130/500k	160708-095147-50mmLens 200A w.s.16cm.m try joinning 5mmPlate	N/A	08.07.2016	N/A	TIG	s304/5	200
131-132/500k	160708-095737-50mmLens 220A w.s.16cm.m try joinning 5mmPlate	N/A	08.07.2016	N/A	TIG	s304/5	220
133-138/500k	160708-100507-50mmLens 235A w.s.16cm.m try joinning 5mmPlate	N/A	08.07.2016	N/A	TIG	s304/5	235
139-146/500k	160708-100937-50mmLens 250A w.s.16cm.m try joinning 5mmPlate	N/A	08.07.2016	N/A	TIG	s304/5	250
147-151/500k	160708-101257-50mmLens 270A w.s.16cm.m try joinning 5mmPlate	N/A	08.07.2016	N/A	TIG	s304/5	270
152-155/500k	160708-110225-50mmLens 200A w.s.16cm.m try joinning 10mmPlate	N/A	08.07.2016	N/A	TIG	s304/10	200
156-162/500k	160708-110523-50mmLens 200A w.s.16cm.m try joinning 10mmPlate	N/A	08.07.2016	N/A	TIG	s304/10	200
163-164/500k	160708-110713-50mmLens 220A w.s.16cm.m try joinning 10mmPlate	N/A	08.07.2016	N/A	TIG	s304/10	220
165-166/500k	160708-111106-50mmLens 235A w.s.16cm.m try joinning 10mmPlate	N/A	08.07.2016	N/A	TIG	s304/10	235
167-168/500k	160708-111323-50mmLens 250A	N/A	08.07.2016	N/A	TIG	s304/10	250

	w.s.16cm.m try joinning 10mmPlate						
168-172/500k	160708-111554-50mmLens 270A	N/A	08.07.2016	N/A	TIG	s304/10	270
	w.s.16cm.m try joinning 10mmPlate						
N/A	160708-113447-50mmLens tacking	N/A	08.07.2016	N/A	TIG	s304/5	
173-177/500k	160708-114501-50mmLens 200A	N/A	08.07.2016	N/A	TIG	s304/5	200
	w.s.Lev8 try joining 5mm Plate						
178-179/500k	160708-114915-50mmLens 200A	N/A	08.07.2016	N/A	TIG	s304/5	200
	w.s.Lev10 try joining 5mm Plate						
180-181/500k	160708-115129-50mmLens 200A	N/A	08.07.2016	N/A	TIG	s304/5	200
	w.s.Lev12 try joining 5mm Plate						
182-183/500k	160708-115340-50mmLens 200A	N/A	08.07.2016	N/A	TIG	s304/5	200
	w.s.Lev14 try joining 5mm Plate						
184-187/500k	160708-115546-50mmLens 200A	N/A	08.07.2016	N/A	TIG	s304/5	200
	w.s.Lev16 try joining 5mm Plate						
188-189/500k	160708-140017-50mmLens 200A	N/A	08.07.2016	N/A	TIG	s304/5	200
	w.s.Lev16 g.f.10L.m try joining 5mm Plate						
190-193/500k	160708-140302-50mmLens 200A	N/A	08.07.2016	N/A	TIG	s304/5	200
	w.s.Lev16 g.f.15L.m try joining 5mm Plate						
194/500k	160708-140555-50mmLens 200A	N/A	08.07.2016	N/A	TIG	s304/5	200
	w.s.Lev16 g.f.35L.m try joining 5mm Plate						
195/500k	160708-140803-50mmLens 200A	N/A	08.07.2016	N/A	TIG	s304/5	200
	w.s.Lev16 g.f.40L.m try joining 5mm Plate						
196-197/500k	160708-142902-50mmLens 350A	N/A	08.07.2016	N/A	TIG	s304/10	350
	w.s.Lev16 g.f.40L.m try joining 10mm Plate						
198-200/500k	160708-143201-50mmLens 300A	N/A	08.07.2016	N/A	TIG	s304/10	300
	w.s.Lev16 g.f.40L.m try joining 10mm Plate						
201-203/500k	160708-143601-50mmLens PROBABLY 250A	N/A	08.07.2016	N/A	TIG	s304/10	
	w.s.Lev16 g.f.40L.m try joining 10mm Plate						
204-205/500k	160708-145105-50mmLens 350A	N/A	08.07.2016	N/A	TIG	s304/10	350
	w.s.Lev16 g.f.20L.m try joining 10mm Plate						
206-207/500k	160708-145314-50mmLens 300A	N/A	08.07.2016	N/A	TIG	s304/10	300
	w.s.Lev16 g.f.20L.m try joining 10mm Plate						
208/500k	160708-145602-50mmLens 250A	N/A	08.07.2016	N/A	TIG	s304/10	250
	w.s.Lev16 g.f.20L.m try joining 10mm Plate						

N/A	160708-145744-50mmLens 200A w.s.Lev16 g.f.20L.m try joining 10mm Plate	N/A	08.07.2016	N/A	TIG	s304/10	200		
209-212/500k	N/A	N/A	31.10.2016	N/A	BG	s304/5			
213-214/500k	N/A	N/A	31.10.2016	N/A	Table moving	s304/5			
215-216/500k	N/A	N/A	31.10.2016	N/A	Table moving	s304/5			
217-218/500k	N/A	N/A	31.10.2016	N/A	Table moving	s304/5			
219-221/500k	N/A	N/A	31.10.2016	N/A	BG	s304/5			
222-231/500k	N/A	N/A	31.10.2016	222-231	Air cooling	s304/5	99	11	
232-236/500k	N/A	N/A	31.10.2016	232-236	Air cooling	s304/5	99	10	
237-241/500k	N/A	N/A	31.10.2016	237-241	Air cooling	s304/5	97	10	
242-271/500k	N/A	N/A	31.10.2016	242-271	Fan	s304/5	99	10	
272-276/500k	N/A	N/A	31.10.2016	272-276	BG	s304/5	130	10	
277-300/500k	N/A	N/A	31.10.2016	277-300	Water	s304/5	130	10	
301/500k	N/A	N/A	31.10.2016	N/A	BG	s304/5	130	10	
302-327/500k	N/A	N/A	31.10.2016	Pass 1	Dry ice	s304/5	130	10	
328-329/500k	N/A	N/A	01.11.2016		BG	s304/5			
330-359/500k	N/A	N/A	01.11.2016	Pass 2	Air cooling	s304/5			
360-386/500k	N/A	N/A	01.11.2016	Pass 3	Water	s304/5			
387-408/500k	N/A	N/A	01.11.2016	Pass 4	Dry ice	s304/5			
409-428/500k	N/A	N/A	01.11.2016	Pass 5	Air cooling	s304/5			
429-448/500k	N/A	N/A	01.11.2016	Pass 6	Dry ice	s304/5			
449-468/500k	N/A	N/A	01.11.2016	Pass 7	Water	s304/5			
469/500k	N/A	N/A	01.11.2016		BG	s304/5			
470-472/500k	N/A	N/A	01.11.2016	Pass 8	Paint	s304/5			
473/500k	N/A	N/A	01.11.2016		BG	s304/5			
475-481/500k	N/A	N/A	01.11.2016	Pass 10		s304/5			
482/500k	N/A	N/A	01.11.2016			s304/5			
483-502/500k	N/A	N/A	01.11.2016	Pass 11		s304/5			
503-522/500k	N/A	N/A	01.11.2016	Pass 12		s304/5			
523-534/500k	N/A	N/A	01.11.2016	Pass 13		s304/5			
535-559/500k	N/A	N/A	01.11.2016			s304/5			
560-583/500k	N/A	N/A	01.11.2016	Pass 17		s304/5			
584-597/500k	N/A	N/A	01.11.2016	Pass 18		s304/5			
620-639/500k	N/A	N/A	14.12.2016	620-639		s304/5			
640-659/500k	N/A	N/A	14.12.2016	640-659		s304/5			
660-679/500k	N/A	N/A	14.12.2016	660-679		s304/5			
680-699/500k	N/A	N/A	14.12.2016	680-699		s304/5			
700-719/500k	N/A	N/A	14.12.2016	700-719		s304/5			
720-769/500k	N/A	N/A	14.12.2016	720-769		s304/5			
772-783/1M	N/A	02022017_Pass5	02.02.2017	Pass 5	Autogenous	CS70/3	70	12	9.8

784-793/1M	N/A	02022017_Pass6	02.02.2017	Pass 6	Wire	CS70/3	70	12	9.8
794-806/500k	N/A	02022017_Pass7	02.02.2017	Pass 7	Autogenous	CS70/3	70	12	9.8
807-819/500k	N/A	02022017_Pass8	02.02.2017	Pass 8	Wire	CS70/3	70	12	9.8
820-840/1M	N/A	02022017_Pass9	02.02.2017	Pass 9	Autogenous	CS70/3	90	12	9.8
841-858/1M	N/A	02022017_Pass10	02.02.2017	Pass 10	Wire	CS70/3	90	12	9.8
859-878/1M	N/A	02022017_Pass12	02.02.2017	Pass 12	Autogenous	CS70/3	90	12	9.8
879-910/500k	N/A	02022017_Pass13	02.02.2017	Pass 13	Wire	CS70/3	90	12	9.8
911-940/1M	N/A	02022017_Pass14	02.02.2017	Pass 14	Autogenous	CS70/3	110	12	9.8
941-970/1M	N/A	02022017_Pass15	02.02.2017	Pass 15	Wire	CS70/3	110	12	9.8
971-985/500k	N/A	02022017_Pass16	02.02.2017	Pass 16	Autogenous	CS70/3	110	12	9.8
986-1000/500k	N/A	02022017_Pass17	02.02.2017	Pass 17	Wire	CS70/3	110	12	9.8
1001-1020/1M	N/A	02022017_Pass18	02.02.2017	Pass 18	Autogenous	CS70/3	130	12	9.8
1021-1032/1M	N/A	02022017_Pass19	02.02.2017	Pass 19	Wire	CS70/3	130	12	9.8
1041-1055/500k	N/A	02022017_Pass20	02.02.2017	Pass 20	Autogenous	CS70/3	130	12	9.8
1056-1070/500k	N/A	02022017_Pass21	02.02.2017	Pass 21	Wire	CS70/3	130	12	9.8
1086-1100/500k	N/A	02022017_Pass23	02.02.2017	Pass 23	Autogenous	CS70/3	90	12	9.8
1101-1115/500k	N/A	02022017_Pass24	02.02.2017	Pass 24	Autogenous	CS70/3	90	12	9.8
1116-1140/1M	N/A	02022017_Pass25	02.02.2017	Pass 25	Autogenous	CS70/3	130	12	9.8
1141-1155/1M	N/A	02022017_Pass26	02.02.2017	Pass 26	Autogenous/Paint	CS70/3	90	12	9.8
1156-1170/1M	N/A	02022017_Pass27	02.02.2017	Pass 27	Copperwire	CS70/3	130	12	9.8
1171-1185/1M	N/A	02022017_Pass28	02.02.2017	Pass 28	Copperwire	CS70/3	90	12	9.8
1186-1210/1M	N/A	02022017_Pass29	02.02.2017	Pass 29	Long weld	CS70/3	70	12	9.8
1211-12351M	N/A	02022017_Pass31	02.02.2017	Pass 31	Long weld	CS70/3	70	12	9.8
1236-1257/1M	N/A	14032017_Pass1	14.03.2017	Pass 1		CS70/3			
1258-1271/1M	N/A	14032017_Pass2	14.03.2017	Pass 2		CS70/3			
1272-1290/1M	N/A	N/A	14.03.2017	N/A		CS70/3			
1291-1311/1M	N/A	14032017_Pass3	14.03.2017	Pass 3		CS70/3			
1312-1329/1M	N/A	14032017_Pass4	14.03.2017	Pass 4		CS70/3			
1330-1344/1M	N/A	14032017_Pass5	14.03.2017	Pass 5		CS70/3			
1345-1355/1M	N/A	14032017_Pass6	14.03.2017	Pass6		CS70/3			
1357-1371/1M	N/A	N/A	01.05.2017	N/A		CS70/3			
1372/1M	N/A	N/A	01.05.2017	N/A		CS70/3			
1373-1374/1M	N/A	N/A	01.05.2017	N/A		CS70/3			
1375-1389/1M	170509-112044	09052017_Pass1	09.05.2017	Pass 1		S527/0.7	60	15	0.6
1390-1399/1M	170509-131849	09052017_Pass2	09.05.2017	Pass 2		s304/0.9	70	15	0.7
1400-1403/1M	170509-131849	09052017_Pass3	09.05.2017	Pass 3		s304/0.9	70	15	0.7
1410/1M	170509-135231	09052017_Pass4	09.05.2017	Pass 4		s304/0.9	80	15	0.7
1411/1M	170509-140409	09052017_Pass5	09.05.2017	Pass 5		s304/0.9	90	15	0.7
1412/1M	170509-143344	09052017_Pass6	09.05.2017	Pass 6		s304/0.9	60	15	0.5
1413/1M	N/A	09052017_Pass7	09.05.2017	Pass 7		s304/0.9	70	15	0.7

1414/1M	170509-154204	09052017_Pass8	09.05.2017	Pass 8	s304/0.9	60	15	0.7
1415-1416/1M	170509-160038	09052017_Pass9	09.05.2017	Pass 9	s304/0.9	70	15	0.5
1417-1418/1M	N/A	N/A	10.05.2017	BG				
1419-1420/1M	170510-114911	N/A	10.05.2017	N/A	s304/0.9	Peak 60/ BG 40 frequency 3	15	0.5
1421-1422/1M	170510-115542	10052017_Pass1	10.05.2017	Pass 1	s304/0.9	Peak 70/ BG 40 frequency 3	15	0.5
1423/1M	170510-133014	10052017_Pass2	10.05.2017	Pass 2	s304/0.9	Peak 80/ BG 40 frequency 3	15	0.5
1424/1M	170510-135515	10052017_Pass3	10.05.2017	Pass 3	s304/0.9	Peak 80/ BG 40 frequency 3	15	0.5
1425/1M	170510-140108	10052017_Pass4	10.05.2017	Pass 4	s304/0.9	Peak 60/ BG 40 frequency 3	15	0.5
1427/1M	170510-155009	10052017_Pass5	10.05.2017	Pass 5	s304/0.9	Peak 125/ BG 40 frequency 3	15	0.5
1428/1M	170510-160135	10052017_Pass6	10.05.2017	Pass 6	s304/0.9	Peak 80/ BG 40 frequency 3	15	0.5
1431/1M	N/A	N/A	10.05.2017	1A	CS70	130	12	9.8
1433/1M	N/A	N/A	10.05.2017	2A	CS70	130	12	9.8
1434/1M	N/A	N/A	10.05.2017	3A	CS70	130	12	9.8
1435/1M	N/A	N/A	10.05.2017	4A	CS70	130	12	9.8
1436/1M	N/A	N/A	10.05.2017	5A	CS70	130	12	9.8
1437/1M	N/A	N/A	10.05.2017	6A	CS70	130	12	9.8
1439/1M	N/A	N/A	10.05.2017	7A	CS70	130	12	9.8
1440/1M	N/A	N/A	10.05.2017	8A	CS70	130	12	9.8
1441/1M	N/A	N/A	10.05.2017	9A	CS70	130	12	9.8
1442/1M	N/A	N/A	10.05.2017	1B	CS70	130	12	9.8
1443/1M	N/A	N/A	10.05.2017	2B	CS70	130	12	9.8
1445/1M	N/A	N/A	10.05.2017	3B	CS70	130	12	9.8
1446/1M	N/A	N/A	10.05.2017	4B	CS70	130	12	9.8
1447/1M	N/A	N/A	10.05.2017	5B	CS70	130	12	9.8
1448/1M	N/A	N/A	10.05.2017	6B	CS70	130	12	9.8
1449/1M	N/A	N/A	10.05.2017	7B	CS70	130	12	9.8
1450/1M	N/A	N/A	10.05.2017	8B	CS70	130	12	9.8
1451/1M	N/A	N/A	10.05.2017	9B	CS70	130	12	9.8
1452-1456/1M	N/A	N/A	10.05.2017	10B	CS70	130	12	9.8
1457-1459/1M	N/A	N/A	10.05.2017	1C	CS70	130	12	9.8
1460-1462/1M	N/A	N/A	10.05.2017	2C	CS70	130	12	9.8

1463-1464/1M	N/A	2607201 7_Pass1	26.07.2017	Pass 1	Wire	CS70	160	18	30
1465-1466/1M	N/A	2607201 7_Pass2	26.07.2017	Pass 2	Wire	CS70	180	12	30
N/A	N/A	2607201 7_Pass3	26.07.2017	Pass 3	Wire	CS70			
1467-1468/1M	N/A	2707201 7_Pass1	27.07.2017	Pass 1	Wire	CS70	190	20	30
1469-1471/1M	N/A	2707201 7_Pass2	27.07.2017	Pass 2	Wire	CS70	160	18	25
1472-1473/1M	N/A	2707201 7_Pass3	27.07.2017	Pass 3	Wire	CS70	130	18	30
1476-1477/1M	N/A	2707201 7_Pass4	27.07.2017	Pass 4	Wire	CS70	160	18	30
1478-1479/1M	N/A	2707201 7_Pass5	27.07.2017	Pass 5	Wire	CS70	130	18	30
1480/1M	N/A	2707201 7_Pass6	27.07.2017	Pass 6	Wire	CS70	130	18	50
N/A	N/A	2707201 7_Pass7	27.07.2017	Pass 7	Wire	CS70	130	18	30
1481-1482/1M	N/A	2707201 7_Pass8	27.07.2017	Pass 8	Wire	CS70	130	18	50
1483/1M	N/A	0108201 7_Pass1	01.08.2017	Pass 1		Al 6082/4	125 (7/3)	12	9.8
1484-1485/1M	N/A	0108201 7_Pass2	01.08.2017	Pass 2		Al 6082/4	125 (3/7)	20	9.8
1486/1M	170801-121333-Al	0108201 7_Pass3	01.08.2017	Pass 3		Al 6082/4	100 (7/3)	12	9.8
1487-1488/1M	170801-144218-Al	0108201 7_Pass4	01.08.2017	Pass 4		Al 6082/4	150 (7/3)	20	15
1489/1M	170801-145156-Al	0108201 7_Pass5	01.08.2017	Pass 5		Al 6082/4	150 (7/3)	20	20
1490-1491/1M	170801-151202-Al	0108201 7_Pass6	01.08.2017	Pass 6		Al 6082/4	150 (7/3)	20	25
1492/1M	170801-152228-Al	0108201 7_Pass7	01.08.2017	Pass 7		Al 6082/4	175 (7/3)	20	30
1493-1494/1M	170801-154557-Al	0108201 7_Pass8	01.08.2017	Pass 8		Al 6082/4	175 (7/3)	20	35
1496-1497/1M	N/A	0208201 7_Pass1	01.08.2017	Pass 1		Al 6082/4	175 (7/3)	20	15
1498-1499/1M	N/A	0208201 7_Pass2	02.08.2017	Pass 2		Al 6082/4	150 (7/3)	20	15
1503-1504/1M	N/A	0208201 7_Pass3	02.08.2017	Pass 3		Al 6082/4	150 (7/3)	20	15
1505/1M	N/A	N/A	02.08.2017	Pass 4		Al 6082/4	150 (7/3)	20	15
1506/1M	N/A	0208201 7_Pass4	02.08.2017	Pass 4(2)		Al 6082/4	150 (7/3)	20	35
1507/1M	N/A	0208201 7_Pass5	02.08.2017	Pass 5		Al 6082/4	150 (7/3)	20	30
1508/1M	N/A	0208201 7_Pass6	02.08.2017	Pass 6		Al 6082/4	150 (7/3)	20	30
1509/1M	N/A	0208201 7_Pass7	02.08.2017	Pass 7		Al 6082/4	100 (7/3)	20	30
1510/1M	170803-114302-Al	0308201 7_Pass1	03.08.2017	Pass 1	Al 5556 (AlMg5Mn)	Al 6082/4	175 (7/3)	20	30
1512/1M	170803-120654-Al	0308201 7_Pass2	03.08.2017	Pass 2	Al 5556 (AlMg5Mn)	Al 6082/4	175 (7/3)	20	30
N/A	170803-121642-Al	0308201 7_Pass3	03.08.2017	Pass 3	Al 5556 (AlMg5Mn)	Al 6082/4	175 (7/3)	20	30
1513/1M	170803-150021-Al	0308201 7_Pass4	03.08.2017	Pass 4	Al 5556 (AlMg5Mn)	Al 6082/4	175 (7/3)	20	30
N/A	N/A	0308201 7_Pass5	03.08.2017	Pass 5	Al 5556 (AlMg5Mn)	Al 6082/4			
1514-1517/1M	170803-151007-Al	0308201 7_Pass6	03.08.2017	Pass 6	Al 5556 (AlMg5Mn)	Al 6082/4	175 (7/3)	20	30
1515/1M	N/A	0308201 7_Pass7	03.08.2017	Pass 7	Al 5556 (AlMg5Mn)	Al 6082/4			
1516/1M	N/A	0308201 7_Pass8	03.08.2017	Pass 8	Al 5556 (AlMg5Mn)	Al 6082/4			

1517/1M	N/A	03082017_Pass9	03.08.2017	Pass 9	Al 5556 (AlMg5Mn)	Al 6082/4			
1519/1M	170803-153414-Al	03082017_Pass10	03.08.2017	Pass 10	Al 5556 (AlMg5Mn)	Al 6082/4	175 (7/3)	20	30
N/A	N/A	03082017_Pass11	03.08.2017	Pass 11	Al 5556 (AlMg5Mn)	Al 6082/4			
1520	170803-154734-Al	03082017_Pass12	03.08.2017	Pass 12	Al 5556 (AlMg5Mn)	Al 6082/4	175 (7/3)	20	30
1521-1530/1M	N/A	08082017_Pass1	08.08.2017	Pass 1		EN8	90	12	9.8
1531-1540/1M	N/A	08082017_Pass2	08.08.2017	Pass 2		EN8	90	12	9.8
1538-1539/1M	N/A	N/A	10.08.2017	Pass 1		EN8	110	12	9.8
N/A	N/A	N/A	10.08.2017	Pass 2		EN8	70	12	9.8
1540-1547/1M	N/A	10082017_Pass1	10.08.2017	Pass 3		EN8	70	20	9.8
1548-1551/1M	N/A	10082017_Pass2	10.08.2017	Pass 4		EN8	70	30	9.8
1552-1565/1M	N/A	10082017_Pass3	10.08.2017	Pass 5		EN8	50	12	25
1566-1570/1M	N/A	10082017_Pass4	10.08.2017	Pass 6		EN8	50	12	9.8
1571-1573/1M	N/A	N/A	10.08.2017	Pass 7		EN8	90	30	9.8
1574-1576/1M	N/A	N/A	10.08.2017	Pass 8		EN8	70	15	9.8
1577-1581/1M	N/A	N/A	11.08.2017	Pass 1		EN8	70	12	9.8
1583-1587/1M	N/A	N/A	11.08.2017	Pass 2		EN8	70	15	9.8
1588-1592/1M	N/A	N/A	11.08.2017	Pass 3		EN8	50	10	9.8
1593-1597/1M	N/A	N/A	11.08.2017	Pass 4		EN8	50	12	9.8
1598-1600/1M	N/A	N/A	11.08.2017	Pass 5		EN8	50	10	9.8
1601-1603/1M	N/A	N/A	11.08.2017	Pass 6		EN8	70	10	9.8
1604-1608/1M	N/A	N/A	11.08.2017	Pass 7		EN8	90	10	9.8
1609-1611/1M	N/A	N/A	11.08.2017	Pass 8		EN8	70	12	15
1612-1615/1M	N/A	N/A	11.08.2017	Pass 9		EN8	80	12	9.8
1616-1619/1M	N/A	N/A	11.08.2017	Pass 10		EN8	90	12	15
1621-1625/1M	N/A	N/A	11.08.2017	Pass 11		EN8	50	12	7
1626-1631/1M	N/A	N/A	11.08.2017	Pass 12		EN8	60	12	7
1632-1633/1M	170815-133921-Al 2mm	N/A	15.08.2017	Pass 1		Al 5083/2	AC negative:77A 50p positive:54A 50p	10	30
1634-1636/1M	170815-134756-Al 2mm	N/A	15.08.2017	Pass 2		Al 5083/2	70	10	30
1637-1639/1M	170815-142052-Al 2mm	N/A	15.08.2017	Pass 3		Al 5083/2	50	10	30
1644-1645/1M	N/A	N/A	15.08.2017	N/A	BG	N/A	N/A	N/A	N/A
1646-1650/1M	170904-112347	N/A	04.09.2017	Pass 1		Al 5083/2	70	12	25
1651-1652/1M	170904-113012	N/A	04.09.2017	Pass 2		Al 5083/2	70	12	25
1653-1655/1M	170904-115503	N/A	04.09.2017	Pass 3		Al 5083/2	60	12	25
1656/1M	170904-115959	N/A	04.09.2017	Pass 4		Al 5083/2	60	12	30
1657-1659/1M	170904-141232	N/A	04.09.2017	Pass 5		Al 5083/2	70	12	35

1660-1662/1M	170904-141730	N/A	04.09.2017	Pass 6		Al 5083/2	80	12	40
1663-1664/1M	170904-145718	N/A	04.09.2017	Pass 7		Al 5083/2	80	12	45
1665/1M	170904-150144	N/A	04.09.2017	Pass 8		Al 5083/2	80	12	50
1666-1668/1M	170904-151845	N/A	04.09.2017	Pass 9		Al 5083/2	70	12	50
1669-1670/1M	170904-152301 170904-155610	N/A	04.09.2017	Pass 10		Al 5083/2	80	12	20
1671-1672/1M	170904-154202	N/A	04.09.2017	Pass 11		Al 5083/2	60	12	20
1673-1678/1M	170904-155523	N/A	04.09.2017	Pass 12		Al 5083/2	70	12	20
1680/1M	170905-110711	N/A	05.09.2017	Pass 1		Al 5083/2	80	12	50
N/A	170905-115602	N/A	05.09.2017	Pass 2		Al 5083/2	80	12	35
1681-1682/1M	170906-104925	06092017_Pass1	06.09.2017	Pass 1		Al 5083/2	80	12	35
1683-1685/1M	170906-113317	06092017_Pass2	06.09.2017	Pass 2		Al 5083/2	100	12	35
1686-1688/1M	170906-114912	06092017_Pass3	06.09.2017	Pass 3		Al 5083/2	100	12	30
1689-1690/1M	170906-120346	06092017_Pass4	06.09.2017	Pass 4		Al 5083/2	100	12	25
1691-1692/1M	170906-141809	06092017_Pass5	06.09.2017	Pass 5		Al 5083/2	100	12	20
1693-1694/1M	170906-143512	06092017_Pass6	06.09.2017	Pass 6		Al 5083/2	100	12	15
1695-1696/1M	170906-144958	06092017_Pass7	06.09.2017	Pass 7		Al 5083/2	100	12	10
1697-1699/1M	N/A	13092017_Pass1	13.09.2017	Pass 1		Al 5083/2	80	12	35
1700-1701/1M	170913-140725-Al 2mm	13092017_Pass2	13.09.2017	Pass 2		Al 5083/2	80	12	30
1702-1703/1M	170913-142501-Al 2mm	13092017_Pass3	13.09.2017	Pass 3		Al 5083/2	80	12	30
1704-1705/1M	170913-143933-Al 2mm	13092017_Pass4	13.09.2017	Pass 4		Al 5083/2	90	12	35
1706-1707/1M	170913-151508-Al 2mm	13092017_Pass5	13.09.2017	Pass 5		Al 5083/2	100	12	40
1708-1709/1M	170913-152931-Al 2mm	13092017_Pass6	13.09.2017	Pass 6		Al 5083/2	100	12	45
1710-1711/1M	170913-154448-Al 2mm	13092017_Pass7	13.09.2017	Pass 7		Al 5083/2	100	12	50
1712-1713/1M	170913-155806-Al 2mm	13092017_Pass8	13.09.2017	Pass 8		Al 5083/2	70	12	20
1725			29.01.2018		Screw nut drop/ h30d10				
1726			29.01.2018		screw nut drop/ h20d10				
1727			29.01.2018		Screw nut drop/ h10d10				
1728			29.01.2018		Screw nut drop/ h30d20				
1729			29.01.2018		Screw nut drop/ h20d20				
1730			29.01.2018		Screw nut drop/ h10d20				
1732			29.01.2018		Screw nut drop/ h30d10				
1733			29.01.2018		Screw nut drop/ h10d10				
1734			29.01.2018		Screw nut drop/ h30d20				
1735			29.01.2018		Screw nut drop/ h20d20				

1736		29.01.2018		Screw nut drop/ h10d20				
1737		29.01.2018		GAS 15L/min				
1740-1741	Pass1	30.01.2018	middles 20180130(1)	Bead on plate	CS70	17.5	41	6.29
1742-1743	Pass2	30.01.2018		bead on plate	CS70	17.5	41	6.29
1744-1745	Pass3	30.01.2018		bead on plate	CS70	17.5	41	6.29
1746	Pass4	30.01.2018		bead on plate	CS70	17.5	41	6.29
1747	Pass5	30.01.2018		bead on plate	CS70	17.5	41	6.29
1760	Pass3 middles20180130(2)	30.01.2018	middles 20180130(2)	butt weld	EN8	16.5	59	5.91
1761	Pass4	30.01.2018		butt weld	EN8	16.5	59	5.91
1762	Pass5	30.01.2018		butt weld	EN8	16.5	59	5.91
1763	Pass8	30.01.2018		butt weld	EN8	16.5	59	5.91
1764	Pass9	30.01.2018		butt weld	EN8	16.5	59	5.91
1765	Pass11	30.01.2018		butt weld	EN8	16.5	59	5.91
1766	Pass1	01.02.2018	middles 20180201a	butt weld	Al5083	14	47	5.84
1767	Pass2	01.02.2018		butt weld	Al5083	14	47	5.84
1768	Pass3	01.02.2018		butt weld	Al5083	14	47	5.84
1770	Pass1	01.02.2018	middles 20180201b	butt weld	Al5083	14	47	5.84
1771	Pass2	01.02.2018		butt weld	Al5083	14	47	5.84
1773	Pass3	01.02.2018		Increasing joint gap	Al5083	14	47	5.84
	Pass1	01.02.2018	middles 20180201c	Increasing joint gap	Al5083	14	47	5.84
1774	Pass2	01.02.2018		Thickness variation	Al5083	14	47	5.84
	Pass1	01.02.2018	middles 20180201d	Thickness variation	Al5083	14	47	5.84
	Pass2	01.02.2018		Voltage too high	Al5083	15	47	5.84
	Pass3	01.02.2018		Voltage too high	Al5083	15.5	47	5.84
	Pass1	01.02.2018	middles 20180201e	Voltage too low	Al5083	13	47	5.84
1775	Pass1	01.02.2018	middles 20180201f	Voltage too low	Al5083	10	47	5.84
	Pass2	01.02.2018		Voltage too low	Al5083	10	47	5.84
	Pass3	01.02.2018		TS too fast	Al5083	14	71	5.84
	Pass4	01.02.2018		TS too fast	Al5083	14	71	5.84
	Pass5	01.02.2018		TS too slow	Al5083	14	29	5.84
1776	Pass6	01.02.2018		TS too slow	Al5083	14	29	5.84
1777	Pass7	01.02.2018		WFS too high	Al5083	14	47	6.93
	Pass8	01.02.2018		WFS too high	Al5083	14	47	5
	Pass9	01.02.2018		WFS too low	Al5083	14	47	5
1778	Pass10	01.02.2018		WFS too low	Al5083	14	47	5.84

	Pass11	01.02.2018		Liner missalignment	Al5083		14	47	5.84
	Pass12	01.02.2018		Liner missalignment	Al5083		14	47	5.84
	Pass13	01.02.2018		Water	Al5083		14	47	5.84
1779	Pass1	05.02.2018	middles 20180205a	butt weld	Al6061		15	35	5.94
	Pass2	05.02.2018		butt weld	Al6061		15	35	5.94
	Pass3	05.02.2018		butt weld	Al6061		15.4	35	5.94
1781	Pass1	06.02.2018	middles 20180206a	butt weld 1mm gap	CS70		19	41	6.37
1782	Pass2	06.02.2018		butt weld 1mm gap	CS70	166	19	41	6.37
1783	Pass3	06.02.2018		butt weld 1mm gap	CS70	168	19	41	6.37
1784	Pass1	06.02.2018	middles 20180206b	Increasing joint gap	CS70		19	41	6.37
1785	Pass2	06.02.2018		Voltage too high	CS70	160	21	41	6.37
1786	Pass3	06.02.2018			CS70		17	41	6.37
1787	Pass4	06.02.2018		Increasing joint gap	CS70		17	41	7.01
1788	Pass5	06.02.2018			CS70		17	41	7.01
1789	Pass6	06.02.2018			CS70		17	41	5.51
1790	Pass7	06.02.2018		Missing joint	CS70		17	41	6.37
1791	Pass8	06.02.2018		Decreasing gap	CS70		17	41	6.37
1792	Pass9	06.02.2018			CS70		17	53	6.37
1793	Pass10	06.02.2018			CS70		17	29	6.37
1794	Pass11	06.02.2018			CS70		17	41	6.37
1795	Pass1	06.02.2018	middles 20180206c		EN8		16.5	47	5.91
1796	Pass2	06.02.2018			EN8		16.5	47	5.91
1797	Pass3	06.02.2018			EN8		16.5	71	5.91
1798	Pass4	06.02.2018			EN8		16.5	71	5.91
1799	Pass5	06.02.2018			EN8		17.5	59	5.91
1800	Pass6	06.02.2018			EN8		17.5	59	5.91
1803	Pass7	06.02.2018			EN8		15.5	59	5.91
1804	Pass8	06.02.2018			EN8	154	15.5	59	5.91
1805	Pass9	06.02.2018			EN8		16.5	59	6.22
1806	Pass10	06.02.2018			EN8	152	16.5	59	6.22
1807	Pass11(TWO WELDS)	06.02.2018			EN8	153	16.5	59	5.5
1808	Pass12	06.02.2018			EN8		16.5	59	5.91
1809	Pass13(TWO WELDS)	06.02.2018			EN8		16.5	59	5.3
1810	Pass14	06.02.2018			EN8		16.5	59	5.91
1811	Pass15	06.02.2018			EN8		16.5	59	5.91
1812	Pass16	06.02.2018		Thickness variation	EN8		16.5	59	5.91
1813	Pass17	06.02.2018		Thickness variation	EN8		16.5	59	5.91

Appendix B: Signal processing tools

Fast Fourier Transform (FFT):

```
Fs = ;              % Sampling frequency
T = 1/Fs;               % Sampling period
L = ;               % Length of signal
t = (0:L-1)*T;          % Time vector
N = fft(filename);
P2 = abs(N/L);
P1 = P2(1:L/2+1);
P1(2:end-1) = 2*P1(2:end-1);
f = Fs*(0:(L/2))/L;
plot(f,P1)
title('' )
xlabel('f (Hz)')
ylabel('|P1(f)|')
```

Short time Fourier Transform (STFT):

```
spectrogram(filename,1000,900,1000,1e6,'yaxis');
view(-150,72)
shading interp
title('spectrogram')
```

Wavelet denoising:

```
WD = wden(filename,'modwtsqtwolog','s','mln',5,'sym5');
```

Root mean square (RMS):

```
y=rms(filename)
```

Coherence:

```
% Method: PSD xcorr
% PSD calculated by welch method
% Cross-correlation of PSD is calculated
window = ;              %Sample window length
overlap = ;                  %Overlap Length
Fs = ;                           % Sampling frequency
delta = window - overlap;
indice_out = 1:delta:length(sig)-window
weight = zeros(1,length(indice_out));
[pxx_templ,f_templ] = pwelch(template1);
```

```
for i = 1:length(indice_out)
    y = sig(indice_out(i):indice_out(i)+window-1,1);
    [pxx_y,f_y] = pwelch(y);

    [acor,lag] = xcorr(pxx_y,pxx_templ);
    weight(i) = acor((length(lag)+1)/2);
end

t_weight = (0:1:length(weight)-
1)/length(weight)*length(sig)/Fs;

figure;
plot(t_weight,weight)
xlabel('time (s)')
ylabel('similarity')
title('Cross-correlation result')
```

Pattern Recognition:

```
% Function ef calculates the difference in the sum of power of
higher frequency and lower frequency.
function C= ef(filename)
Fs = ;              % Sampling frequency
T = 1/Fs;               % Sampling period
L = ;               % Length of signal
t = (0:L-1)*T;          % Time vector
N = fft(filename);
P2 = abs(N/L);
P1 = P2(1:L/2+1);
SL = sum(P1(0.05*L+1:0.18*L));      %Sum of power of lower
frequency (51-180kHz)
SH = sum(P1(0.25*L+1:0.38*L));     %Sum of power of higer
frequency (251-380kHz)
C = minus(SL,SH);
Y=Fs/500;
j=1
for i=1:Y
dataname=data(j:j+499)
C(i,:)=ef(dataname)
j=j+500
end
Time=L/Fs
plot(Time,C)
title('Pattern recognition analysis result')
xlabel('t(s)')
ylabel('Similarity')
```